Electron Transfer and Ligand Binding Properties of Cytochromes

Pedro Oliveira Quintas

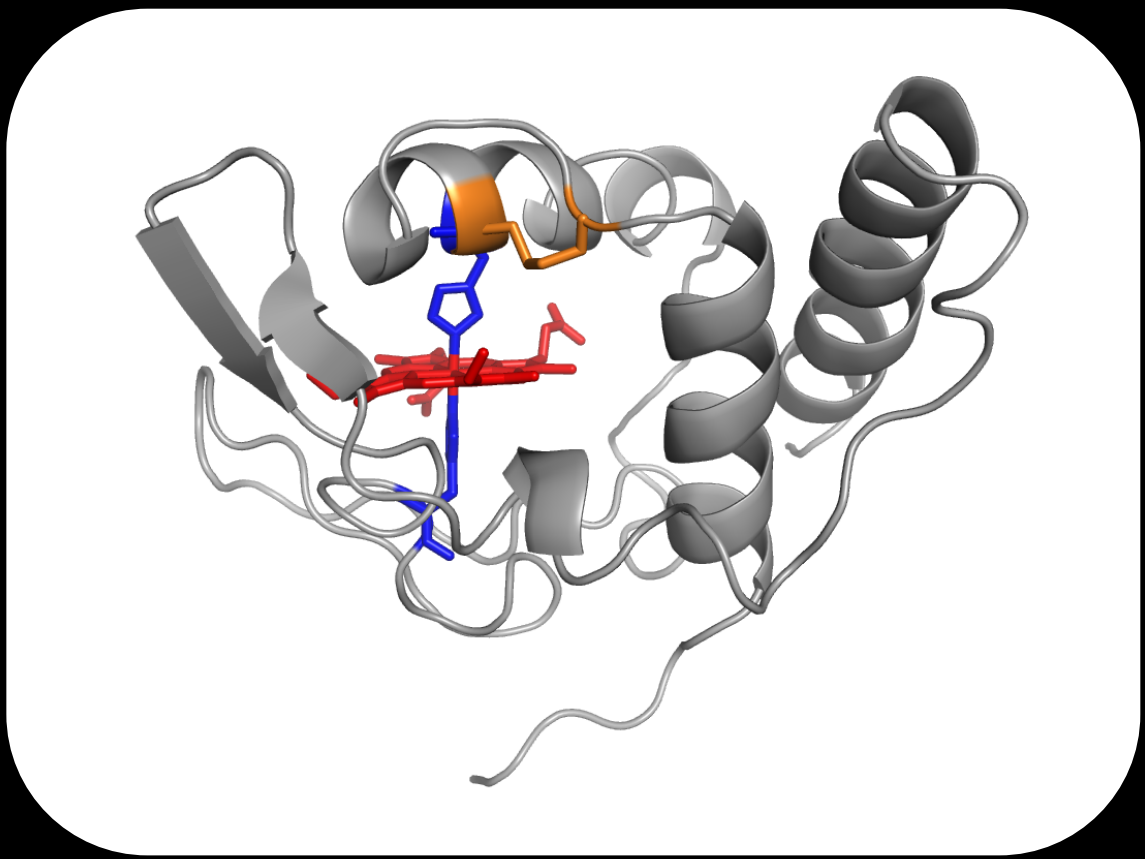

Dissertation presented to obtain the Ph.D degree in Biochemistry

Instituto de Tecnologia Química e Biológica | Universidade Nova de Lisboa

Oeiras,
June, 2013

INSTITUTO
DE TECNOLOGIA
QUÍMICA E BIOLÓGICA
/UNL

Knowledge Creation

Electron Transfer and Ligand Binding Properties of Cytochromes

Pedro Oliveira Quintas

Dissertation presented to obtain the Ph.D degree in Biochemistry

Instituto de Tecnologia Química e Biológica | Universidade Nova de Lisboa

Oeiras, June, 2013

FCT Fundação para a Ciência e a Tecnologia
MINISTÉRIO DA EDUCAÇÃO E CIÊNCIA

INSTITUTO DE TECNOLOGIA QUÍMICA E BIOLÓGICA /UNL
Knowledge Creation

ACKNOWLEDGEMENTS

Like all scientific work, this would have been much harder to accomplish without the precious help from a number of people.

In the first place I must thank my supervisors Prof. David Turner and Prof. Teresa Catarino for all the help and support during these years. It is hard to imagine how much I have learned in this time, and most of it was owed to them.

I would also like to acknowledge Prof. Helena Santos and the rest of the group for listening and discussing a subject that was very different from what they were used to. Also, one can hardly think of a better group of people to be with every day. Thank you all for everything.

Most of the experimental work was a lonely affair, however, towards the end of the PhD I had the invaluable support of Márcia Oliveira and Andreia Cepeda, which was greatly appreciated.

I necessarily had to learn a few new techniques in order to perform my work and therefore I wish to express my gratitude to the following people: Dr. Nuno Borges for the lessons in molecular biology; Dr. Melinda Noronha for the instructions on the growth of *E. coli* and the expression of proteins; Prof. Carlos Salgueiro who provided plasmid pVA203, which greatly improved the expression of our proteins; Isabel Pacheco for the training in protein purification, and Dr. Pedro Lamosa and Dr. Ricardo Louro for the assistance with the NMR. The small part of the thesis that involved Raman spectroscopy would not have been possible without the help of Dr. Smilja Todorovic. Thanks also to Patrícia Almeida, easily one of the most helpful persons I have met, and to Fátima Madeira for the assistance with all the bureaucratic details and the company in some rather lonely times.

Additionally, I would like to express my appreciation to Prof. António Xavier for believing in my capacities and giving me the opportunity to join his group.

Finally, I would like to thank ITQB for providing all the conditions to perform my work and FCT for funding.

Apoio financeiro da Fundação para a Ciência e Tecnologia (FCT) e do FSE no âmbito do Quadro Comunitário de Apoio, Bolsa de Doutoramento SFRH/BD/36716/2007.

SUMMARY

Haem proteins are one of the most versatile groups of proteins in nature. They are able to perform several functions, such as transport and storage of oxygen, electron transfer, sensing of small molecules, and catalysis. The nature of the haem, the presence or absence and the nature of the axial ligands to the iron atom, and the effect of the polypeptide chain of the protein on the environment of the haem all contribute to this versatility. The work presented in this thesis focuses on the mechanisms of electron transfer and the discrimination of small ligands by cytochromes containing haem *c* with axial histidines.

Several haem proteins are known to bind and discriminate small ligands. Selectivity is thought to be achieved by regulating the relative binding affinities of the ligands through electrostatic interactions with the nearby aminoacids and/or steric hindrance. Some ligands also cause conformational changes on binding that change the active/inactive state of the protein. One of the proteins that is selective towards nitric oxide (NO), and has been implicated in the protection of cells against toxic levels of NO, is cytochrome *c*', which is produced by several organisms, such as *Alcaligenes xylosoxidans*, *Paracoccus denitrificans* and *Rhodobacter sphaeroides*. A protein featuring some similarities to cytochrome *c*' has been isolated from *Methylophilus methylotrophus* and named cytochrome *c*''. Previous studies of this protein focused on the characterization of electron transfer processes, as well as the determination of the three-dimensional structure. Because of its similarities to cytochrome *c*', we sought to characterize in detail the ligand binding and selectivity of cytochrome *c*''. We used nitric oxide (NO), carbon monoxide (CO) and cyanide (CN^-) as ligands and found that only NO is able to bind at physiological pH and room temperature. By partially unfolding the protein with temperature or urea we were able to bind the other two

ligands and determine binding energies by extrapolation to normal conditions. Despite having a lower affinity and rate of binding than other NO-binding proteins, the selectivity of cytochrome *c*" for NO is bigger. The study of the kinetics of NO binding by the stopped-flow technique revealed a slower and NO-independent process that follows the initial binding. Using resonance Raman spectroscopy to get information about the environment around the haem and understand the structural implications of NO binding, we concluded that the NO-bound form of cytochrome *c*" is 5-coordinated. We attributed the second process to detachment of the proximal axial histidine following the binding of NO.

Another goal of this work was the study of electron transfer in haem proteins. This topic has recently grown in importance following the discovery of organisms that are able to perform the extracellular reduction of metal oxides, such as those from the genera *Geobacter* and *Shewanella*. This characteristic has potential uses in bioremediation of contaminated environments or in energy production by microbial fuel cells. Electrons are exported to the extracellular space by several multihaem proteins; therefore, the detailed thermodynamic and kinetic characterization of these proteins is of great importance. Haem reduction potentials, as well as the interactions between haems and those with ionisable centres, can be determined by following redox titrations using a combination of NMR and UV-visible spectroscopies. The kinetic properties of individual haems have been studied by the reduction of multihaem cytochromes with sodium dithionite in stopped-flow experiments, and then using the thermodynamic parameters for the individual haems with the Marcus theory of electron transfer to separate the contributions of each haem. It is assumed that variations in the rates of reduction of each haem depend only on the driving force, while any changes in electrostatic interactions were neglected, otherwise the model would fail. Using cytochrome *c*" as a model, we aimed to test this assumption. By studying the dependence of the rate of reduction of cytochrome *c*" by dithionite on ionic strength, we were able to determine the rates at infinite ionic strength to

eliminate electrostatic interactions. The change in these rates with pH can be compared with the change predicted by the Marcus theory of electron transfer, based solely on the driving force of the reaction. We concluded that most of the effect was caused by the change in the driving force; hence the assumption made in the model, that changing electrostatic interactions between the protein and dithionite may be neglected, now has an experimental basis.

The final part of the work concerned the electron transfer between two cytochromes c_3 from *Desulfovibrio africanus*, identified as cytochrome c_3 type I (TpIc_3) and cytochrome c_3 type II (TpIIc_3). It is believed that these cytochromes are physiological partners and are involved in the transfer of electrons from the periplasmic hydrogenase to the transmembrane electron-transfer complex. Based on their thermodynamic properties, it is also possible that two electrons could be transferred in the same encounter between the two cytochromes. The study involved the determination of electron exchange rates by ^{1}H-NMR. Electron transfer between TpIc_3 and TpIIc_3 was much faster than transfer between TpIc_3 molecules, which is good evidence for the two cytochromes being physiological partners. However, no evidence was found for two-electron transfers occurring in the lifetime of the TpIc_3 encounter complexes.

In summary, the work presented in this thesis further advances the characterization of cytochromes. The ligand selectivity by cytochrome *c*" is another example of ligand discrimination by a haem protein, which extends the knowledge of these mechanisms. The verification of the main assumption of the kinetic model, that the changes in rates of reduction depend exclusively on the driving force, clears the way for the utilization of the model in the characterization of other multihaem cytochromes, such as those from *Geobacter* and *Shewanella*. The methodology developed to determine the electron exchange rates between proteins confirmed that TpIc_3 and TpIIc_3 from *Desulfovibrio africanus* are physiological partners and proved to be a useful tool in the kinetic characterization of protein-protein interactions.

Resumo

As proteínas hémicas são um dos mais versáteis grupos de proteínas na natureza. São capazes de executar funções tão distintas como transporte e armazenamento de oxigénio, transferência de eletrões, deteção de pequenas moléculas e catálise. Para esta versatilidade contribuem vários fatores, tais como a natureza do grupo hemo, a presença ou ausência e a natureza dos ligandos axiais ao átomo de ferro e o efeito da sequência polipeptídica da proteína na proximidade do hemo. O trabalho apresentado nesta tese foca-se nos mecanismos de transferência eletrónica e na discriminação de pequenos ligandos por citocromos que contêm hemos *c* com histidinas axiais.

Diversas proteínas hémicas são capazes de ligar e discriminar pequenos ligandos. Pensa-se que a seletividade é alcançada através da regulação das afinidades relativas dos ligandos por meio de interações eletrostáticas com os aminoácidos vizinhos e/ou limitações espaciais. Alguns ligandos causam ainda mudanças conformacionais que alteram o estado ativo/inativo da proteína. Uma das proteínas que é seletiva para o óxido nítrico (NO), e foi implicada na proteção das células contra níveis tóxicos do NO, é o citocromo *c*', que é produzido por diversos organismos, tais como *Alcaligenes Xylosoxidans*, *Paracoccus Denitrificans* e *Rhodobacter Sphaeroides*. Uma proteína que possui algumas semelhanças com o citocromo *c*' foi isolada de *Methylophilus Methylotrophus* e denominada citocromo *c*''. Estudos anteriores nesta proteína focalizaram-se na caracterização de processos de transferência eletrónica, e na determinação da sua estrutura tridimensional. Devido às similaridades com o citocromo *c*', procurou caracterizar-se em detalhe a ligação de pequenas moléculas e a seletividade do citocromo *c*''. Usou-se óxido nítrico (NO), monóxido de carbono (CO) e cianeto (CN^-) como ligandos e descobriu-se que apenas o NO é capaz de se ligar a pH fisiológico e temperatura ambiente. Através do desenrolamento parcial da proteína com temperatura ou ureia foi possível ligar os outros dois ligandos e determinar energias de ligação por extrapolação para as condições normais. Constatou-se que,

apesar de ter uma afinidade e uma velocidade de ligação mais baixas do que outras proteínas que ligam NO, a seletividade do citocromo *c*" para o NO é maior. O estudo da cinética de ligação do NO por *stopped-flow* revelou um processo mais lento e independente do NO que ocorre após a ligação. Usando espectroscopia de ressonância de Raman, de modo obter informação sobre o ambiente em torno do hemo e compreender as implicações estruturais da ligação do NO, concluiu-se que o citocromo *c*" ligado ao NO apresenta o hemo na forma penta-coordenada. Atribuiu-se, portanto, o segundo processo ao afastamento da histidina proximal, que ocorre na sequência da ligação do NO.

Outro objetivo deste trabalho era o estudo da transferência de eletrões em proteínas hémicas. Este tópico tem crescido recentemente em importância, na sequência da descoberta de organismos capazes de executar a redução extracelular de óxidos de metais, como, por exemplo, bactérias dos géneros *Geobacter* e *Shewanella*. Esta característica tem aplicações potenciais na biorremediação de ambientes contaminados ou na produção de energia por pilhas de combustível microbianas. Os eletrões são exportados para o espaço extracelular por diversas proteínas multihémicas, logo, a caracterização detalhada das propriedades termodinâmicas e cinéticas destas proteínas é de grande importância. Os potenciais de redução dos hemos, assim como as interações entre hemos e destes com centros ionizáveis, podem ser determinados através de titulações redox usando uma combinação de espectroscopias de NMR e UV-visível. As propriedades cinéticas dos hemos individuais foram estudadas pela redução dos citocromos multihémicos com ditionito do sódio em experiências de *stopped-flow*, usando depois os parâmetros termodinâmicos dos hemos individuais e a teoria de Marcus para a transferência eletrónica de modo a separar as contribuições de cada hemo. Assume-se que as variações nas velocidades de redução de cada hemo dependem apenas da diferença de energia (*driving force*), ao passo que quaisquer mudanças em interações eletrostáticas são negligenciadas, caso contrário o modelo falharia. Usando o citocromo *c*" como modelo, pretendeu testar-se esta hipótese restritiva. Estudando a

dependência da velocidade de redução do citocromo *c*'' pelo ditionito com a força iónica, foi possível determinar as velocidades a força iónica infinita, de modo a eliminar as interações eletrostáticas. A variação da velocidade com o pH pode ser comparada com a mudança prevista pela teoria de Marcus para a transferência eletrónica, baseada apenas na *driving force* da reação. Concluiu-se que a maior parte do efeito é causada pela mudança na *driving force*; portanto, a suposição feita no modelo de que variações nas interações eletrostáticas entre a proteína e o ditionito podem ser negligenciadas, tem agora um fundamento experimental.

A parte final do trabalho debruçou-se sobre a transferência de eletrões entre dois citocromos c_3 de *Desulfovibrio africanus*, designados citocromo c_3 tipo I (TpIc_3) e citocromo c_3 tipo II (TpIIc_3). Supõe-se que estes citocromos são parceiros fisiológicos e estão envolvidos na transferência de eletrões da hidrogenase periplasmática para o complexo transmembranar de transferência eletrónica. Com base nas suas propriedades termodinâmicas, é também possível que dois eletrões possam ser transferidos no mesmo encontro entre os dois citocromos. O estudo envolveu a determinação das velocidades de permuta eletrónica por ^{1}H-NMR. A transferência eletrónica entre o TpIc_3 e o TpIIc_3 é muito mais rápida do que transferência entre as moléculas de TpIc_3, o que é um forte indício de que os dois citocromos são parceiros fisiológicos. Contudo, nenhuma evidência foi encontrada para a transferências de dois eletrões durante o tempo de vida dos complexos.

Em resumo, o trabalho apresentado nesta tese é mais um passo no avanço da caracterização de citocromos. A seletividade dos ligandos pelo citocromo *c*'' é mais um exemplo de discriminação de ligandos por uma proteína hémica, o que contribui para o aumento do conhecimento a respeito destes mecanismos. A verificação da hipótese restritiva do modelo cinético, de que as mudanças nas velocidades de redução dependem exclusivamente da *driving force*, permite a utilização do modelo na caracterização de outros citocromos multihémicos, tais como os de *Geobacter* e de *Shewanella*. A metodologia desenvolvida para determinar as velocidades de permuta eletrónica

entre proteínas confirmou que o TpIc_3 e o TpIIc_3 de *Desulfovibrio africanus* são parceiros fisiológicos e provou ser uma ferramenta útil na caracterização cinética de interações proteína-proteína.

ABBREVIATIONS

2D – Two dimensional

5cc – five-coordinated

6cc – six-coordinated

ATP – Adenosine-5'-triphosphate

ATPase – ATP synthase

Cyt – Cytochrome

DTT – Dithiothreitol

EDTA – Ethylenediaminetetraacetic acid

ET – Electron transfer

EXSY – Exchange spectroscopy

Hase – Hydrogenase

Hb – Haemoglobin

HS – High-spin

HSQC – Heteronuclear single quantum coherence

IPTG – Isopropyl β-D-1-thiogalactopyranoside

IUB – International union of biochemistry

IUPAC – International union of pure and applied chemistry

LS – Low-spin

Mb – Myoglobin

MeV – Methyl viologen

NMR – Nuclear magnetic resonance

NOESY – Nuclear Overhauser enhancement spectroscopy

OD – Optical density

PDB – Protein data bank

PCR – Polymerase chain reaction

rB^+ – Positive redox-Bohr effect

rB^- – Negative redox-Bohr effect

Red5cc – Reduced five-coordinated

Red6cc – Reduced six-coordinated

RMSD – Root-mean-square deviation

ROS – Reactive Oxygen Species

RR – Resonance Raman

SDS-PAGE – Sodium dodecyl sulfate polyacrylamide gel electrophoresis

sGC – Soluble Guanylate Cyclase

Tmc – Transmembrane electron-transfer complex

TpIc_3 – Type I cytochrome c_3

TpIIc_3 – Type II cytochrome c_3

Tris – Tris(hydroxymethyl)aminomethane

UV – Ultra-violet

Wt – Wild-type

Amino acid abbreviations

Alanine	Ala	A
Arginine	Arg	R
Asparagine	Asn	N
Aspartate	Asp	D
Cysteine	Cys	C
Glutamate	Glu	E
Glutamine	Gln	Q
Glycine	Gly	G
Histidine	His	H
Isoleucine	Ile	I
Leucine	Leu	L
Lysine	Lys	K
Methionine	Met	M
Phenylalanine	Phe	F
Proline	Pro	P
Serine	Ser	S
Threonine	Thr	T
Tryptophan	Trp	W
Tyrosine	Tyr	Y
Valine	Val	V

CONTENTS

FIGURE INDEX

TABLE INDEX

Chapter 1

Introduction

CONTENTS

HAEM PROTEINS

Haem proteins are one of the most versatile groups of proteins in nature. Found in all forms of life, they are involved in many different types of reactions such as electron transfer, oxygen transport and storage, oxygen reduction, nitric oxide production, sensing and transport, oxygenation, and reduction of peroxides. Most of this versatility arises from the presence of an iron-porphyrin prosthetic group – the haem. The nature of the haem, the presence or absence and the nature of the axial ligands to the iron atom, and the effect of the polypeptide chain of the protein on its surroundings all contribute to this diversity of properties. Of the different types of haem (Figure 1.1) the most common is haem *b*. It is present for example in haemoglobin and myoglobin, with a single axial iron ligand, where it serves as the binding site for oxygen. It is also present in catalase where it is part of the active site, assisting in the conversion of hydrogen peroxide into oxygen and water. Haem *c*, which appears in most electron transfer proteins with two axial iron ligands, is very similar to haem *b* but is covalently attached to the polypeptide chain via thioether bonds. Other less common haems include, among others, haem *a*, present in cytochrome *c* oxidase, and characterized by the presence of a hydroxyethylfarnesyl group at position 3 and a formyl group at position 18 of the porphyrin ring (according to IUPAC-IUB nomenclature (Moss 1988)); and haem d_1, present in nitrite reductase, and character-

ized by the presence of saturated bonds in the porphyrin ring. In regard to the axial ligands, most haem proteins have at least one histidine coordinated to the haem. The sixth ligand is most commonly another histidine or a methionine, but asparagines (Leys *et al.* 2000), cysteines (Meier *et al.* 2001; Bamford *et al.* 2002), tyrosines (Fulop *et al.* 1995; Arnoux *et al.* 2000) and others have also been observed. In some cases, the sixth coordination site may also be empty or occupied by a water molecule. Not surprisingly, the nature of the aminoacid residues around the haem also contributes to the properties of the haem protein as different interactions can stabilize or destabilize reagents, products or intermediates.

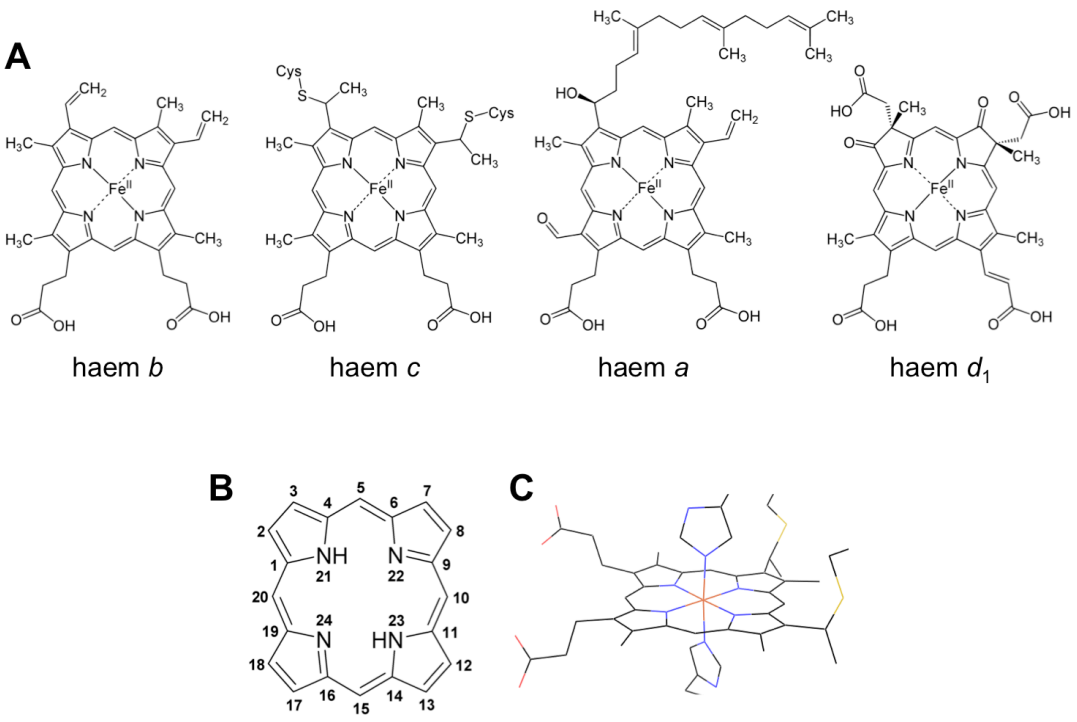

Figure 1.1 (A) Different types of haem groups. **(B)** Porphyrin numbered according to IUPAC-IUB nomenclature (Moss 1988). **(C)** Haem *c* with bis-histidinyl coordination.

Cytochromes *c* are a particular group of haem proteins that are mainly involved in the transfer of electrons in respiratory pathways, both aerobic and anaerobic, covering a reduction potential range from -400 to +400 mV (Figure 1.2). They contain one or more covalently attached haems *c* and can be soluble or membrane associated. The number of haems per protein can range from just one to more than twenty. The reason for the increase in the number of haems seems to be efficiency, since it not only maximises the likelihood of a successful electron transfer, but also allows the transfer of more electrons at the same time. Moreover, the presence of more than one haem enables the occurrence of cooperativity, where the redox state of one centre influences the reduction potential of other centres, allowing the fine tuning of the reduction potential in order to optimize the interaction with other electron transfer partners in different physiological situations (Santos *et al.* 1984a). In this work two different kinds of cytochromes *c* were studied: the single-haem cytochrome *c*" and a pair of tetrahaem cytochromes c_3. The objective is to use these cytochromes as models to further understand the mechanisms and functions of these proteins.

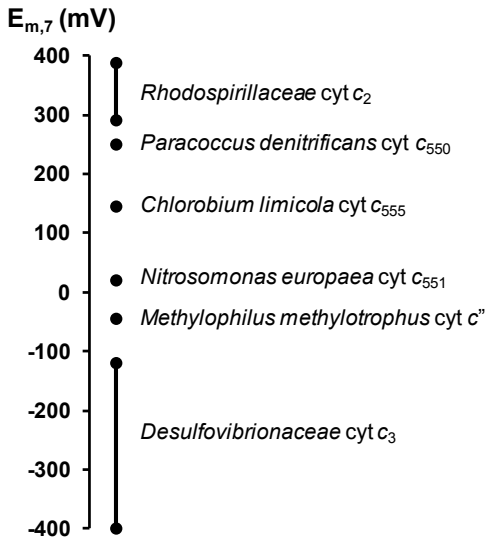

Figure 1.2 Reduction potential range of *c*-type cytochromes (Pettigrew and Moore 1987).

CYTOCHROME *c*”

Cytochrome *c*” is a 14.2 kDa periplasmic protein isolated from the obligate aerobe *Methylophilus methylotrophus* (Santos and Turner 1988). This organism is a restrictive facultative methylotroph, meaning that it is capable of using single-carbon molecules like methanol or methylamines as both carbon and energy sources, but is also able to utilize a limited range of other organic compounds, such as glucose and fructose (Jenkins *et al.* 1987). It is considered an important organism for industrial applications and has been used in the production of Single-Cell Protein since the 1980s (Windass *et al.* 1980). Other possible applications include the production of small metabolites and the isotope labelling of proteins or nucleic acids (Batey *et al.* 1996), with the main advantage of utilizing methanol, a relatively inexpensive substrate.

Cytochrome *c*” is a monomer with 124 aminoacid residues and a single haem covalently bound via thioether bonds to cysteines 49 and 52. An extra pair of cysteines (96 and 104) forms a disulfide bond not far from the haem, which confers rigidity to the structure (Brennan *et al.* 2001) (Figure 1.3).

In the oxidised state the haem is coordinated by two histidinyl residues (H53 and H95) in a near-perpendicular orientation (Berry *et al.* 1990), but upon reduction the cytochrome undergoes an unusual spin-state transition from low-spin to high-spin, with the detachment of histidine 95 (Costa *et al.* 1993) (Figure 1.4). However, the chemical disruption of the disulfide bond prevents this detachment from happening (Brennan *et al.* 2001) (Figure 1.4). This histidine-detachment mechanism is also thought to allow the coupling of electrons and protons in a process that is known as the redox-Bohr effect (Costa *et al.* 1992). In fact, there is a clear variation of the reduction potential with the pH from 82 mV at pH 4 to -100 mV at pH 10 (Figure 1.5). The experimental points were analyzed using a model that considers two distinct and non-interacting ionizing groups: one in which the pKa changes from <2.5 to 8.1

upon reduction that has been attributed to the detached histidine; and one in which the pKa decreases from 6.4 to 5.4 that has been attributed to haem propionate 17. Therefore, a mechanism was proposed where, upon reduction at physiological pH, the detached histidine picks up a proton, resulting in no change in the charge around the haem. The movement of the detached histidine closer to the haem propionate, increasing the local charge and slightly lowering the p*K*a, can explain the anti-electrostatic process observed in the propionate.

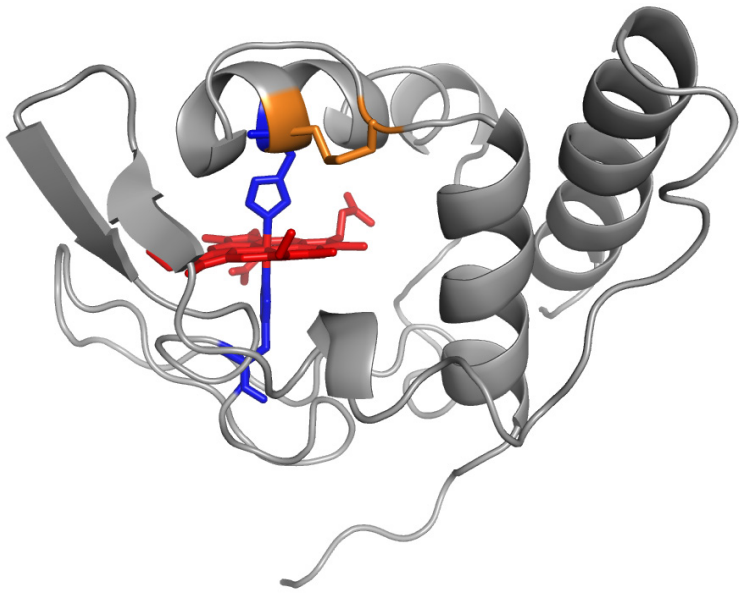

Figure 1.3 Structure of oxidised cytochrome *c*" (pdb: 1E8E (Brennan *et al.* 2001)). In red the haem group, in blue the two histidinyl axial ligands and in orange the disulfide bond.

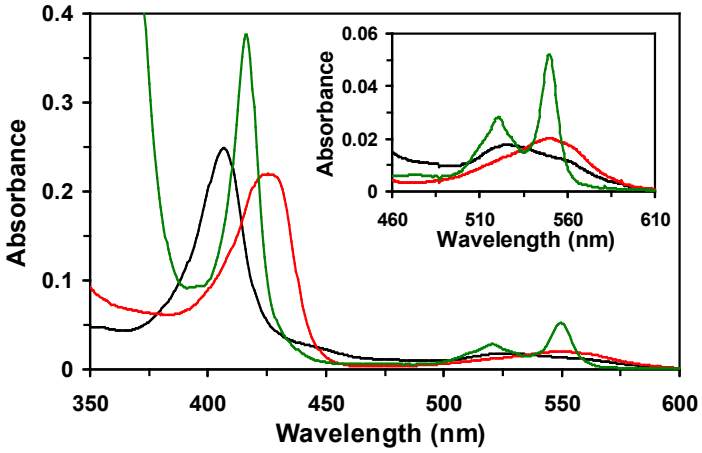

Figure 1.4 UV-visible spectra of cytochrome *c*" oxidised (black), reduced 5-coordinated (red) and reduced 6-coordinated (green) (Santos and Turner 1988; Brennan *et al.* 2001). The reduced 6-coordinated protein was obtained at pH 11.8 in the presence of 5 mM sodium dithionite.

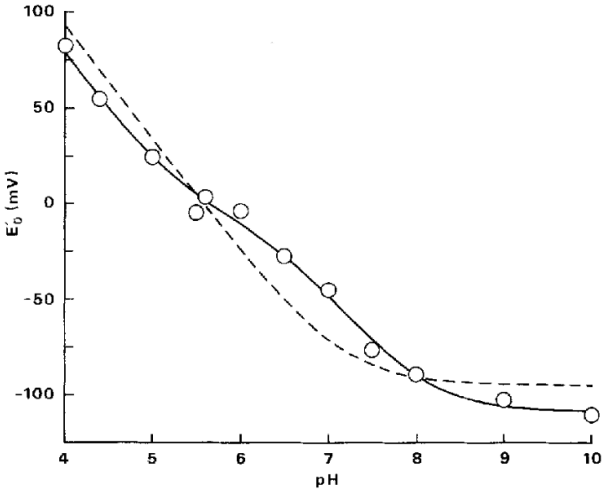

Figure 1.5 pH dependence of the reduction potential of *M. methylotrophus* cytochrome *c*" at 25 °C. The dashed line is the best fit to a theoretical model that considers a single ionizing group. The solid line represents the best fit to a model that assumes two distinct and non-interacting ionizing groups influencing the reduction potential. Adapted from (Costa *et al.* 1992).

It has been previously reported that cytochrome *c*" was able to bind cyanide in both redox states, but only at high pH, and carbon monoxide at physiological pH, but only in the reduced form (Santos and Turner 1988). Nitric oxide binding had never been tested. Therefore, because of the growing importance of this small molecule and the similarities between cytochrome *c*" and cytochrome *c*', which has been implicated in NO metabolism in *Paracoccus denitrificans* (Moir 1999) and has been used as a model to understand the mechanism of soluble guanylate cyclase, the human sensor for NO, we went on to study the binding of this ligand in detail as well as quantifying the binding of the other small molecules. Cytochrome *c*" proved to be highly selective for NO when compared to other haem proteins. The binding of CO and CN^- was rather challenging because of the very low affinities of these ligands to cytochrome *c*". This limitation was overcome by performing the experiments at higher temperature, higher pH or in the presence of a high concentration of urea. However, a severe complication arises from the disulfide bond because of its tendency to become reduced when the haem iron was reduced in the conditions necessary for the binding, hence altering all of the properties of the cytochrome. The results of these studies are presented in chapter 2 of this thesis.

A previous study on the kinetics of reduction of cytochrome *c*" has shown that the rate of reduction decreases with the pH (Coletta *et al.* 1997), as does the reduction potential (Figure 1.5). This result led us to investigate whether this decrease in the rate was due to changes in the electrostatic properties of the protein as was suggested or rather to the observed decrease in the driving force, which, according to the theory of Marcus, is one of the factors controlling the rate of electron transfer (Marcus and Sutin 1985). In fact, the theory of Marcus is the basis of the model used in the study of multihaem cytochromes (Catarino and Turner 2001). The changes in the driving force are used to obtain the kinetic parameters, and the method would fail if surface charge was a more important factor. Using cytochrome *c*" as a model it was established that the change in the driving force is in fact more important for the control of

reduction rates than the change in electrostatics, validating the approach used in multihaem cytochromes. Results are presented in chapter 3 of this thesis.

TETRAHAEM CYTOCHROMES C_3

Cytochromes c_3 are a group of tetrahaem cytochromes present in sulphate-reducing bacteria. These organisms are considered one of the oldest forms of bacterial life on earth (Barton and Fauque 2009). They are found in anaerobic environments, both aquatic and terrestrial and are located at the end of the microbial food chains, thus performing the important environmental role of further oxidizing the fermentation products from other microorganisms (Muyzer and Stams 2008). They couple the oxidation of these small organic compounds, such as lactate or pyruvate, and molecular hydrogen to the reduction of sulfate to sulfide (Hansen 1994). Sulfate-reducing bacteria are also industrially relevant for distinct reasons. On the one hand they are a source of major concern to industries like the petro-chemical because of the corrosion to the metal surfaces caused by sulfides (Hamilton 2003; Coetser and Cloete 2005). On the other hand they can also be applied beneficially in bioremediation, such as the removal of heavy metals from waste water (Lovley 2001).

The first cytochrome c_3 was isolated in 1954 from *Desulfovibrio vulgaris* (Ishimoto *et al.* 1954; Postgate 1954), but several others were later isolated from other members of the *Desulfovibrionaceae* family. They are small (~15 kDa) and very stable globular proteins. The polypeptide chains comprise 102-118 aminoacid residues and the four *c*-type haems have bis-histidinyl coordination. Despite low homology in aminoacid sequence (Magro *et al.* 1997), the general folding and the haem architecture is strictly conserved (Matias *et al.* 2005) among them. Furthermore, the soluble cytochromes c_3, called type I (TpIc_3), possess a conserved patch of positive charges close to haem IV, composed mostly of lysine residues, that is supposed to be the site of interaction with its partners (Matias *et al.* 2001). They are present in large quantities

in the periplasm and are proposed to play a role in the hydrogen metabolism in sulphate-reducing bacteria (Matias *et al.* 2005) (Figure 1.6).

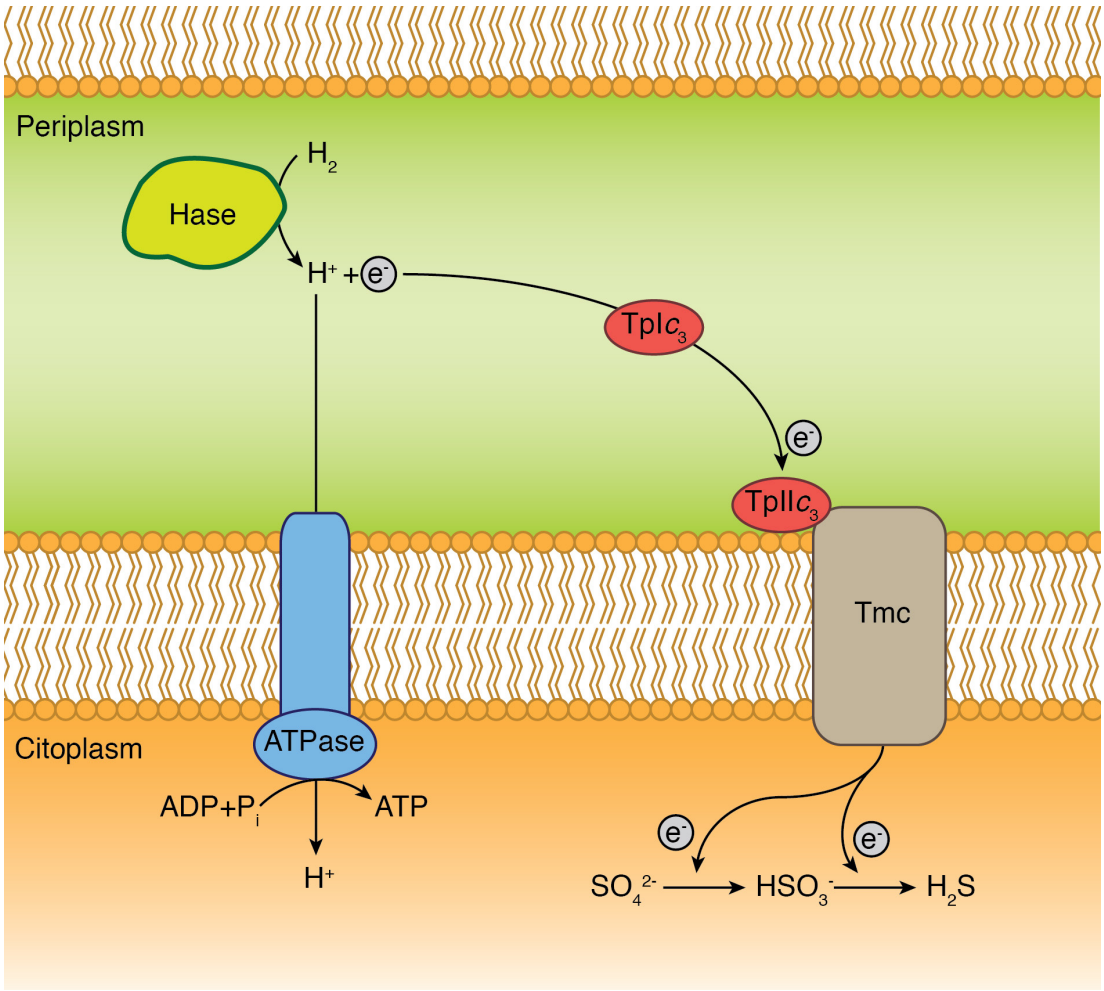

Figure 1.6 Proposed hydrogen metabolism in *Desulvovibrio africanus*. Hase: Hydrogenase; ATPase: ATP synthase; Tmc: Transmembrane complex; TpIc_3: Type I cytochrome c_3; TpIIc_3: Type II cytochrome c_3.

Molecular hydrogen is converted to electrons and protons by periplasmic hydrogenases. The resulting protons are released to the periplasm but the electrons are transferred to the transmembrane electron transfer complex and eventually are used in the reduction of the terminal electron acceptor, sulphate. This process generates a proton gradient across the membrane that is used to produce ATP. In the membrane, the electron acceptor is thought to be one of the multihaem cytochromes associated with the transmembrane complexes. Several different cytochromes have been identified so far, including a sixteen-haem cytochrome in *D. vulgaris* Hildenborough (Pollock *et al.* 1991), *D. vulgaris* Miyazaki (Ogata *et al.* 1993) and *Desulfovibrio gigas* (Chen *et al.* 1994); a nine-haem cytochrome in *Desulfovibrio desulfuricans* ATCC 27774 (Liu *et al.* 1988; Matias *et al.* 1999), and a tetrahaem cytochrome c_3, denoted type II (TpIIc_3), in *Desulfovibrio africanus* (Pieulle *et al.* 1996), *D. vulgaris* Hildenborough (Valente *et al.* 2001) and *D. gigas* (Di Paolo *et al.* 2006). TpIIc_3 are structurally similar to the periplasmic ones but lack the lysine patch (Nørager *et al.* 1999). (Figures 1.7 and 1.8) Perhaps because of the absence of a lysine patch, TpIIc_3 shows low reactivity with hydrogenase, but the presence of TpIc_3 increases the rate of electron transfer between those two proteins (Pieulle *et al.* 1996). Hence, it is proposed that TpIc_3 and TpIIc_3 are physiological partners, with TpIc_3 receiving electrons from hydrogenase and then delivering them to TpIIc_3 associated to the transmembrane complex. However, despite evidence of complex formation between TpIc_3 and TpIIc_3 (Pieulle *et al.* 2005), the two proteins have not been shown to interact functionally.

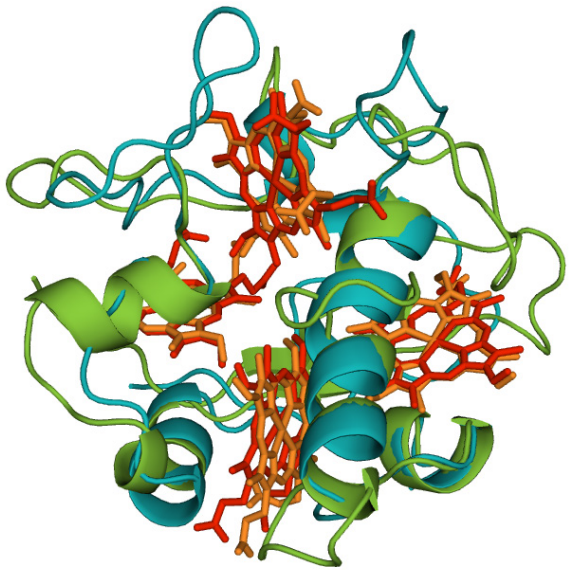

Figure 1.7 Superimposed 3-dimensional structures of TpIc_3 (green, red haems, pdb: 2BQ4 (Pieulle *et al.* 2005)) and TpIIc_3 (blue, orange haems, pdb: 3CAO (Nørager *et al.* 1999)).

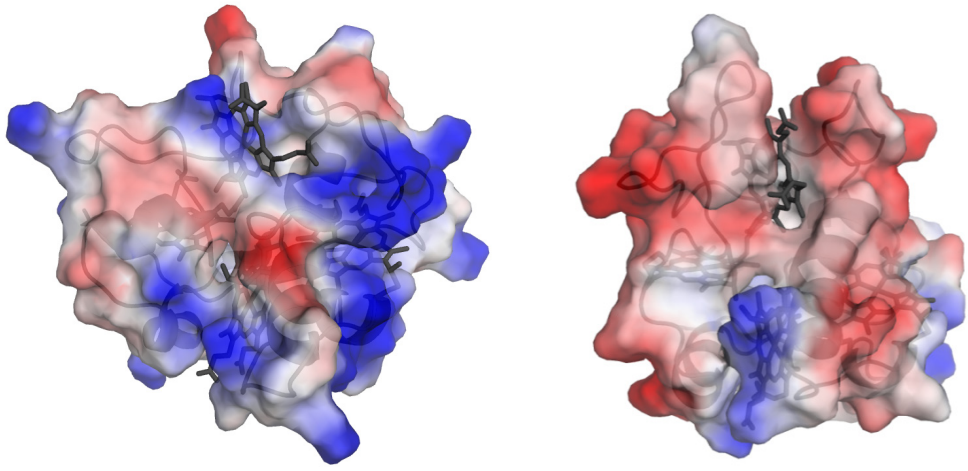

Figure 1.8 Surface charge at pH 7 of TpIc_3 (left, pdb: 2BQ4 (Pieulle *et al.* 2005)) and TpIIc_3 (right, pdb: 3CAO (Nørager *et al.* 1999)). Positive charges are in blue and negative charges are in red. The proteins are presented with the same haem orientation. The lysine patch is the blue region at the right-hand side of the TpIc_3 structure, which is absent from the TpIIc_3 structure.

Due to their tightly packed haems, with distances of 11-18 Å between the iron atoms, the redox properties of each haem are affected by neighbouring ones (homotropic cooperativity). Moreover, the protonation state of some ionisable groups also interferes with the redox properties of the haem centres (heterotropic cooperativity, also known as the redox-Bohr effect). The thermodynamic properties of several TpIc_3 have been studied in detail (Turner and Catarino 2012). In all cases, cooperative processes have been observed. At least one ionisable group is affected by the redox state of the protein with its pK_a increasing with the reduction and decreasing with the oxidation. This positive redox-Bohr effect (rB^+) is easily explained by electrostatics since it involves charges of opposite signs. Also easily explained by electrostatics is negative homotropic cooperativity, where the reduction of one haem makes the reduction of another haem less favourable, in this case because the charges have the same sign. However, most cytochromes c_3 have one haem-haem interaction in which the reduction of one haem facilitates the reduction of the other. These positive homotropic cooperativities must involve some conformational changes in the proximity of the haems, presumably a decrease in the exposure to the solvent, which stabilises the reduced state (Messias *et al.* 1998). This increased affinity for a second electron following the uptake of the first one is the basis for the proposed concerted two-electron transfer step, *i.e.* the transfer of two electrons during the same encounter, that would efficiently channel the electrons from hydrogenase to the membrane acceptor.

In some TpIc_3, the redox-Bohr group appears to be critical for a two-electron transfer. In the fully oxidised state, the pK_a of the ionisable centre is sufficiently low that it is deprotonated at physiological pH. Upon receiving electrons from the periplasmic hydrogenase, the pK_a increases, leading to the capture of one proton. This in turn increases the reduction potential of the haems resulting in further reduction. The whole process is reversed at the membrane, with the pK_a becoming lower as the oxidation progresses and the reduction potential becoming more negative when the

ionisable centre is deprotonated. This results in energy transduction by converting weakly acidic protons into more acidic protons by dissipation of the reducing power of the coupled electrons. This mechanism has been called "proton thrusting" (Louro 2007).

Although the proteins possess the necessary thermodynamic properties, the two-electron transfer step has never been observed experimentally. Therefore, we sought to determine the nature of electron transfer between *D. africanus* TpIc_3 and the soluble *D. africanus* TpIIc_3. We found that they are likely physiological partners but the two-electron transfer step could not be observed, however it should not be ruled out. The results are presented in chapter 4.

FURTHER SIGNIFICANCE OF MULTIHAEM PROTEINS

The interest surrounding organisms that are able to perform extracellular reduction of insoluble metal oxides has been growing tremendously. These organisms couple the oxidation of electron donors to the reduction of extracellular electron acceptors. The acceptors can be large organic molecules (Lovley *et al.* 1996) or soluble metal chelates (Coppi *et al.* 2007; Shelobolina *et al.* 2007), but those of greatest interest are insoluble metal oxides, such as Fe^{III} and Mn^{IV} oxides (Lovley *et al.* 2004). Coupling the oxidation of toxic organic compounds to the reduction of these metals could be an important method for bioremediation (Lovley *et al.* 1989; Lovley 1997). Moreover, if the metal is on the surface of an electrode, it could be a way of generating electricity (Lovley 2006a; Lovley 2006b). Organisms capable of extracellular metal reduction include the Gram-negative genera *Geobacter* and *Shewanella* (Shi *et al.* 2007), and the Gram-positive *Thermincola potens* (Carlson *et al.* 2012). Understanding how these organisms are able to transfer the electrons to the outside of the cell and to the electron acceptors is therefore of great importance. In all cases a large number of multihaem cytochromes have been identified and have been implicated in the

electron transport chains that transfer the electrons from the inner membrane to the extracellular medium.

Detailed characterization of each of the multihaem cytochromes involved in these processes is necessary and some of the methodologies described in this thesis may be useful for that task.

CHAPTER 2

HIGHLY SELECTIVE LIGAND BINDING BY *METHYLOPHILUS METHYLOTROPHUS* CYTOCHROME *C*"

Results published in:
Quintas, P. O., Catarino, T., Todorovic, S., and Turner, D. L. (2011) Highly selective ligand binding by *Methylophilus methylotrophus* cytochrome *c*", Biochemistry **50**, 5624-5632.

The majority of this work was performed by the author of the thesis. The analysis of the resonance Raman spectra was performed by S. Todorovic.

CONTENTS

ABSTRACT

Cytochrome *c*" (cyt *c*") from *Methylophilus methylotrophus* is unusual insofar as the haem has two axial histidine ligands in the oxidised form but one is detached when the protein is reduced. Despite having an axial site available for binding small ligands, we show here that only NO binds readily to the ferrous cyt *c*". Binding of CO, as well as CN^-, on the other hand requires considerable structural reorganisation, or reduction of the disulfide bridge close to the haem. Standard free energies for the binding of NO and CO reveal high selectivity of the ferrous cyt *c*" for NO, indicating a possible physiological role. In this work we characterize in detail the kinetics of NO binding and the structural features of the Fe^{2+}-NO adduct, by stopped-flow and resonance Raman spectroscopy, respectively.

INTRODUCTION

Gaseous diatomic molecules are found in a wide variety of both unicellular and multicellular organisms. Their functions are usually related to the metabolism or signal transduction and vary depending on the organism. O_2 is mostly recognized as the final acceptor of the electron transport chain in aerobic organisms or the product of water photodissociation in photosynthesis. It is also the main source of reactive oxygen species (ROS) which, besides their role in oxidative stress and cell death, are also regulators of intracellular signalling pathways (Thannickal and Fanburg 2000; Apel and Hirt 2004). NO is an intermediate in the nitrogen cycle, occurring during the process of denitrification (Zumft 1993). In humans it is formed from L-arginine and has been implicated in various processes in the cardiovascular, nervous and immune systems, namely vasodilation and neurotransmission (Moncada *et al.* 1991; Dröge 2002). CO originates from both natural processes and human activities. It can be used as carbon and energy source by both aerobic and anaerobic microorganisms. In humans it originates mainly from haem degradation and acts as a signalling

molecule, much like NO, in processes of vasodilation and neurotransmission. It has also been involved in anti-inflammatory and anti-proliferative processes (Gullotta *et al.* 2012). Several haem proteins have been associated with the sensing, transport and synthesis of these molecules.

Binding of gaseous diatomic molecules to haem proteins is, therefore, of utmost importance for living cells. The haem group is indeed engineered to provide optimized binding of O_2, NO and CO (*i.e.* XO), via effective back-donation of Fe(II) $d\pi_x$ electrons to low-lying π^* orbitals of these diatomic molecules (Soldatova *et al.* 2010). However, despite their almost identical size and shape, some haem proteins are able to discriminate these ligands. Selectivity is thought to be achieved by regulating the relative binding affinities to the ligands through electrostatic interactions with the nearby aminoacids and/or steric hindrance (Jain and Chan 2003). One example of this happens in haemoglobin and myoglobin (Springer *et al.* 1994; Olson and Phillips 1997). The haem is 5-coordinate, with a histidinyl residue as the proximal axial ligand. Despite the empty distal position, and the higher affinity of CO to the free haem, myoglobin is able to discriminate in favour of O_2 because of the way the haem pocket is organized. The presence of a histidine residue in the distal side of the haem is significant because it reduces the space available for ligand binding. CO usually binds perpendicularly to the haem while O_2 binds at an angle, so, by hindering the space on the distal side of the haem, it becomes harder for CO to bind. In fact, the binding of CO happens because of an opening of the haem pocket and not a tilting of the ligand. Moreover, the presence of this histidine residue helps stabilize the binding of the O_2 molecule by electrostatic interactions, and thus increasing its affinity. Other examples exist, such as the O_2 sensor FixL (Gong *et al.* 1998; Gong *et al.* 2000). While steric hindrance does not seem to play a role, the electrostatic interaction between O_2 and an arginine residue most likely contributes for the increased affinity of FixL. Moreover, this interaction brings about a conformational change that triggers the response of the sensor. Another protein where a conformational change brought by

the binding of one ligand triggers a response is the soluble guanylate cyclase (Zhao *et al.* 1999). In this case only NO activates the protein. The haem is coordinated by one histidine residue and CO binds to the distal side. However, NO seems to bind to the proximal side, displacing the histidine, and this may be the trigger for its activation. A similar process happens in CooA (Aono *et al.* 1996; Reynolds *et al.* 2000), a CO sensor, where the CO-bound form is 6-coordinated and the NO-bound form is 5-coordinated, but only the former activates the protein. The mechanisms that allow haem proteins to discriminate between diatomic ligands are therefore of considerable interest.

Here we have investigated the ligand selectivity by cytochrome *c*" (cyt *c*"), a soluble monohaem protein isolated from the obligate aerobe *Methylophilus methylotrophus* that undergoes a redox-linked spin-state transition from low-spin (LS) in the oxidised form to high-spin (HS) in the reduced form (Santos and Turner 1988) (see Figure 1.4). The axial ligands are two histidinyl residues with a near perpendicular orientation in the oxidised form and a single proximal histidinyl residue in the reduced form (red5cc) (Berry *et al.* 1990). Previous work has also shown that reduction and alkylation of a disulfide bridge located near the haem led to a 6-coordinated reduced form (red6cc), presumably with the previously detached histidine coordinated back to the haem iron (Brennan *et al.* 2001). So far, the physiological function of this cytochrome has not been determined, however, because of its ability to couple electron and proton transfer (Costa *et al.* 1992), it has been suggested that it could serve as a model for more complex systems, such as cytochrome *c* oxidase (Xavier 2002).

In this work we addressed the ability of cyt *c*" to bind diatomic ligands. Typically, CO and O_2 bind to ferrous haem, since their π^* orbitals do not match the contracted dπ orbitals in ferric proteins (Soldatova *et al.* 2010). NO is able to bind to both ferric and ferrous proteins, often forming only a transient adduct in the former case. In that respect cyt *c*" is unusual since, despite the vacant distal axial position, it

binds CO only upon major conformational rearrangement, brought on by high temperature or pH, in the presence of high concentrations of urea, or upon reduction of the disulfide bond. Under these conditions, the protein undergoes a spin state transition that results in a red6cc species (Figure 1.4) which binds CO and CN^- more readily. Moreover, ferrous cyt *c*" does not bind O_2, and the ferric protein does not bind NO. Nevertheless, NO is able to bind to ferrous cyt *c*" at physiological pH and temperature.

Binding of CO, CN^- and NO, followed by UV-visible spectroscopy, was performed in order to obtain binding affinities of those diatomic molecules for cyt *c*". Since CO and CN^- do not bind at physiological pH and temperature, these parameters, along with the concentration of urea, were varied so that the binding was achieved. The results were then extrapolated to physiological conditions for comparison. The NO binding, as the only one that occurs at physiological conditions, was analysed further. Stopped-flow experiments were used to obtain the kinetic rate constants for the reaction and to understand its mechanism. In order to assess the structural implications of the binding of NO and evaluate the proposed mechanism, resonance Raman spectra of the NO adduct were also obtained. Detailed comparison of standard free energies for the binding of NO and CO revealed high selectivity of the ferrous cyt *c*" for NO, leading us to propose that it may be functionally relevant.

MATERIALS AND METHODS

EXPRESSION AND PURIFICATION OF CYTOCHROME *C*"

The plasmid containing the cyt *c*" gene (pHS1) (Price *et al.* 2000) was transformed into *Escherichia coli* strain BL21(DE3) harbouring plasmid pEC86 encoding genes for cyt *c* maturation (Arslan *et al.* 1998). Plasmid pHS1 confers resistance to ampicillin and pEC86 to chloramphenicol. For selective growth of transformed cells, antibiotics were added to a concentration of 100 μg/mL ampicillin and 25 μg/mL

chloramphenicol. Cells were grown aerobically at 37 °C and 250 rpm in LB medium. To induce expression, IPTG was added to a concentration of 350 μM at a cell density of $OD_{600\,nm}$ = 3. IPTG blocks the action of the lac repressor, allowing the transcription of the genes under the control of the lac promoter, such as the one encoding for cyt *c*'' in pHS1. After 3-4 hours cells were harvested by centrifugation (6500 ×g, 20 min, 10 °C). Periplasmic fractions were isolated by osmotic shock, by resuspending the cells in 160 mL of 20% sucrose in 30 mM Tris-HCl buffer (pH 7.5) containing 1 mM EDTA per litre of culture, followed by centrifugation (12500 ×g, 20 min, 4 °C). The pellet was then resuspended in 60 mL of cold 5 mM $MgSO_4$, shaken for 10 min in an ice bath and centrifuged in the same conditions.

Cyt *c*'' was purified from the resulting supernatant by column chromatography in three steps: (i) anion exchange on a Q-Sepharose column (GE Healthcare) equilibrated with 5 mM Tris-HCl pH 7.6 (cyt *c*'' does not adsorb to this column and elutes with the equilibrating buffer); (ii) cation exchange by applying the red fractions from (i) to an SP-Sepharose column (GE Healthcare) equilibrated with 5 mM Tris-HCl pH 7.6 and eluted with a salt gradient of 0-1M NaCl prepared in the same buffer; (iii) fractions containing cyt *c*'' were concentrated by ultrafiltration (Amicon) and loaded onto a Superdex-75 gel-filtration column (GE Healthcare) equilibrated with 100 mM potassium phosphate buffer pH 7.5. The purification procedure was monitored by UV-visible spectroscopy and SDS-PAGE (Figure 2.1). Polyacrylamide gels were prepared with 12% acrylamide (running) and 3% acrylamide (stacking) and were stained with Coomassie blue.

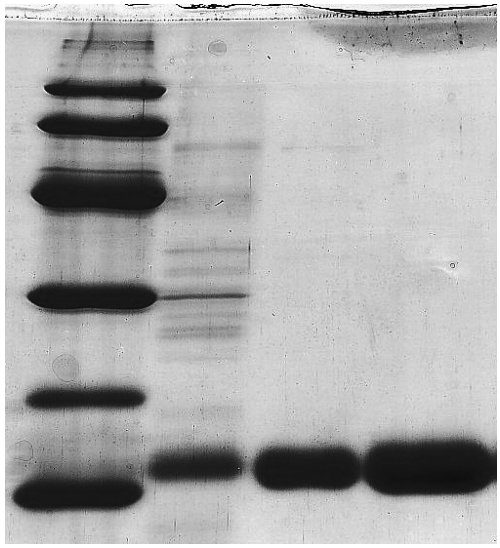

Figure 2.1 SDS-PAGE gel of the purification of cytochrome *c*". The lanes correspond to (from left to right): the molecular weight markers (lowest to highest: 14, 20, 30, 45, 66 and 97 kDa), the pool of fractions collected from the Q-Sepharose column, the SP-Sepharose column, and the Superdex-75 column (pure fractions).

BINDING OF SMALL MOLECULES.

The binding of nitric oxide (NO) was followed by optical absorption spectroscopy in a Shimadzu UV-1203 spectrophotometer placed inside an anaerobic chamber (<2 ppm of O_2). Because it may react with the NO releasing compound or NO itself, care was taken to minimise the excess of sodium dithionite used to reduce cyt *c*". The addition of NO was performed by injecting a small volume of a diethylamine NONOate solution in 10 mM NaOH with a gas-tight syringe ($[NONOate]_{final}$ = 50 μM). The protein sample was prepared in 100 mM phosphate buffer (pH 7.5). At this pH, each NONOate molecule releases 1.5 molecules of NO ($t_{½}$ = 16 min, at 25 °C, pH 7.4). The amount of NO present in solution at each time was obtained by studying the decay of the NONOate peak under the same conditions (ε_{250nm} = 6.5 mM^{-1} cm^{-1}) (Keefer *et al.* 1996).

The binding of carbon monoxide (CO) and cyanide (CN^-) was followed by optical absorption spectroscopy on a Shimadzu UV-1603 spectrophotometer, using a quartz optical cell with a path-length of 10 mm, sealed with a silicone septum. Samples were prepared by injecting a few microliters of a concentrated protein solution into a degassed solution of the desired buffer. Reduction of the haem was achieved by adding excess sodium dithionite solution with a gas-tight syringe. In order to reduce the disulfide bond, 5 mM dithiothreitol (DTT) was added to some samples. The addition of CN^- was performed by injecting a small volume of a potassium cyanide solution in the same buffer as the sample ($[CN^-]_{final}$ = 10 mM). The addition of CO was achieved by replacing argon in the headspace of the cuvette containing the protein sample with CO from a gas cylinder: this results in approximately 1 mM of CO dissolved at 20 °C (Stephen *et al.* 1963).

In each case, the amount of bound and unbound protein was determined by treating each spectrum as a weighted sum of the spectra of the two pure forms (Figure 2.2).

Effect of temperature

The temperature was controlled by a circulating water bath connected to the spectrophotometer. Samples were prepared in degassed 100 mM phosphate buffer (pH 7.5). After the addition of the ligand, the temperature was increased until full binding was achieved (approximately 60 °C for CO and 70 °C for CN^-) and the temperature was quickly lowered by substituting the hot water with water at room temperature. The effect of the temperature on the protein without any ligand was also studied using samples prepared in 100 mM phosphate buffer (pH 7.0) and 100 mM glycine/NaOH buffer at various pH values from 8.7 to 11.8.

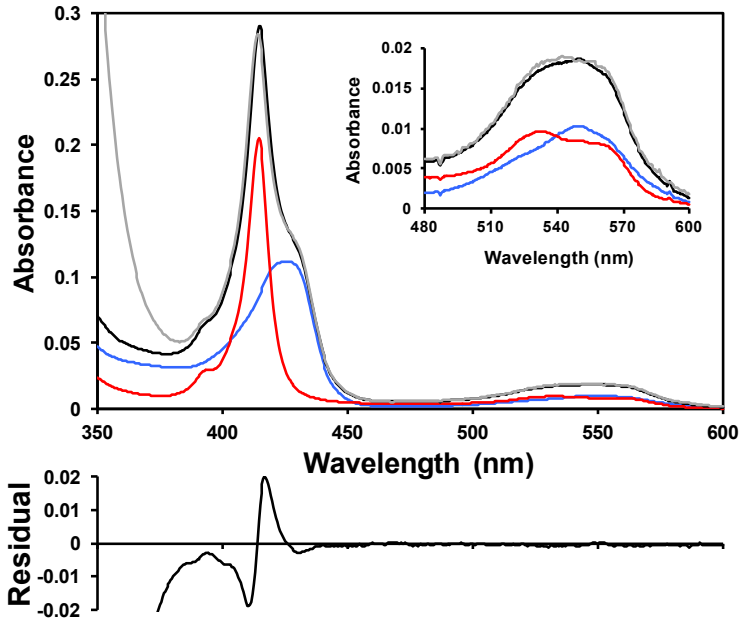

Figure 2.2 Deconvolution of the UV-visible spectrum during CO binding experiments. The experimental spectrum (grey) can be deconvoluted into a fraction of the pure CO-bound (blue) and reduced unbound forms (red), in this case 44% and 56%, respectively. Adjustment was performed by the least squares method. The residual is the difference between the spectrum resulting from the deconvolution (black) and the experimental spectrum (grey). The same strategy can be used to study any conversion between different forms.

Effect of urea

Samples were prepared in degassed 100 mM phosphate buffer (pH 7) with various urea concentrations up to 6 M. Reversibility of the transition was studied by removing urea with a HiTrap desalting column (GE Healthcare). The effect of urea on the protein without any ligand was also studied using samples prepared in 100 mM phosphate buffer (pH 7.0) and 100 mM glycine/NaOH buffer at various pH values from 8.7 to 11.8.

Effect of DTT

In addition to binding experiments in the presence of DTT, protein samples treated with 5 mM DTT were titrated with reduced methyl viologen to determine the state of the disulfide bond. Untreated protein was titrated as a control, with 6 M urea as a denaturant in each case. A stock solution of methyl viologen was reduced by zinc under an anaerobic atmosphere and its concentration was obtained from its UV-visible spectrum, using the value of absorbance at 605 nm and the extinction coefficient of 13.7 mM^{-1} cm^{-1} (Watanabe and Honda 1982). 20 μL aliquots were added to the protein sample, followed by recording the UV-visible spectrum. The spectra recorded after each addition of methyl viologen were deconvoluted to obtain the contributions of the oxidised protein, the red5cc form, and the red6cc form, which are illustrated in Figure 1.4. Deconvolution was performed as shown in Figure 2.2, using three spectra instead of two.

Kinetic experiments

Stopped-flow kinetic experiments were performed at a constant temperature of 25 °C using a SF-61 DX2 stopped-flow apparatus (Hi-Tech Scientific) placed inside an anaerobic chamber (<2 ppm of O_2). Solutions of reduced protein and NO were mixed and the variation in absorbance in the UV-visible was followed. The protein solution was prepared in the desired 100 mM phosphate buffer (pH range: 6.5-7.8) by adding a small amount of a concentrated stock; NO solutions were prepared by adding concentrated NONOate in 10 mM NaOH, to the same buffer as the protein in 1.8 mL flasks with no head-space. The solutions were then left for at least one hour so that the NO was fully released, resulting in known final NO concentrations in the range 150 μM to 1.5 mM. The reaction was followed by either irradiating the sample with monochromatic light and measuring the absorbance at a single wavelength or irradiating the sample with light from a xenon lamp and detecting the transmitted light with a photodiode array (512 diodes, 280-700 nm

range). All reactions were performed under pseudo-first order conditions ([NO] >> [protein]) and traces were fitted with exponentials, or biexponentials when two processes were observed. Second order rate constants were obtained by measuring pseudo-first order rate constants as a function of [NO].

RESONANCE RAMAN SPECTROSCOPY

All RR measurements were performed with a confocal microscope coupled to a Raman spectrometer (Jobin Yvon U1000) equipped with 1200 l/mm grating and liquid-nitrogen-cooled back-illuminated CCD detector. Samples were placed in a quartz rotating cell and excited with the 413 nm line from a krypton ion laser (Coherent Innova 302). Oxidised (as purified) and sodium dithionite reduced cyt *c*" samples (100-200 μM) were measured at room temperature in the presence or absence of NO with a laser power of 8 mW and accumulation times of 60 s. The samples of reduced cyt *c*" in the presence of NO were prepared in an anaerobic chamber (<2 ppm of O_2) by the addition of excess NONOate to the cell filled with the protein solution in 10 mM Tris-HCl buffer, pH 7.6. UV-visible spectra were recorded after the Raman experiments to confirm the state of the sample.

After polynomial background subtraction, the positions and line-widths of Raman bands were determined by component analysis in which the spectra of the individual species were fitted to the measured spectra using home-made software.

RESULTS AND DISCUSSION

BINDING OF NO TO CYT *c*"

Binding of NO to ferrous cyt *c*" was followed via the characteristic blue shift of the Soret band (Figure 2.3 and Table 2.1), observed upon addition of small aliquots of NO releasing diethylamine NONOate to dithionite reduced protein. The UV-visible spectra were measured and in each case, the amount of NO-bound and free protein was determined by treating each spectrum as a weighted sum of the spectra of the two pure forms with electronic transitions at 398 and 426 nm.

At 20 °C and pH 7.5, NO binds to the reduced cyt *c*", forming a 1:1 complex with a dissociation constant of 0.37 μM, which corresponds to a ΔG° for the binding of -36.1 kJ/mol (Figure 2.4). The UV-visible spectra in the presence of excess NO show no evidence of further reaction such as nitrosylation of the cysteines. Binding is fully reversible since removal of NO results in the UV-visible spectra of the ligand-free native HS state of ferrous cyt *c*".

Table 2.1 UV-visible spectroscopic properties of cyt *c*" and its adducts.

	λ (nm) (ε (mM^{-1} cm^{-1}))							
	Soret		β		α		other	
Fe^{3+} 6cc	407	(97.5)	526	(6.9)				
Fe^{2+} 5cc	426	(86.2)	550	(7.9)				
Fe^{2+} 6cc	416	(147.6)	521	(11.1)	550	(20.4)		
Fe^{2+}-NO 6cc	410	(67.5)	538	(7.9)				
Fe^{2+}-NO 5cc	398	(62.7)	535	(8.0)			482	(7.6)
Fe^{2+}-CO	415	(193.5)	532	(9.1)	563	(7.4)		
Fe^{2+}-CN^-	420	(123.7)	525	(12.7)	554	(14.5)		
Fe^{3+}-CN^-	412	(84.9)	534	(9.0)				

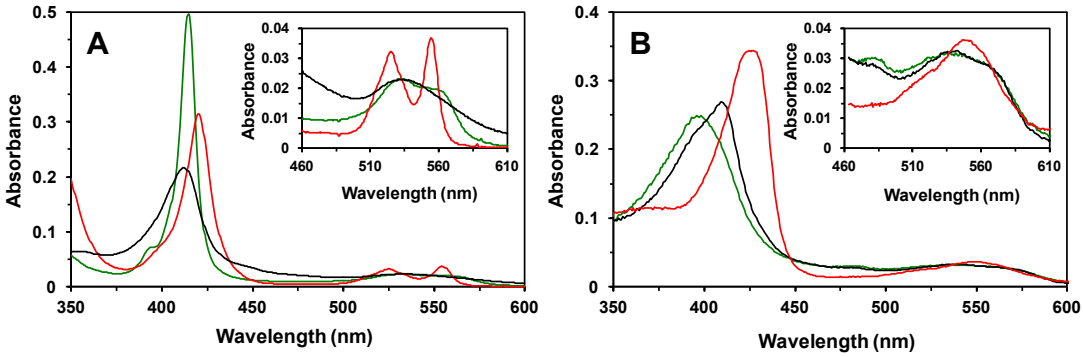

Figure 2.3 (A) UV-visible spectra of oxidised cyt *c*" bound to cyanide (black) and reduced cyt *c*" bound to cyanide (red) and carbon monoxide (green). **(B)** UV-visible spectra of reduced cyt *c*" in its native 5cc form (red) and reduced cyt *c*" bound to nitric oxide in the 6cc form (black) and 5cc form (green). The shoulder at ~400 nm in the spectrum of the 6cc form arises from imperfect deconvolution.

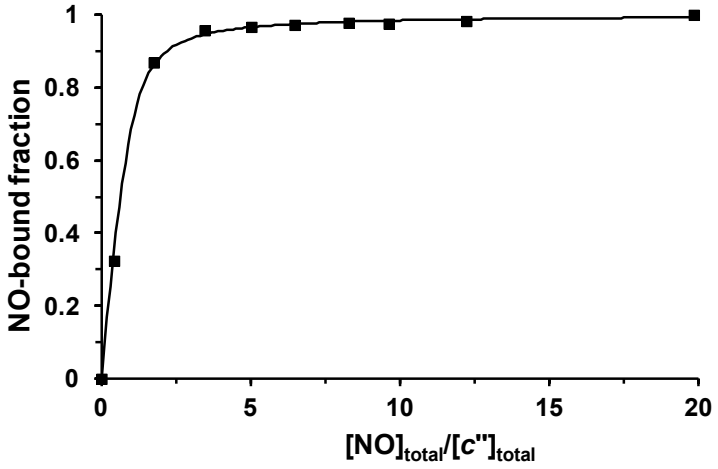

Figure 2.4 Binding curve of NO to reduced cyt *c*" (100 mM phosphate buffer pH 7.5, T = 20 °C, [*c*"] = 2.5 μM). The NO-bound fraction accounts for the concentration ratio of NO-bound cyt *c*" to total cyt *c*". The curve results from the fit to the experimental points of a rearrangement of the equation K_d = [NO]$_{free}$[unbound-cyt*c*"]/[bound-cyt*c*"]. The $\Delta G°$ value is obtained from $\Delta G° = RT\ln(1/K_d)$.

In the next step, stopped-flow experiments were carried out to study the kinetics of the reaction of reduced cyt *c*" with NO. An excess of ligand was used to ensure that the reaction occurred under pseudo-first-order conditions.

The reaction was followed by measuring the change in absorbance with time at 393, 407 and 426 nm, chosen by inspection of spectra obtained with the diode array, and corresponding to different mixtures of the NO-bound 5-coordinated (5cc), NO-bound 6-coordinated (6cc) and red5cc forms. The time-course traces show an increase in the absorbance at 393 nm and a decrease at 426 nm, while at 407 nm an increase is observed followed by a decrease (Figure 2.5). This suggests a mechanism in which NO binds to the reduced cyt *c*", forming a 6cc NO-Fe-His intermediate, that is then converted to a 5cc NO-Fe form, with the detachment of the axial histidine. Each trace was fitted with a sum of two exponentials, as appropriate for consecutive reactions, to obtain first-order rate constants k_1 and k_2 for the NO binding and histidine detachment, respectively. The rates show no dependence on the pH in the 6.5-7.8 range. Note that it is not necessary for the traces to represent pure forms in order to extract the rate constants; in fact the wavelengths used here have contributions from more than one form. No change in the rates was observed when traces obtained at different wavelengths were used for the fitting.

The second-order rate constant for the binding of NO was determined from the slope of the straight line obtained by plotting the values of k_1 at different NO concentrations (Figure 2.6). The value obtained for k_{on} (5.7×10^3 M^{-1} s^{-1}) is lower than that determined for cytochrome *c*' (cyt *c*') and much lower than the ones for myoglobin and soluble guanylate cyclase (sGC) (Table 2.2) (Moore and Gibson 1976; Makino *et al.* 1999; Andrew *et al.* 2002). The second process is clearly NO independent, with a rate constant k_2 of 0.06 ± 0.01 s^{-1}, suggesting that NO does not bind to the proximal side of the haem, contrary to what was observed in the case of cyt *c*' (Andrew *et al.* 2002).

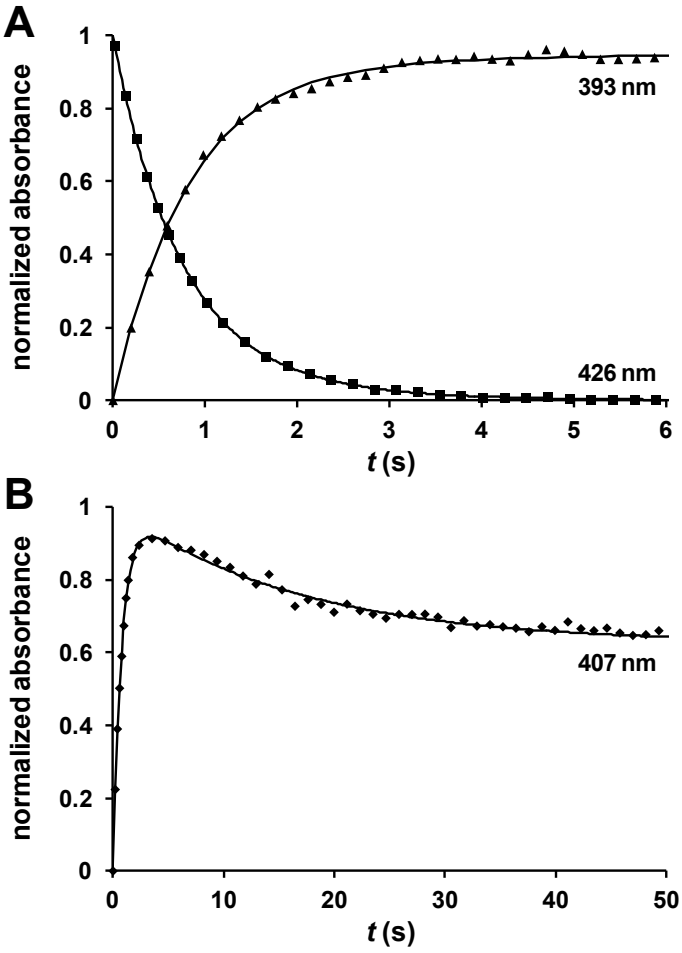

Figure 2.5 Time-course traces at 393 and 426 nm **(A)** and 407 nm **(B)** for the reaction of 3 μM cyt *c*" with 300 μM NO (100 mM phosphate buffer pH 7.0, T = 25 °C). Solid lines represent the data fitted to the sum of two exponentials.

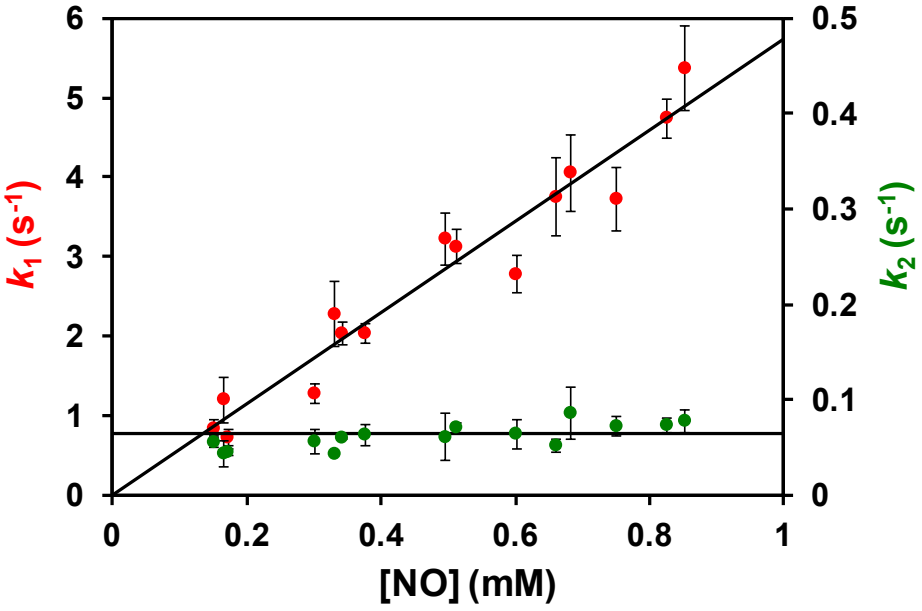

Figure 2.6 Dependence of k_1 (red) and k_2 (green) on the concentration of NO. Values of k_1 and k_2 were obtained by fitting time-course traces to a sum of two exponentials. Each point represents an average of separate fittings at different wavelengths, with the error bars representing twice the standard deviation.

Table 2.2 Rate constants for the binding of NO to ferrous haemproteins.

Protein	Temperature (°C)	k_{on} (M^{-1} s^{-1})	Reference
cyt *c*''	25	$(5.7 \pm 0.2) \times 10^3$	This work
cyt *c*'	25	4.4×10^4	(Andrew *et al.* 2002)
Mb	20	1.7×10^7	(Moore and Gibson 1976)
sGC	15	$> 1 \times 10^7$	(Makino *et al.* 1999)

In order to understand the structural implications of NO binding, resonance Raman (RR) spectra of cyt *c*" in the ferric, ferrous and ferrous-NO forms were measured. Vibrational modes ν_4, ν_3, ν_2 and ν_{10}, that appear in the high-frequency region (1300-1700 cm^{-1}) of the RR spectra, are sensitive marker bands of the spin, oxidation and coordination state of the haem iron, allowing the identification and detailed characterization of the different states of cyt *c*".

In the ferric state the haem is mainly LS 6cc, as indicated by ν_4, ν_3, ν_2 and ν_{10} marker bands at 1378, 1507, 1590 and 1640 cm^{-1} (Figure 2.7A) (Rivas *et al.* 2001). A minor contribution from a HS species, with ν_4 and ν_3 bands at 1371 and 1472 cm^{-1}, was also detected. It was present in all preparations and probably originates from cytochrome where one of the axial histidines detached from the haem (Rivas *et al.* 2001). In the ferrous state, only the red5cc form is present, with ν_4, ν_3, ν_2 and ν_{10} marker bands at 1355, 1471, 1575 and 1605 cm^{-1} (Figure 2.7B). The RR spectrum of the reduced protein shows strong similarities with that of cyt *c*' (Andrew *et al.* 2001), with down shifted ν_4 and unusually intense modes at 1400 and 1430 cm^{-1}. Upon re-oxidation of the ferrous cyt *c*", the two-population state of the oxidised form is fully re-established. In addition to out-of plane porphyrin modes and deformation modes, an intense band at 228 cm^{-1} was detected in the low frequency region (Figure 2.8 and Table 2.3). We assign this mode to the Fe^{2+}-N(His) stretching coordinate that typically appear in the 190-250 cm^{-1} range. A relatively high frequency of this mode indicates H bonding interactions of the proximal His that bring about a partial imidazolate character (Othman *et al.* 1996).

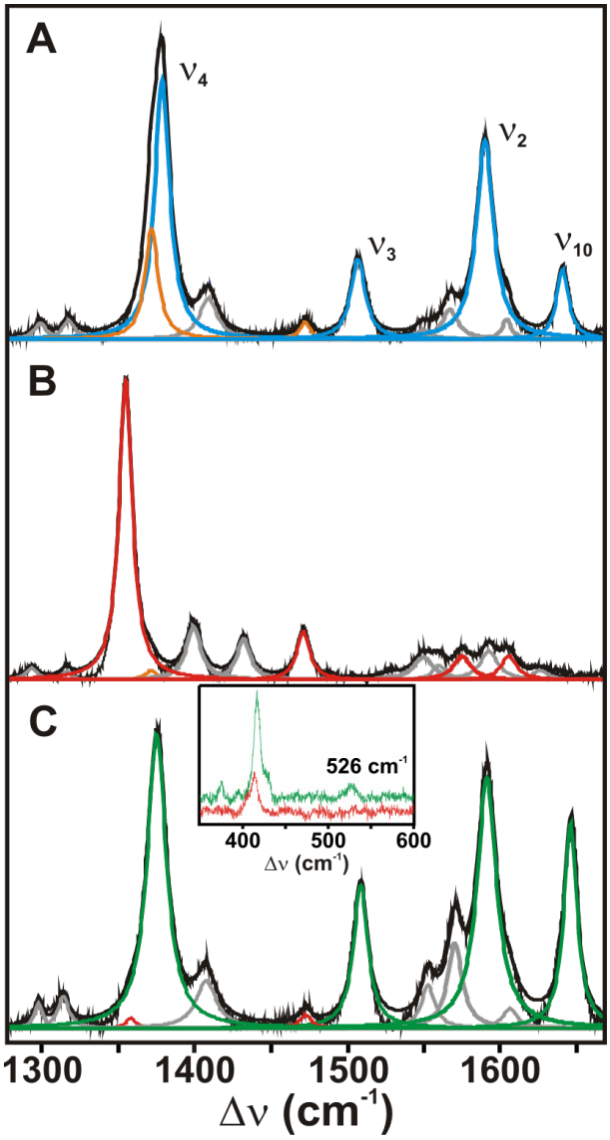

Figure 2.7 Experimental and component resonance Raman spectra of cyt *c*" in the oxidised **(A)**, reduced **(B)** and reduced NO-bound **(C)** forms, obtained with 413 nm excitation and 8 mW laser power. Marker bands are designated: oxidised 5cc (orange), oxidised 6cc (blue), reduced 5cc (red) and reduced NO-bound 5cc (green). Inset: low frequency region of the NO-bound ferrous cyt *c*" (upper trace) and ferrous cyt *c*" (lower trace). Haem state non-specific bands are represented in grey. Putative assignment of the bands is provided in Table 2.3.

Table 2.3 Vibrational modes (stretching, ν_i, and bending, δ, cm^{-1}) of cyt *c*" in the ferric (Fe^{3+}), native ferrous five-coordinated (5cc Fe^{2+}), urea treated ferrous six-coordinated (6cc Fe^{2+}), and ferrous NO bound state (Fe^{2+}-NO) in the high frequency region, and of the Fe-axial modes in the low frequency region.

mode	Fe^{3+}	5cc Fe^{2+}	6cc Fe^{2+}	Fe^{2+}-NO
ν (Fe-N(His))		228		
N (Fe-NO)				526
δ (CH)	1299 1317	1293 1316	1296 1315	1297 1313
ν_4	1371 (mn) 1378	1355 1371 (tr)	1360	1357 (tr) 1375
ν_{29}	1408	1400		1407
ν_{20}		1430		
ν_3	1472 (mn) 1507	1471	1493	1472 (tr) 1508
ν_{11}	1549	1549	1539	1552
ν_{19}	1567	1560	1560	1570
ν_2	1590	1575	1591	1592
ν_{37}	1604	1592	1607	1506
ν_{10}	1640	1605	1622	1647
n.a.		1528 (tr) 1626 (tr)		

(tr) refers to population present in trace amount, (mn) to a minor component, n.a. non-assigned.

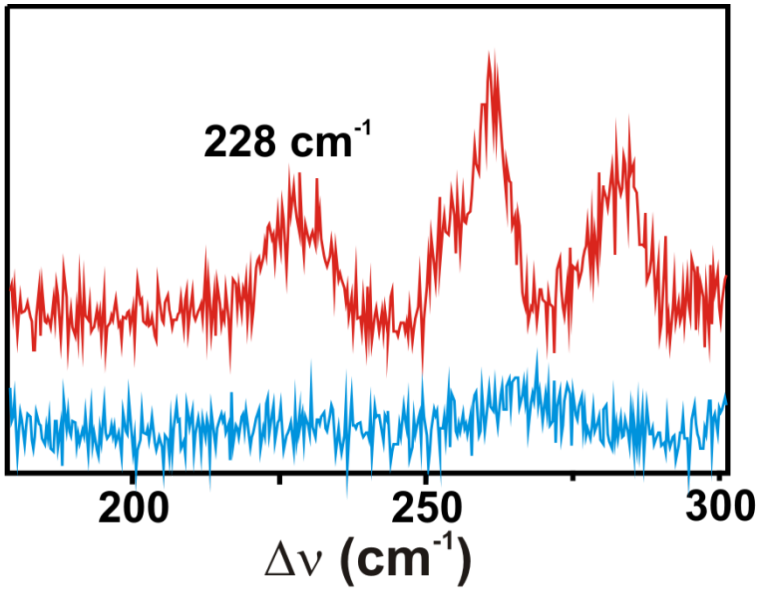

Figure 2.8 Low-frequency region of RR spectra of the Fe^{2+} (upper trace) and the Fe^{3+} cyt *c*". The spectra were recorded with 413nm excitation laser focused onto 2 μL of frozen 2 mM protein (dithionite-reduced or in the resting state), in phosphate buffer, pH 7.5, with laser power of 1.3 mW and accumulation time of 20s, using N_2(l)-cooled cryostat (Liknam) mounted onto the microscope stage and set at -190 °C.

The RR spectrum of the ferrous NO-bound complex shows a population with ν_4, ν_3, ν_2 and ν_{10} modes at 1375, 1508, 1592 and 1647 cm^{-1} (Figure 2.7C). The values of the ν_4 frequencies are unusually high for a reduced haem due to the decrease in electron density of the π^* antibonding orbitals of the porphyrin macrocycle by back-bonding to the NO through the iron d_π orbitals (Soldatova *et al.* 2010). Similar frequencies were reported for NO adducts of ferrous sGC, CooA and cyt *c*' (Deinum *et al.* 1996; Reynolds *et al.* 2000; Andrew *et al.* 2001), and attributed to a high-spin 5cc state, with NO bound to the haem and no proximal histidine ligand (Table 2.4).

Table 2.4 Resonance Raman Frequencies (cm^{-1}) for 5-coordinated nitrosyl adducts.

Protein	ν_4	ν_3	ν_2	ν_{10}	Reference
cyt *c*"	1375	1508	1592	1647	This work
cyt *c*'	1373	1506	1592	1641	(Andrew *et al.* 2001)
sGC	1375	1509	1584	1646	(Deinum *et al.* 1996)
CooA	1376	1506	1582	1641	(Reynolds *et al.* 2000)

Further evidence for the formation of a 5cc nitrosyl complex, comes from the low-frequency region of the RR spectrum (300-600 cm^{-1}), where an additional broad band appears at 526 cm^{-1} in the presence of NO (Figure 2.7 inset, upper trace). This band is clearly absent from the spectra of the ferrous protein (Figure 2.7 inset, bottom trace). The frequency of the band falls into the 520-526 cm^{-1} range observed in other 5cc NO adducts of *c*-type cytochromes and coincides with the Fe-NO stretching measured in the 5cc cyt *c*'-NO adduct (Andrew *et al.* 2001). The 6cc nitrosyl adducts of haem proteins, on the other hand, tend to have a stronger Fe^{2+}-NO bond, with the stretching frequency in the range 536-576 cm^{-1} (Lukat-Rodgers and Rodgers 1997).

In the UV-visible experiments, the final product is only reached after >100 s. Kinetic experiments with detection by a photodiode array show a fivefold increase in the rate constant k_2, compared to the single wavelength data obtained with the photomultiplier (Figure 2.9). This cannot be an effect of temperature because the Arrhenius activation energies have been determined as 57.3±8.1 $kJmol^{-1}$ for k_1 and 171±16 $kJmol^{-1}$ for k_2 (Figure 2.10) but k_1 is not affected when the diode array is used. We attribute this effect to the fact that in kinetic experiments with the photodiode array, the sample is exposed to intense light, which may facilitate the detachment of the axial histidine. This was tested in the stopped flow apparatus by switching on the light source after the reaction had proceeded for various times in the absence of light. In each case, the reaction proceeded normally and accelerated immediately when the light source was switched on.

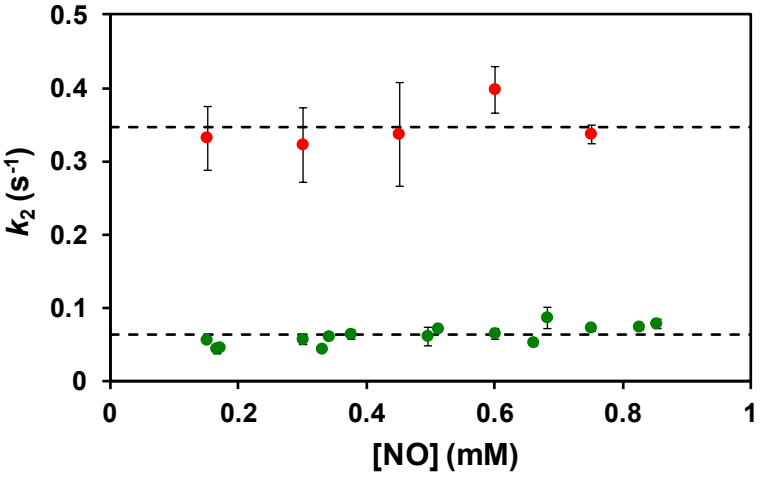

Figure 2.9 Dependence of the values of k_2 obtained in experiments with the photodiode array (red) and in single wavelength mode (green) on the concentration of NO. Each point represents an average of separate fittings at different wavelengths, with the error bars representing the standard deviation. The dashed lines represent the average of the measurements.

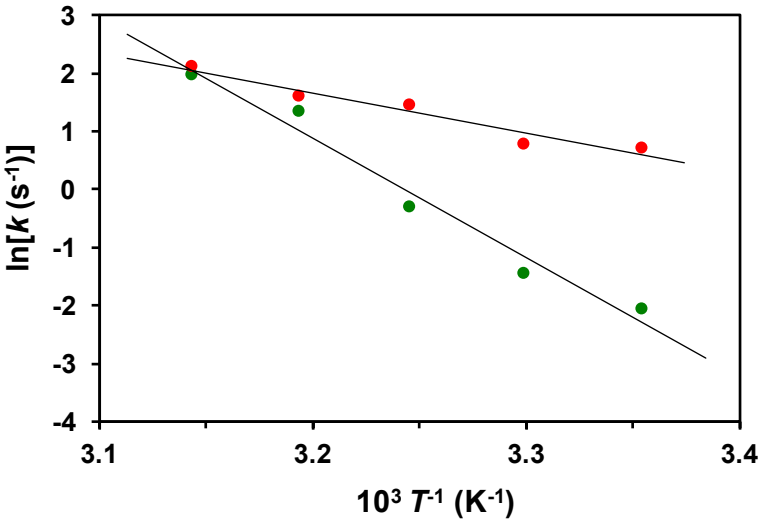

Figure 2.10 Arrhenius plot (k = A exp(-E_A/RT)) of k_1 (red) and k_2 (green) obtained from the reaction of 3 μM cit *c*" with 500 μM NO at different temperatures (100 mM phosphate buffer pH 7.6).

BINDING OF CO AND CN^- TO CYT *C*"

In the next step we investigated the binding of other small ligands to cyt *c*" by UV-visible spectroscopy. Under reducing conditions at 25 °C and pH 7.0, only about 10% of the protein binds CO, while under the same conditions the binding of CN^- is negligible. Binding CO and CN^- to the red5cc form is only achieved in the presence of urea or at increased temperatures. UV-visible spectra of the complexes of cyt *c*" with CO and CN^- are shown in Figure 2.3 and the respective peak positions are listed in Table 2.1.

Raising the temperature results in an increase in the amount of the CO-bound form, with full binding achieved at about 60 °C. Lowering the temperature brings the protein back to its original, partially bound, state. Spectra were deconvoluted to obtain the bound (B) and unbound (U) fractions and hence the equilibrium constant K=[B]/([U][CO]) at each temperature (*T*). Plotting ln(*K*) vs. 1/*T* (Figure 2.11A) and extrapolating to 293 K provided the value of ΔG° for the binding of CO at this temperature (Table 2.5).

Table 2.5 Standard free energies of binding and of the reduced 5-coordinated to 6-coordinated transition obtained when either the urea concentration or the temperature was varied (values at 20 °C, pH 7 for urea and pH 7.5 for temperature).

	ΔG° (kJ/mol)			
	Fe^{2+}-CO binding	Fe^{2+}-CN^- binding	Fe^{3+}-CN^- binding	red5cc-red6cc transition
Temperature	-3.5 ± 0.9	21 ± 2	16.9 ± 0.9	48 ± 4
Urea	-6 ± 1	17 ± 2	6.6 ± 0.2	38 ± 2

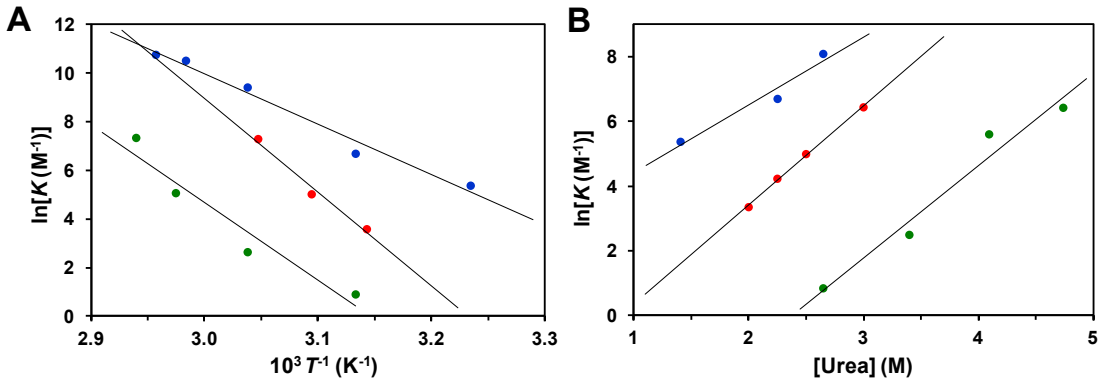

Figure 2.11 (A) Temperature dependence of the equilibrium constant of CO binding to reduced cyt *c*" (blue) and CN^- binding to reduced (green) and oxidised (red) cyt *c*" (100 mM phosphate buffer pH 7.5, [CO] = 0.5–1 mM, [CN^-] = 10 mM, [*c*"] = 2.5 μM). **(B)** Variation of the equilibrium constant of CO binding to reduced cyt *c*" (blue) and CN^- binding to reduced (green) and oxidised (red) cyt *c*", with the concentration of urea (100 mM phosphate buffer pH 7, T = 20 °C, [CO] = 1 mM, [CN^-] = 10 mM, [*c*"] = 2.5 μM).

Full binding of cyanide to ferrous cyt *c*" can also be achieved by increasing the temperature to about 70 °C. Cyanide commonly binds to the iron in oxidised type-*c* cytochromes, but CN^- only binds fully to oxidised cyt *c*" at about 60 °C. In fact, the value found for ΔG° is similar to that for cyanide binding to the reduced form (Table 2.5). Lowering the temperature brings the protein back to the ligand-free form, in both cases. The binding of CO and CN^- to ferrous cyt *c*" is fully reversible for most of the sample. The small fraction of bound protein present at the start of each experiment is slightly increased when the temperature is lowered at the end (ca. 5% increase in the experiments with CO and 10% in the experiments with CN^-). This may be due to some irreversible denaturation of the protein at high temperature which increases the affinity of the protein for the ligands. The effect is less pronounced in the binding of CO, probably because the temperatures reached in these experiments were lower.

Similarly, high concentrations of urea (up to 6M) facilitate the binding of CO to the reduced and of CN^- to the reduced and oxidised forms of cyt *c*". Approximate binding energies can be obtained by plotting ln(*K*) against the concentration of urea (Makhatadze 1999) (Figure 2.11B) and extrapolating to zero concentration (see Table 2.5). As in the case of elevated temperatures, the transition to the bound form is less favourable in the case of CN^- than CO. Removal of urea returns the protein to the reduced form with release of the ligand.

The binding of CN^- to the oxidised form is also favoured by increasing the concentration of urea, but agreement with the $\Delta G°$ value obtained from the temperature dependence is less good than for the reduced form (Table 2.5).

Effect of temperature in the reduced form

Raising the temperature causes the UV-visible spectrum typical of the red5cc form to change to that of red6cc cyt *c*" (see Figure 1.4) with a transition temperature that is pH dependent, as shown in Figure 2.12A. At the highest pH value studied (11.8), the protein is already in the red6cc form at 23 °C, while at pH 7.0 only 35% of the protein is in this state at the highest temperature (80 °C). Assuming a two state transition, we determined an equilibrium constant at 20 °C by extrapolation for each pH value (Figure 2.12B). A plot of ln(*K*) vs. ln($[H^+]$) (Figure 2.12C) extrapolated to pH 7 then gave the value of $\Delta G°$ included in Table 2.5. Moreover, the slope of the plot gives the number of protons transferred in the process (1.5 ± 0.6) (Wyman 1964). We can rationalize the loss of one proton in the transition by formation of an imidazolate ion at high pH which may bind the iron more tightly than uncharged histidine. The change in conformation is almost fully reversible in this pH range, with only ca. 10% of the protein remaining in the red6cc form when the temperature is restored to ambient.

The UV-visible spectrum of the oxidised form does not change in the range of temperatures tested, although it should be noted that the ferric haem is already 6-coordinate.

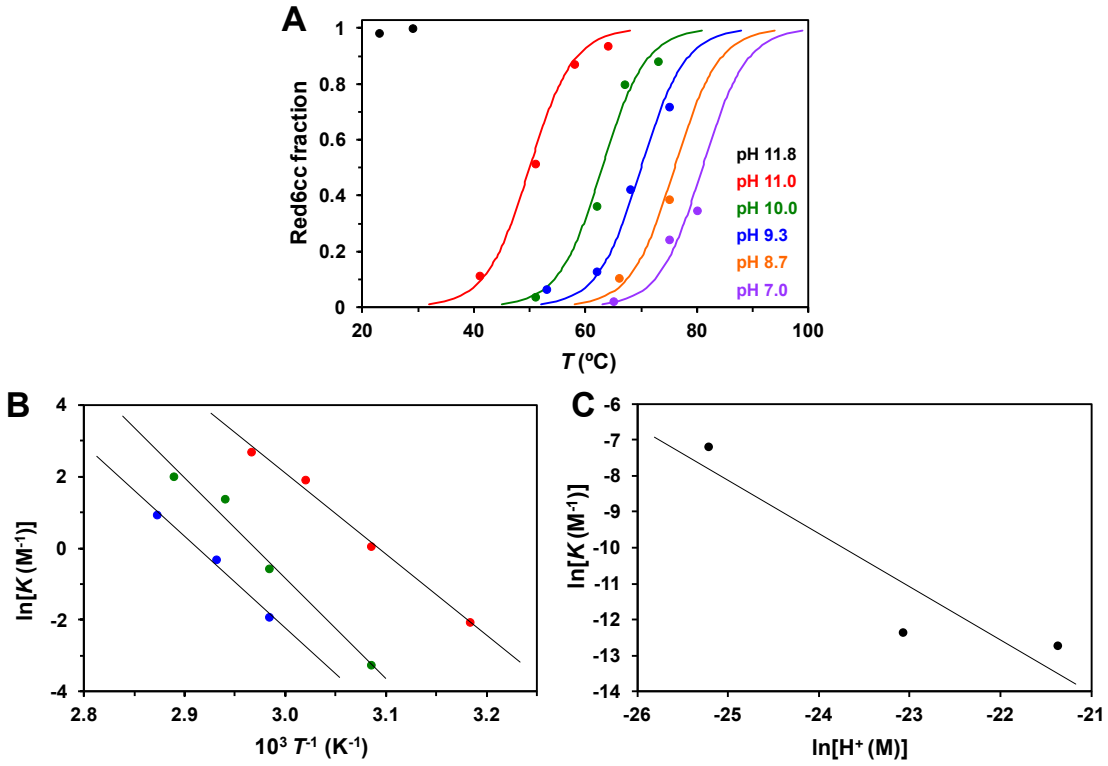

Figure 2.12 (A) Temperature dependence of the fraction of cyt *c*" in the reduced 6-coordinated form at different pH values in 100 mM glycine buffer, except pH 7.0 in 100 mM phosphate buffer. The curves drawn for pH 7 and 8.7 are illustrative because of limitations of temperature. **(B)** Variation of the equilibrium constant of the reduced 5-coordinated to 6-coordinated transition with temperature (100 mM glycine/NaOH buffer pH 9.3 (blue), 10.0 (green) and 11.0 (red)). **(C)** pH dependence of the equilibrium constants obtained from B by extrapolating to 20 °C.

EFFECT OF UREA IN THE REDUCED FORM

The UV-visible spectrum of the reduced HS cyt *c*" also shows a conversion to the red6cc LS form with the addition of urea. The reversibility of the transition was proved by removal of urea by gel filtration, which brings the protein back to the native red5cc form. As demonstrated in the case of elevated temperature, high pH also facilitates the spin-state transition in the presence of urea. The $\Delta G°$ of the transition was calculated using the same procedures as before (see Figure 2.13 and Table 2.5). The slope of the ln(*K*) vs. ln([H^+]) curve is also compatible with the loss of one proton (0.7 ± 0.2). As before, the UV-visible spectrum of the oxidised form does not change with urea in the absence of ligands. RR spectra further confirmed the formation of the red6cc species in urea treated cyt *c*", with ν_4 and ν_3 bands at 1360 and 1493 cm^{-1} (Figure 2.14). Furthermore, as judged from the RR spectra in the presence/absence of urea, no structural alterations at the level of the haem cavity seem to occur in the ferric cyt *c*".

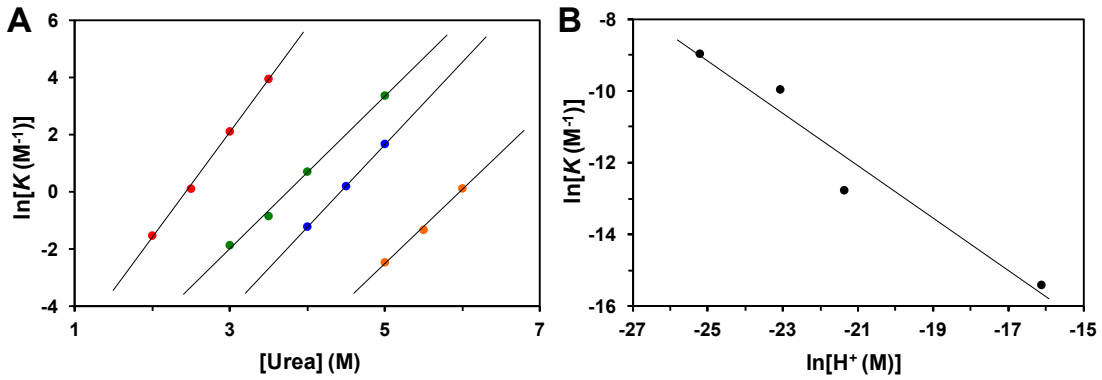

Figure 2.13 (A) Variation of the equilibrium constant of the reduced 5-coordinated to 6-coordinated transition with the concentration of urea, determined in 100 mM glycine/NaOH buffer pH 11.0 (red), 10.0 (green) and 9.3 (blue) and 100 mM phosphate buffer pH 7.0 (orange). **(B)** pH dependence of the equilibrium constants obtained from A by extrapolating to zero concentration of urea.

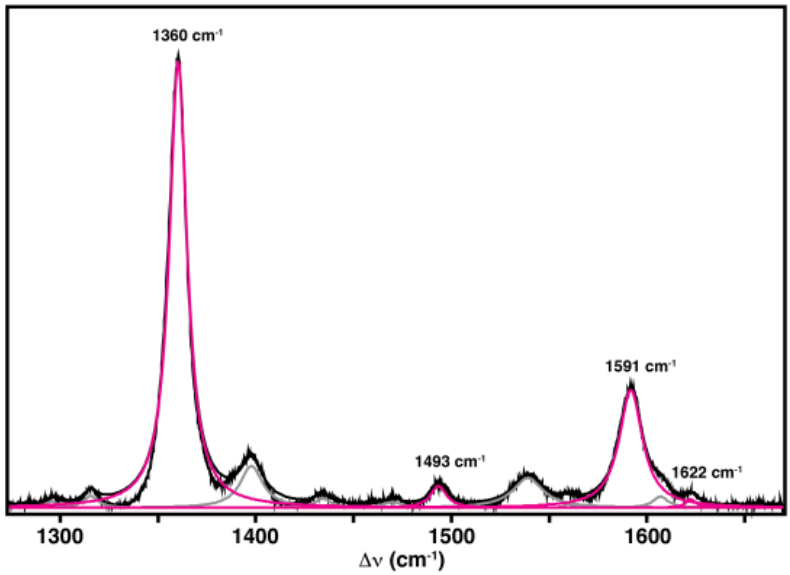

Figure 2.14 Experimental and component resonance Raman spectrum of cyt *c*" in the reduced six-coordinated form, obtained with 413 nm excitation and 8 mW laser power. Marker bands for the red6cc form are represented in pink. Haem state non-specific bands are represented in grey. Putative assignment of the bands is provided in Table 2.3.

In view of the report that chemical modification of the disulfide bond near the haem produced a 6-coordinate reduced cyt *c*" (Brennan *et al.* 2001), we sought to establish whether simple reduction of the disulfide would have the same effect. Treating the protein with DTT converted approximately half of the sample to the red6cc, which binds both CO and CN^- readily. Because strong absorption by the haem in the UV-visible spectrum makes it impractical to use the Ellman assay, it was confirmed that the disulfide was reduced by titrating protein samples in 6 M urea with reduced methyl viologen. As a control, oxidised cyt *c*" was titrated with methyl viologen, which yielded red6cc, red5cc and the ferric protein in the proportions 6:4:1, determined by deconvolution of UV-visible spectra (Figure 2.15A). Analysis of the titration curves showed that one equivalent of methyl viologen is required to generate the red5cc protein, and a further two equivalents are required to produce the

red6cc form, as expected for reduction of the haem followed by reduction of the disulfide. Comparison with the data obtained in the titration of the sample treated with DTT showed that the red6cc produced in this way does not react further with methyl viologen (Figure 2.15B). Thus, we conclude that the disulfide bridge is reduced in this form. The 5-10% of red6cc haem found in the reduced protein when restoring ambient temperature may therefore result from partial reduction of the disulfide by sodium dithionite.

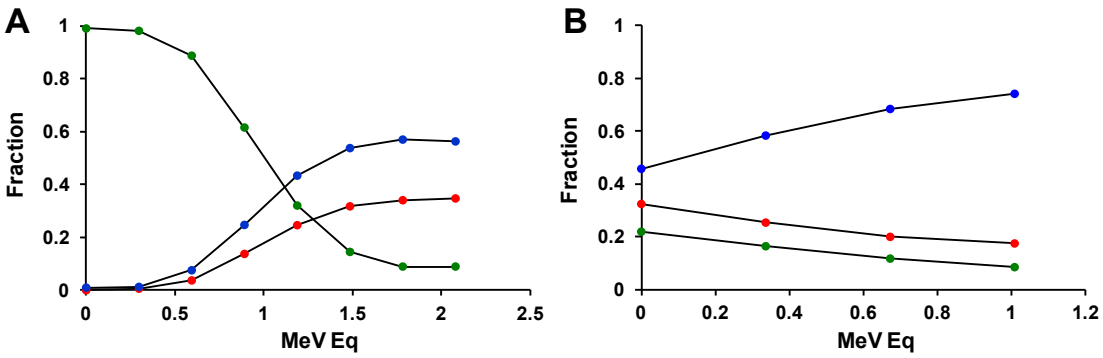

Figure 2.15 Titration of 3 μM cyt *c*" with methyl viologen (MeV) in the presence **(B)** or absence **(A)** of 5mM DTT (100 mM phosphate buffer (pH 7.0) + 6 M urea. T = 25 °C). The curves show the variation of the oxidised (green), red5cc (red) and red6cc (blue) fractions with the addition of MeV. The number of MeV equivalents used to reach the end states of A and B agrees with the predicted number of equivalents, assuming that the red6cc is produced by the reduction of the haem followed by the reduction of the disulfide bond.

CONCLUSIONS

Elucidating the binding properties of cyt *c*" proved difficult because of the unusual characteristics of this cytochrome. We show here that the stable 5-coordinate form of reduced cyt *c*" reveals a high selectivity for NO, which is able to bind fully under physiological conditions (Figure 2.16). Other small ligands like CO and CN^- are only able to bind to cyt *c*" upon structural rearrangement. This conformational transition can take place under moderately denaturing conditions (high temperature, high pH or high urea concentrations) or upon reduction of the disulfide bond, located in the vicinity of the haem. These denaturing conditions also promote reattachment of the distal histidine ligand in the reduced protein and accelerate the reduction of the disulfide by DTT.

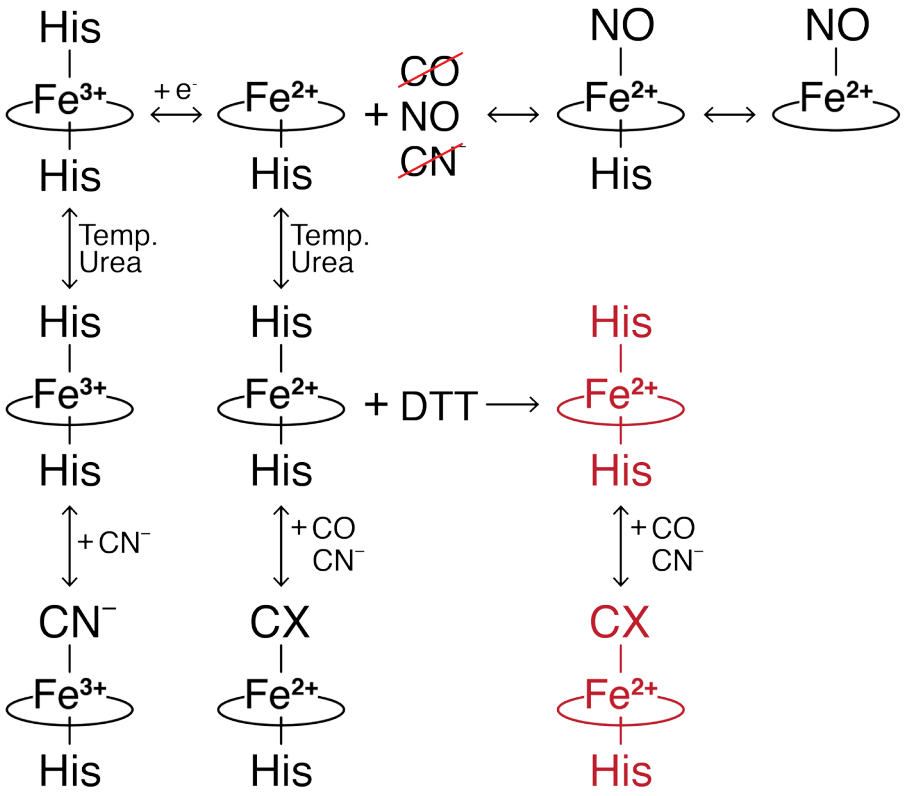

Figure 2.16 Schematic representation of the ligand binding properties of cyt *c*". Reduction leads to the detachment of the distal histidine. The reduced form is then able to bind NO but not CO or CN^-, under physiological conditions. Binding of NO leads to the detachment of the proximal histidine. Upon partial unfolding of the reduced cyt *c*" with temperature or urea, the haem becomes six-coordinated with the previously detached histidine as the sixth ligand. This transition is reversible and this red6cc form is able to bind CO and CN^-. If the red6cc form is treated with DTT in order to reduce the disulfide bond close to the haem, the red5cc-red6cc transition becomes irreversible. This form also binds CO and CN^-. Forms with the reduced disulfide bond are represented in red. No ligands were able to bind to the oxidised cyt *c*" under physiological conditions. The unfolding of this form with temperature or urea does not change the coordination of the haem, but enables the binding of CN^-.

According to the published structure of the reduced cyt *c*" (Enguita *et al.* 2006), the distance from the haem iron to the ring of the detached distal histidine is 5.6 Å, which is comparable with a distance of 6.1 Å between the iron and the ring of the detached proximal histidine in the NO complex of *Alcaligenes xylosoxidans* cyt *c*' (Lawson *et al.* 2000). Hence, steric hindrance is unlikely to be significant for NO when it is on the distal side of the haem in cyt *c*", though the low rate constant for binding suggests that the entrance to the haem pocket may be hindered. Much lower affinity of the haem for CO might be a consequence of steric hindrance for a ligand that prefers to bind more nearly perpendicular to the haem. The distal histidine residue in cyt *c*" immediately precedes Cys96 of the disulfide bridge that braces a loop in the structure (Cys96-Cys104) and lends rigidity to that side of the haem pocket (see Figure 1.3). The $\Delta G°$ values presented here do suggest that CO binding requires a significant conformational rearrangement of the protein. Therefore, by keeping the haem pocket tight, the presence of the disulfide plays a major role in the selectivity of the protein for NO. Although the selectivity of cyt *c*" is not at the level of sGC (see Table 2.6), it is greater than that observed in cyt *c*', a small, soluble monohaem protein that has been associated with the capture and transfer of NO (Moir 1999). If the protein is brought into the "relaxed" form by a thermodynamically unfavourable structural rearrangement or partial denaturation, ligand binding is facilitated and the selectivity for NO binding is lost.

Table 2.6 Standard free energies for the binding of nitric oxide, carbon monoxide and cyanide to different haem proteins.

	ΔG° (kJ/mol)				
	Fe^{2+}-NO	Fe^{2+}-CO	Fe^{3+}-CN^-	Fe^{2+}-CN^-	References
Hb	-68 (R)/-56 (T)	-50 (R)/-34 (T)	-51	0	a, b, c
Mb	-63	-37	-41	-3	c, d
Cyt *c*	-31	-	-35	13	c, e
Cyt oxidase	-50	-37	-34	-19	c, f
sGC	-67	-23	-17	-	c, g, h
Cyt *c*'	-39	-17/-34	-11	-	i, j
CooA	-	-35	-	-	k
Cyt *c*"	-36	-4	17	21	this work

[a](Antonini and Brunori 1971); [b](Cassoly and Gibson 1975); [c](Cooper 1999); [d](Cox and Hollaway 1977); [e](Schejter *et al.* 2006); [f](Jones *et al.* 1984); [g](Stone and Marletta 1995); [h](Stone *et al.* 1996); [i](Kassner 1991); [j](Mayburd and Kassner 2002); [k](Kuchinskas *et al.* 2006)

In *A. xylosoxidans* cyt *c*', which is 5-coordinate in both the oxidised and reduced forms, with histidine as the axial ligand, the crystal structures of the ferrous ligand-bound forms show that NO is bound to the proximal side of the haem, replacing the histidine, while CO binds to the distal side, with the histidine still attached on the proximal side (Lawson *et al.* 2000). A similar process is observed in the activation of sGC by NO, though it is not clear whether the active form has the NO bound to the proximal or to the distal side (Russwurm and Koesling 2004; Fernhoff *et al.* 2009). In ferrous cyt *c*" the detachment of the proximal histidine is also verified, by both UV-visible and resonance Raman spectroscopies. The spectra show high similarity to other 5cc NO adducts, such as cyt *c*', sGC and CooA (Stone and Marletta 1994; Deinum *et al.* 1996; Reynolds *et al.* 2000; Andrew *et al.* 2001). NO is able to displace the proximal ligand in cyt *c*' from *A. xylosoxidans* and *Rhodobacter sphaeroides (Lee et al. 2009)*, but no evidence for this was observed in cyt *c*". The physiological role of cyt *c*" remains to be further investigated, including a possible role

in transporting NO, but the high selectivity towards NO that we demonstrate in this work strongly suggests that its binding is functionally relevant.

Unbalanced levels of NO in the cell can be harmful. Noxious effects of NO can arise, among others, from its high affinity for metal centres in proteins, or its reactivity with reactive oxygen species (ROS), producing highly reactive molecules that can modify macromolecules such as proteins, lipids and DNA (Beckman and Koppenol 1996; Davis *et al.* 2001). NO originates mainly from two distinct pathways. One is the oxidation of L-arginine to L-citruline and NO, catalyzed by NO synthase. Genome search of *M. methylotrophus* and other *Methylophilaceae* (http://img.jgi.doe.gov/w) returns genes annotated as being this enzyme. The other source of NO is the reduction of nitrogen oxides known as denitrification, more specifically the reduction of nitrite by nitrite reductase. Again, genome search of *M. methylotrophus* returns likely candidates for a nitrite reductase. NO is further reduced by NO reductase and *M. methylotrophus* also appears to possess this enzyme. The analysis of the proposed aminoacid sequences suggests that NO reductase is a transmembrane protein. Also from the proposed aminoacid sequences, the nitrite reductases found in different *Methylophilaceae* appear to be localized both in the periplasm and the cytoplasm, since sequences with and without a signal peptide were observed. Cyt *c*", as stated before, is a periplasmic protein. Therefore, cyt *c*" could function as an NO scavenger in the periplasm, delivering the captured NO to the NO reductase in the membrane, thus preventing the toxic effects of this radical.

CHAPTER 3

RELATIVE IMPORTANCE OF DRIVING FORCE AND ELECTROSTATIC INTERACTIONS IN THE REDUCTION OF MULTIHAEM CYTOCHROMES BY SMALL MOLECULES

Results published in:

Quintas, P. O., Cepeda, A. P., Borges, N., Catarino, T., and Turner, D. L. (2013) Relative importance of driving force and electrostatic interactions in the reduction of multihaem cytochromes by small molecules, Biochimica et Biophysica Acta (BBA) - Bioenergetics **1827**, 745-750.

The majority of this work was performed by the author of the thesis, with the production and purification of the cyt *c*" mutants carried out by A. Cepeda.

CONTENTS

ABSTRACT

Multihaem cytochromes are essential to the energetics of organisms capable of bioremediation and energy production. Several have been characterized, both kinetically and thermodynamically. The kinetic characterization of individual haems used the Marcus theory of electron transfer and assumed that the change in the rates of reduction of each haem depend only on the driving force, while electrostatic interactions were neglected. To determine the relative importance of these factors in controlling the rates, we studied the effect of ionic strength on the reduction potential and the rate of reduction by sodium dithionite of native *Methylophilus methylotrophus* cytochrome *c*" and three mutants at different pH values. We found that the main factor determining the rate is the driving force and that Marcus theory describes this satisfactorily. This validates the method of simultaneous fitting of kinetic and thermodynamic data in multihaem cytochromes and opens the way for further investigation into the mechanisms of these proteins.

INTRODUCTION

Organisms that can be used in biodegradation and bioremediation of contaminated environments are receiving increasing attention. Gram-negative bacteria from the *Geobacter* and *Shewanella* genera have been shown to be able to reduce toxic compounds containing chromium or uranium (Anderson *et al.* 2003), as well as insoluble compounds containing iron or manganese (Nealson and Saffarini 1994; Lovley *et al.* 2004) through dissimilatory metal reduction. Moreover, they are being applied to the production of energy through the development of microbial fuel cells (Lovley 2006b; Logan 2009). These organisms produce a large number of multihaem cytochromes (Fredrickson *et al.* 2008) that are present in the periplasm and in the outer membrane; they are crucial to the transfer of electrons to the cell exterior. These features are not restricted to Gram-negative bacteria. Recently, a thermophilic Gram-positive organism, *Thermincola potens* JR, was isolated from the anode of a microbial fuel cell operating at 55 °C. Its genome codes for 32 multihaem cytochromes and it was demonstrated that some of them are localised in the cell surface and are involved in dissimilatory metal reduction (Carlson *et al.* 2012). Detailed characterization of these cytochromes is therefore essential, not only structurally but also in terms of their thermodynamic and kinetic properties.

The thermodynamic characterization of the redox centres in multihaem cytochromes is complicated, but reduction potentials as well as the interactions between haems and with ionisable centres can be determined by following redox titrations using a combination of NMR and UV-visible spectroscopies (Salgueiro *et al.* 1992; Turner *et al.* 1996; Pessanha *et al.* 2006). After the assignment of the haem signals in the NMR spectrum, these can be followed throughout the process of oxidation. This is facilitated by the shifting of the signals out of the main envelope of signals due the paramagnetic Fe^{III}. The extent of the paramagnetic shift of each haem signal is proportional to the oxidation fraction of that particular haem (Santos *et al.* 1984a). During the oxidation process, a tetrahaem protein can be in one of five oxidation

stages (labelled *0-4*), depending on the number of oxidised haems (Santos *et al.* 1984a). Because of the close proximity of the haems, the electrons present at a certain oxidation stage are able to flow between them, and this intramolecular electron transfer is fast in the NMR timescale. If this exchange was slow, each methyl group would give rise to a maximum of 16 resonances, corresponding to all the possible microscopic oxidation states (Figure 3.1). By being fast, the result is a set of five peaks for each haem signal, corresponding to the five macroscopic oxidation stages. The intensity of the signal is proportional to the amount of protein in each oxidation stage at that particular solution potential. The intermolecular electron transfer, on the other hand, is slow and this results in the signals of the five different oxidation stages being always at the same position throughout the oxidation. If it was fast, the signals would move continuously during the oxidation from their positions in stage *0* (fully reduced) to their final positions in stage *4* (fully oxidised). Moreover, because the intermolecular electron transfer is slow, 2D-NOESY experiments can be performed where cross-peaks appear between signals of the same nucleus in different oxidation stages (Santos *et al.* 1984b; Salgueiro *et al.* 1992). This allows us to follow the complete pattern of oxidation of each particular haem signal. The experiments are repeated at different pH values in order to assess the influence of the ionisable centre.

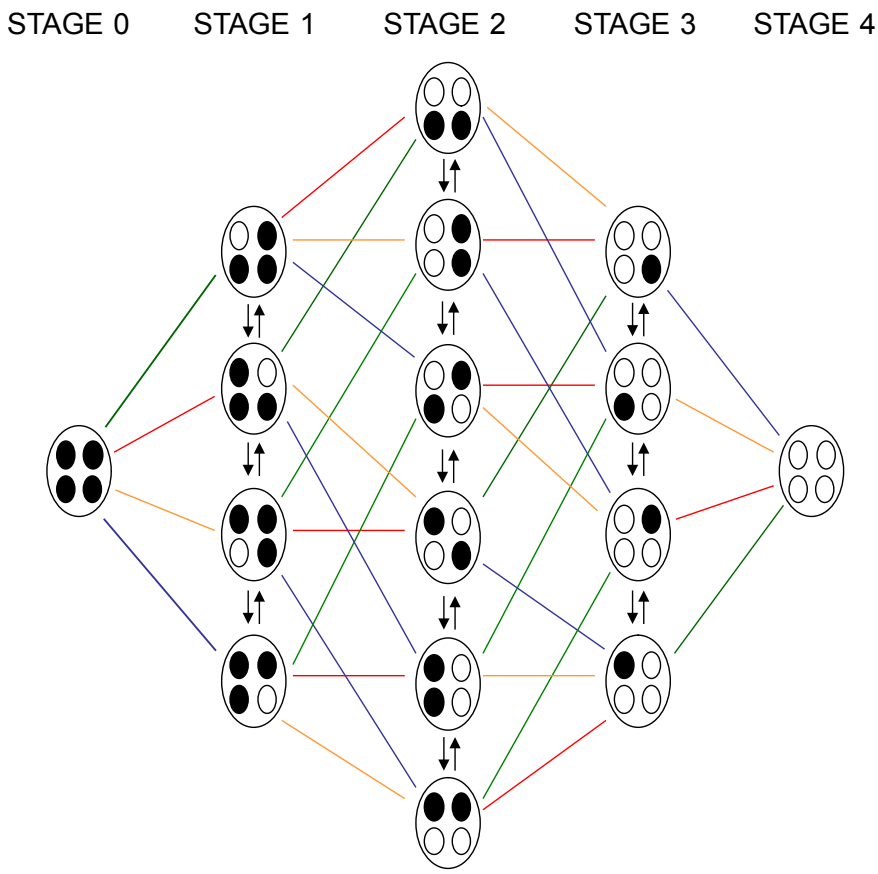

Figure 3.1 Schematic representation of electron exchange in a tetrahaem cytochrome. Small circles represent the four haems that can be either reduced (black) or oxidised (white). The coloured lines represent intermolecular electron exchange involving haem I (green), haem II (red), haem III (yellow) and haem IV (blue). The arrows represent intramolecular electron exchange. The number of the macroscopic stage corresponds to the number of oxidised haems.

Although NMR is able to provide the pattern of oxidation and the relative reduction potentials of the haems, the absolute values are not known and must be obtained by redox titrations followed by UV-visible spectroscopy performed at different pH values. For a tetrahaem cytochrome, a model (Turner *et al.* 1996) considering five interacting centres, four haems and one ionisable group (although occasionally more are required (Paquete *et al.* 2007b)), is then used to fit the data and obtain the thermodynamic properties. If only two-site interactions are considered the model involves the following set of parameters: four reduction potentials, one for each haem, six haem-haem interactions, one pK_a value for the ionisable centre and four interactions between the haems and the ionisable centre. Kinetic properties have been determined by studying the sodium dithionite reduction of the cytochromes by the stopped-flow method and then using the thermodynamic parameters for the individual haems and the Marcus theory of electron transfer (Marcus and Sutin 1985) to separate the contributions of the spectroscopically similar haems (Catarino and Turner 2001; Paquete *et al.* 2010). The simultaneous analysis of data from all experiments, including kinetics, has found significant use in refining the thermodynamic parameters of multihaem cytochromes (Paquete *et al.* 2007b).

According to the theory of Marcus, the rate of electron transfer depends on two components, one that is related to the distance and the environment between the donor and acceptor, and one that is related to the energetic parameters:

$$k = A \cdot \exp(-\beta d) \cdot \exp\left(-\frac{(\Delta G + \lambda)^2}{4\lambda \mathrm{R}T}\right) \quad (1)$$

The first component decreases exponentially with the distance multiplied by a factor (β), which is related to the orbitals overlap of donor and acceptor. The second component contains the energetic parameters, ΔG, the Gibbs energy difference between the two reagents, and λ, the reorganization energy, which is defined as the energy required to distort the equilibrium nuclear geometry of the reactant state into

the equilibrium geometry of the product state without electron transfer. The rate of electron transfer depends on the thermodynamic driving force, increasing with the increase in $-\Delta G$ until it reaches a maximum at $-\Delta G=\lambda$ and then decreasing with $-\Delta G$ values greater than λ. The pre-exponential parameter A is a frequency factor that is a function of temperature.

In the kinetic analysis of the reduction of multihaem proteins by small molecules, each haem is assigned a reference rate constant, k_0, in which the microscopic reduction potential of the centre i is set equal to zero. The reference rate constant accounts for differences in binding, solvent exposure and general electrostatic environment of the haem. The actual rate constants of the microscopic steps are related to the reference rates by a factor γ_i that accounts for the driving force associated with each particular step:

$$\gamma_i = \frac{k_{ET}^{i}}{k_{ET}^{0}} = \exp\left(\frac{-(\Delta G_i + \lambda)^2 + (\Delta G_0 + \lambda)^2}{4\lambda \mathrm{R}T}\right) \tag{2}$$

Assuming that the pre-exponential and distance dependence terms are constant for each haem during the electron transfer steps, the ratio of the rate constants cancels out these terms, isolating the contribution of the driving force. The reorganization energy, λ, is also assumed to be constant. The value of the driving force depends on the difference in reduction potential between the electron donor and acceptor, $\Delta G = \mathrm{F}(E_\mathrm{D}-E_\mathrm{i})$ where F is the Faraday constant, resulting in

$$\gamma_i = \exp\left(\frac{-(F(E_D - E_i)+\lambda)^2 + (FE_D + \lambda)^2}{4\lambda \mathrm{R}T}\right) \tag{3}$$

which can be rearranged to give Eq. 4:

$$\gamma_i = \exp\left(\frac{E_i \mathrm{F}}{2\mathrm{R}T}\left(1+\frac{E_\mathrm{D}\mathrm{F}}{\lambda}-\frac{E_i \mathrm{F}}{2\lambda}\right)\right) \tag{4}$$

NMR shows that the intermolecular electron transfer is slow while intramolecular electron transfer is fast on the experiment timescale (Moura *et al.* 1982; Santos *et al.* 1984a), which collapses the scheme of figure 3.1 in four consecutive one-electron transfer steps. By using an excess of reducing agent, these steps are effectively irreversible and pseudo-first order. Crucially, the variation in the rates of reduction of individual haems as the reduction of the multihaem protein proceeds is ascribed entirely to the variation in driving force that arises from haem-haem interactions, and haem-proton interactions, which account for their pH dependence. This raises an important question: what part is played by electrostatic interactions between electron transfer partners?

Methylophilus methylotrophus cytochrome *c*" (cyt *c*") is a monohaem protein that undergoes a spin-state transition on reduction: the haem is coordinated by two histidines in the oxidised form but only one in the reduced form (Santos and Turner 1988; Costa *et al.* 1993). Both the rate of reduction and the reduction potential are strongly dependent on pH (Costa *et al.* 1992; Coletta *et al.* 1997). It has been proposed that the protonation state of one of the haem propionates is responsible for this behaviour. Haem propionates are also involved in the pH dependence of reduction potentials (the redox-Bohr effect) observed in multihaem cytochromes (Park *et al.* 1996; Turner *et al.* 1996). However, it is not clear to what extent the decrease in the rate with pH is due to electrostatic repulsion by the deprotonated propionate (Coletta *et al.* 1997) or to the observed decrease in the driving force, hence cyt *c*" is an excellent test case.

The ionic strength of a solution influences the rate of reduction through shielding of electrostatic interactions; when the charges of the electron donor and the protein have the same sign, increasing ionic strength leads to an increase in the rate (McArdle *et al.* 1974; Reid and Mauk 1982), and when the charges are opposite the rate decreases (Hodges *et al.* 1974; Lim and Mauk 1985). Moreover, changing the charge on the protein by varying the pH of the solution may change and even invert

the effect (Goldkorn and Schejter 1979). We aim to clarify the relative contributions of electrostatic interactions between charges on the protein surface and the charge of the electron donor and the effect of changes in driving force by using cyt *c*" as a model.

We have studied the effect of ionic strength on the rate of reduction by dithionite and the reduction potential of native cyt *c*" and three mutants in order to assess the importance of these two factors in the control of the electron transfer rates. The three pH values chosen, in ascending order, have the haem propionates fully protonated, then one haem propionate is deprotonated, and finally the protein becomes negatively charged as the isoelectric point is passed. Two of the three mutants have positive charges close to the exposed haem edge removed and the third is the double mutant. Extrapolation to infinite ionic strength eliminates the electrostatic contribution, thus isolating the effect of driving force.

The interest of this work is twofold. First, it tests the validity of the kinetic model proposed by Catarino and Turner (Catarino and Turner 2001) that is being used to extract information about individual haems in multihaem proteins in different systems. As noted above, the kinetic model does not consider changes of the protein charge while it is being loaded with electrons, or at different pH values: this is an important assumption that requires experimental validation. Second, this study contributes to a better understanding of biological electron transfer in situations where redox proteins interact with small electron donors or acceptors. This improves our knowledge of the molecular mechanisms involved in the bioenergetics of microorganisms that perform dissimilatory metal reduction, with potential application to the optimization of bioremediation and energy production processes.

MATERIALS AND METHODS

EXPRESSION AND PURIFICATION

Recombinant protein was produced using *E. coli* BL21 (DE3) cells co-transformed with plasmids pCDP1 containing the cyt *c*" gene and pEC86 encoding genes involved in the maturation of *c*-type cytochromes (Arslan *et al.* 1998). pCDP1 was prepared by inserting the DNA fragment coding for mature cyt *c*" amplified by PCR from pHS1 (Price *et al.* 2000) and digested with restriction enzymes NotI and HindIII, into vector pVA203 (Pokkuluri *et al.* 2004) digested with the same enzymes. Point mutations were obtained using "QuikChange Site-Directed Mutagenesis Kit" from Agilent. The primers used for PCR amplification and mutagenesis are shown in Table 3.1. Growth and purification was performed as described in chapter 2. In this case ampicillin resistance is conferred by pCDP1. The SDS-Page gels of the different purification fractions are shown in Figure 3.2.

Table 3.1 Oligonucleotide primers used in PCR amplification and site-directed mutagenesis of cytochrome *c*". In bold the NotI restriction site (PCR Fwd), the HindIII restriction site (PCR Rev) and the mutated aminoacid codon (Mutagenesis).

PCR	Oligonucleotide sequence (5'-3')
Fwd	AAATTA**GCGGCCGC**CGACGTGACTAACGCTGAAAAG
Rev	CGC**AAGCTT**TTATTTGGTAGGCTTGGTTTCTG
Mutagenesis	**Oligonucleotide sequence (5'-3')**
K80Q	GCACCACGCGTCAATACC**CAG**CGCTTCACAGATATCGAC
K68Q	TAAAAACATTGTTACCGGC**CAG**GAAATCCCACCACTGGCAC

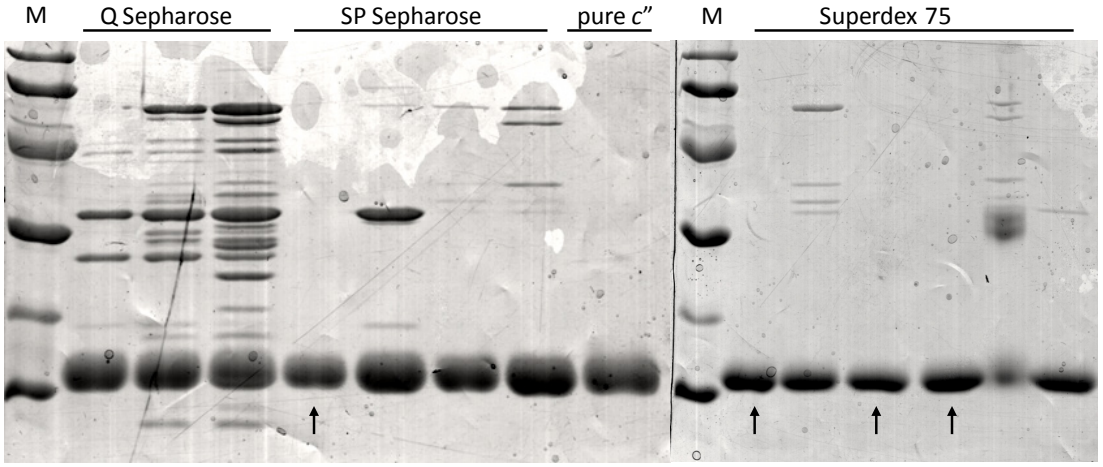

Figure 3.2 SDS-PAGE gels of the purification of native cytochrome *c*". The lanes correspond to: the molecular weight markers (lowest to highest: 14, 20, 30, 45, 66 and 97 kDa), the fractions collected from the Q-Sepharose column, the SP-Sepharose column, and the Superdex-75 column. Fractions marked with an arrow were used in the experiments.

SAMPLE PREPARATION

Buffers at different ionic strengths (0.01-0.2 M) were prepared by diluting a concentrated KCl solution in 50 mM acetate buffer pH 4.5, 5 mM phosphate buffer pH 7.7 or 10 mM Glycine buffer pH 10.0; small pH variations were corrected by adding concentrated HCl or KOH. Protein solutions were prepared by diluting a concentrated stock solution in the desired buffer. Dithionite solutions were prepared in the same buffer as the protein for the experiments at pH 7.7 and pH 10.0. For the experiments at pH 4.5, solutions were prepared in 2.5 mM phosphate buffer pH 7.0 to avoid dithionite decomposition in acidic conditions, with KCl added to the desired ionic strength.

KINETIC EXPERIMENTS

Stopped-flow kinetic experiments were performed at 25 °C using a SF-61 DX2 stopped-flow apparatus (Hi-Tech Scientific) placed inside an anaerobic chamber (<2 ppm O_2). The reaction was initiated by mixing a protein and a dithionite solution (1:1) with the same ionic strength, prepared as above. The change in absorbance at 406 nm (Soret peak in oxidised cyt *c*") and 426 nm (Soret peak in reduced cyt *c*") was followed as a function of time.

Protein and dithionite concentrations were determined in every experiment by mixing each solution with the buffer where it was prepared and recording the absorbance at 406 nm and 315 nm, respectively, using the following extinction coefficients: $\varepsilon_{\text{cyt } c\text{", 406 nm}}$ = 97.5 mM^{-1} cm^{-1} (Santos and Turner 1988), $\varepsilon_{\text{dithionite, 315 nm}}$ = 8 mM^{-1} cm^{-1} (Dixon 1971). The pH values were measured after mixing.

It has been determined previously that the reducing agent is not dithionite but the product of its dissociation, $SO_2^{\bullet-}$ (Coletta *et al.* 1997). Despite the very low dissociation constant, the concentration of $SO_2^{\bullet-}$ is practically constant due to the high concentration of dithionite and the very fast rate of dissociation, making the reaction pseudo-first-order (Catarino and Turner 2001). Rate constants k_{obs} were obtained by single exponential fitting to the traces. Second-order rate constants k were obtained as:

$$k = k_{\text{obs}}\left(\left[dithionite\right] \times K\right)^{-\frac{1}{2}} \tag{5}$$

where K is the equilibrium dissociation constant of dithionite. The variation of K with the ionic strength was taken into account via an extended Debye-Hückel equation (Chien and Dickinson 1978):

$$\ln K = \ln k_1^{\infty} - \ln k_{-1}^{\infty} + \frac{2Z^2\alpha\sqrt{I}}{1+\kappa R} - \frac{4Z^2\alpha\sqrt{I}}{1+2\kappa R} \tag{6}$$

where Z=-1, α = 1.17 $M^{-½}$, $\kappa = 0.329\sqrt{I}$ $Å^{-1}$ and the effective radius of dithionite R = 1.5 Å (Balahura and Johnson 1987). We obtain $\ln k_1^{\infty} - \ln k_{-1}^{\infty} = -19.93$ from the data of Thorneley and Lowe by using I = 0.03 M and $K = 1.60 \times 10^{-9}$ M (Thorneley and Lowe 1983).

REDOX TITRATIONS

Potentiometric titrations were performed inside an anaerobic chamber (<2 ppm O_2) at a constant temperature of 25 °C. Protein samples were prepared as above to a final concentration of 5 μM. Indigo disulfonate, indigo trisulfonate, indigo tetrasulfonate and methylene blue were used as redox mediators, each with a final concentration of 1 μM. Redox mediators are necessary for a good communication between the protein and the electrode. The solution potential was measured with a combined platinum-Ag/AgCl electrode (Crison ref. 52-65) and corrected to the standard hydrogen electrode (correction value = +207 mV, at 25 °C). The calibration of the electrode was performed at the beginning and at the end of the experiment with saturated solutions of quinhydrone at pH 4.0 and pH 7.0, using the reference values of 255 mV and 78 mV, respectively (Bühler and Baumann 1982). The difference between the average of the measurements before and after the experiment, and the references at the two pH values was used to draw a straight line between the two points, which was subsequently used to obtain a calibration value by extrapolation to the experiment pH.

Reduction was achieved by adding small volumes of a sodium dithionite solution prepared as above and oxidation was achieved by addition of air with a gas-tight syringe. The redox state of the protein was monitored by recording the UV-visible spectrum after each addition once a stable potential reading had been attained. Each spectrum was fitted as a sum of the spectra of the pure reduced and oxidised forms to obtain the fractions (see Figures 1.4 and 2.2). The fraction of reduced protein was then plotted against the measured potential and the reduction potential was obtained

from the fitting of a single electron Nernst curve to the experimental points (Figure 3.3).

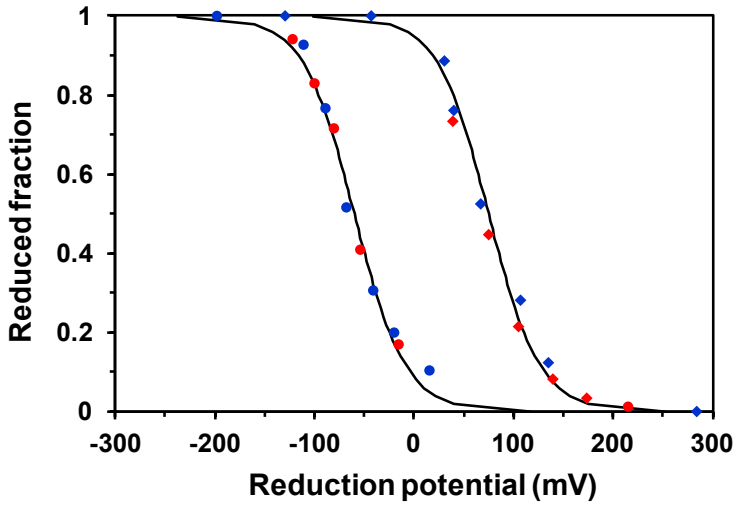

Figure 3.3 Redox titration of native cytochrome *c*'' at pH 7.7 (circles, I = 13.4 mM, $E°$ = −60 mV) and pH 4.5 (diamonds, I = 19.5 mM, $E°$ = 75 mV). Blue corresponds to the reduction and red to the oxidation.

The fit of the ionic strength dependence of the reduction potentials, as well as the extrapolation to infinite ionic strength and the effective charge on the protein, Z_1, were made with Eq. 7 (Mauk *et al.* 1980):

$$\Delta E° = \Delta E^{\infty} - 0.09182\left(\frac{\exp(-\kappa R_1)}{1+\kappa R_2} + \frac{\exp(-\kappa R_2)}{1+\kappa R_1}\right)\left(\frac{Z_1 Z_2 - Z_1' Z_2'}{R_1 + R_2}\right) \qquad (7)$$

where $\Delta E°$ is the reduction potential at ionic strength I, ΔE^{∞} is the reduction potential at infinite ionic strength, Z_1 and Z_2 are the charges and R_1 and R_2 are the radii of the reactants. The primed terms represent the products. The values of the charge and radius of the reducing agent used in the fit were Z_2=-1, Z_2'=0, and R_2=1.5 Å (Balahura and Johnson 1987), and $\kappa=0.329\sqrt{I}$ Å^{-1} for water at 25 °C. Since the best

value for R_1 is unknown, fits were performed with R_1 = 5 and 8 Å, which correspond to the distance from the exposed haem edge or haem propionate to the iron, respectively.

RESULTS AND DISCUSSION

The objective of this work is to distinguish the influence of driving force and of electrostatic interactions in electron transfer reactions between proteins and small molecules. Both the rate of reduction of cyt *c*" by sodium dithionite and its reduction potential show a strong dependence on pH (Costa *et al.* 1992; Coletta *et al.* 1997), making the protein a suitable model. The overall electron transfer process

$$D^- + A^+ \overset{K_{ass}}{\rightleftharpoons} [D^- - A^+] \xrightarrow{k_{ET}} [D - A] \overset{K_{diss}}{\rightleftharpoons} D + A$$

can be simplified if the electron transfer is the rate limiting step and the electron transfer is effectively unidirectional. The reaction then becomes:

$$D^- + A^+ \xrightarrow{k} D + A$$

where the second order rate constant of the electron transfer reaction is the product of the equilibrium association constant for complex formation between electron donor and electron acceptor and the rate constant for electron transfer, $k = K_{ass} \times k_{ET}$ (Catarino and Turner 2001). The rate constant for electron transfer is described as explained above and depends on the driving force among other factors. The driving force is the difference between the reduction potential of the reducing agent $SO_2^{\bullet -}$ (Coletta *et al.* 1997), which is constant and equal to -0.30 V (Neta *et al.* 1987), and the reduction potential of the cyt *c*", which depends on pH and ionic strength. The reduction potential of cyt *c*" was determined from redox titrations followed by visible spectroscopy. The ionic strength dependence of the reduction potentials of the native

cytochrome *c*" at pH 4.5 and 7.7 were fitted with Eq. 7 to obtain the reduction potentials at infinite ionic strength and the results are shown in Figure 3.4.

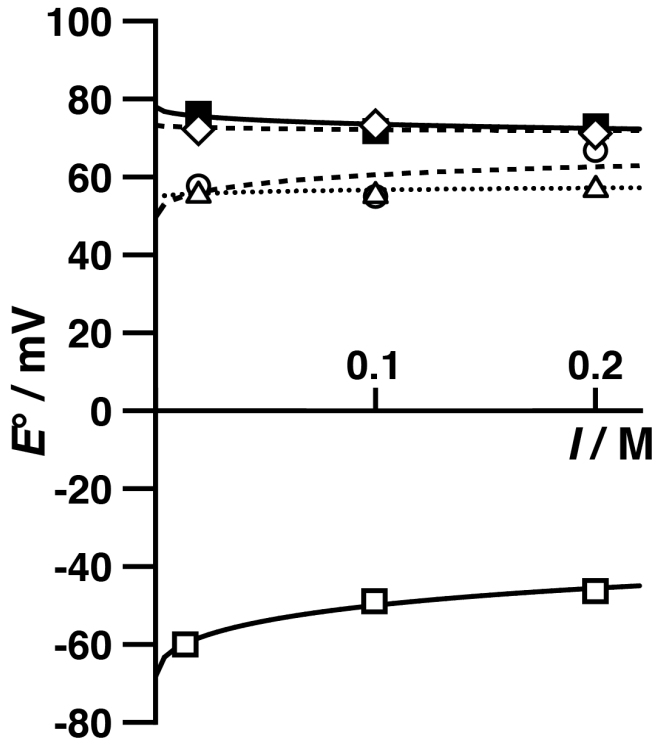

Figure 3.4 Dependence of the reduction potential, $E°$, of cyt *c*" on the ionic strength, *I*, at pH 7.7 (WT – open squares, solid line) and pH 4.5 (WT – filled squares, full line; K80Q – open circles, dashed line; K68Q – open diamonds, dashed line; K68/80Q – open triangles, dotted line). The lines are the result of the fit of Eq. 7 to the data points. The values of the reduction potentials extrapolated to infinite ionic strength were obtained from the fit and are presented in Table 3.6.

These data show that the value of $E°$ at pH 7.7 is about 120 mV lower than that at pH 4.5. Also, the reduction potential increases with ionic strength at pH 7.7, whereas the dependence on ionic strength is small at pH 4.5. This difference can be explained by the influence of the haem propionate group that is protonated at pH 4.5 and deprotonated at pH 7.7. The negative charge of the deprotonated propionate makes it more difficult to reduce the iron at pH 7.7, so that the reduction potential decreases with respect to that at pH 4.5, and partial shielding of the propionate charge would cause the increase in reduction potential with ionic strength.

To investigate the role played by electrostatic interactions, the rate of reduction of cyt *c*" by sodium dithionite was studied at pH 4.5, 7.7 and 10.0, as a function of ionic strength. The second order rate constants obtained are presented in Table 3.2. These values show that the rate constant of the reaction decreases with increasing pH, as observed before (Coletta *et al.* 1997). The change from pH 4.5 to pH 7.7 can be explained by the decrease in driving force and/or increase in repulsive interactions (or decrease in attractive interactions) due to the deprotonation of the haem propionate. There is little change in the reduction potential between pH 7.7 and pH 10 (Costa *et al.* 1992) (see Figure 1.5) but the overall charge on the protein becomes negative since pH 10 is well above the isoelectric point of 8.7 (Santos and Turner 1988).

Table 3.2 Second order rate constants ($/10^8$ $s^{-1}M^{-1}$) for the reduction of cyt *c*" with sodium dithionite.

I (mM)	pH 4.5	pH 7.7	pH 10
19.5	7.59	1.57[a]	0.882[b]
30	7.07	1.52	0.875[c]
50	6.09	1.41	0.918
100	5.07	1.25	0.912
150	4.29	1.18	0.913
200	3.76	1.11	0.872

a) I = 13.4 mM; b) I = 7 mM; c) I = 20 mM

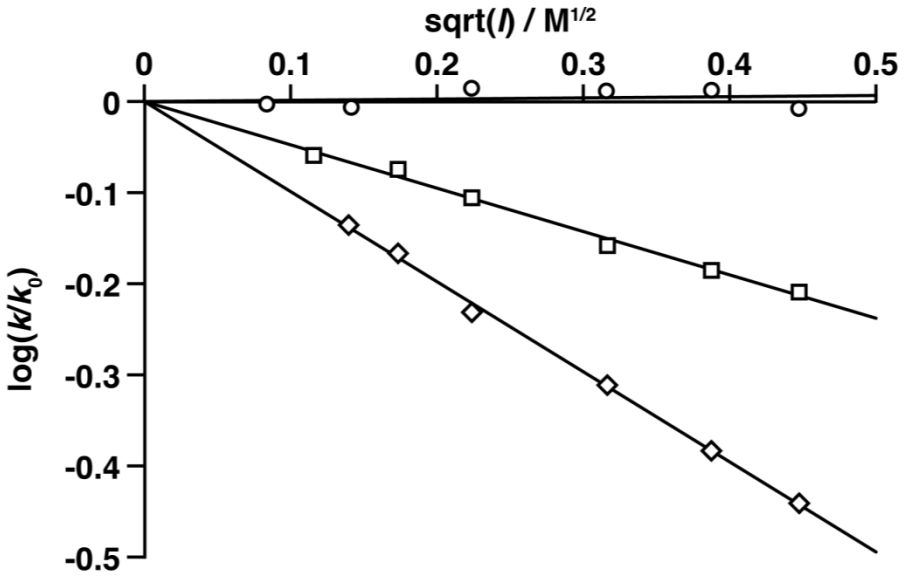

Figure 3.5 Dependence of $log(k/k_0)$ on the square root of the ionic strength at different pH values (diamonds pH 4.5, squares pH 7.7 and circles pH 10.0); k_0 is the rate constant extrapolated to zero ionic strength.

The decimal logarithmic plot of the relative rate constants as a function of the square root of the ionic strength is shown in Figure 3.5: a positive slope indicates repulsive interactions, a negative slope indicates attractive interactions and a slope equal to zero shows that there are no significant electrostatic interactions. A qualitative understanding of the magnitude of the slope is given by the equation of the Debye-Hückel Limiting Law, $\log(k/k_0) = 1.02\ Z_1 Z_2\ \sqrt{I}$ (Atkins and de Paula 2006) that shows that the slope is proportional to the product of the interacting charges. Because the rate constants decrease when the shielding of the interacting charges increases, Figure 3.5 shows that this reaction is influenced by attractive electrostatic interactions. It should be noted that the negative slopes are not an effect of driving force because the driving force for electron transfer is practically independent of ionic strength at pH 4.5, and at pH 7.7 it actually increases. Since the reducing agent is

negatively charged, this implies interactions with positive charges on the protein. Moreover, since the slope is close to zero at pH 10, these data demonstrates clearly that the overall charge of the protein is not the deciding factor. Since the distribution of charge at pH 10 is not known, this pH will not be considered further. As noted above, the major change between pH 4.5 and pH 7.7 is the deprotonation of a haem propionate, and the effective charge on the protein clearly becomes less positive. The slope decreases by about 0.5 units in response to the unit change in the propionate charge, which again shows that the dependence cannot be described by the Debye-Hückel Limiting Law with the overall protein charge.

The electrostatic potential on the surface of cyt *c*" calculated by APBS (Baker *et al.* 2001) at pH 4.5 and pH 7.7 is presented in Figure 3.6: a region near the exposed haem edge is positively charged (blue) at both pH values despite having a negatively charged propionate at pH 7.7. This region includes Arg81, Lys80 and Lys68 and is a likely region for the access of $SO_2^{\bullet -}$ to the haem.

The arginine was not mutated because of its proximity to the haem and the fact that it establishes a hydrogen bond with one of the haem propionates. A mutation of this residue, if successful, would most likely lead to changes in both the reduction potential of the haem and the pK_a of the propionate, which would greatly complicate the interpretation of the results. The lysine residues K68 and K80 were replaced by glutamine, which is also polar but not charged, and the reduction potentials and kinetics of reduction by sodium dithionite of the mutants K68Q, K80Q and double mutant K68/80Q were studied at pH 4.5 as a function of ionic strength. This study was performed at pH 4.5 to avoid interference from deprotonation of the haem propionates, which might have different pK_a values in the mutants. Hence, the introduction of a negative charge on the propionate at pH 7.7 may be compared with the removal of two positive charges close to the haem at pH 4.5. The results obtained are presented in Table 3.3 and Figure 3.7. As can be seen in Figure 3.4, replacing lysine 68, has a negligible effect on the reduction potential of cyt *c*" whereas the

substitution of lysine 80 by glutamine leads to ca. 15 mV decrease, and the effect of the double mutant is similar. These effects are small by comparison with the effect of deprotonating the haem propionate at pH 7.7, that shifts the reduction potential by 120 mV. The distance from the nitrogen of the ε-amino group in K68 to the haem iron is 12.9 Å in the oxidised crystal structure (Enguita *et al.* 2006) and the distance from K80 to the haem iron is 18.3 Å, both of which are much larger than the 7.8 Å between the carboxylate group of the propionate and the haem iron. The differences decrease further at higher ionic strengths, and extrapolation to infinite ionic strength gives similar values of the reduction potentials for the wild type and the mutants.

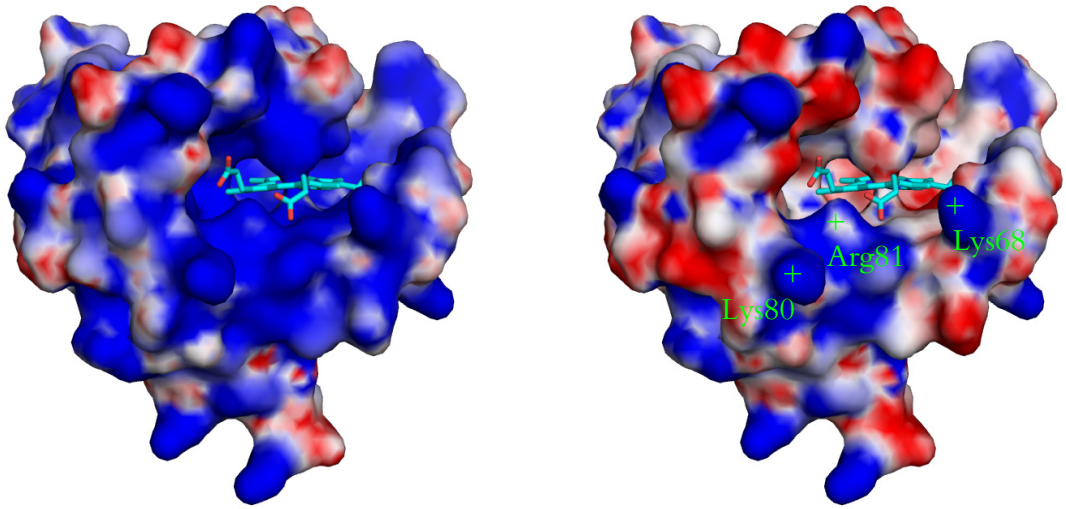

Figure 3.6 Electrostatic potential on the surface of cytochrome *c*" (PDB: 1GU2) at pH 4.5 (left) and pH 7.7 (right), calculated by APBS (Baker *et al.* 2001) using the default parameters. Blue corresponds to positive charge and red to negative charge, with levels ranging from +7 to -7. Prediction of pK_a values by PropKa (Li *et al.* 2005) and preparation of structure for electrostatic calculations by PDB2PQR (Dolinsky *et al.* 2004) using the PARSE forcefield. The figures were prepared with PyMOL (The PyMOL Molecular Graphics System 2006).

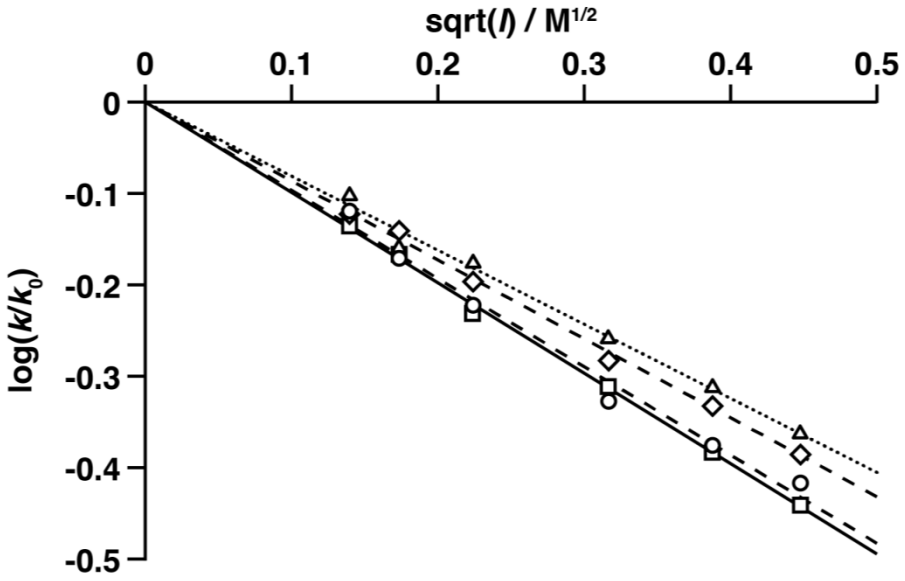

Figure 3.7 Dependence of $\log(k/k_0)$, the relative rates, on the square root of the ionic strength at pH 4.5. Comparison between native cyt *c*" (squares, solid line) and mutants K80Q (circles, dashed line), K68Q (diamonds, dashed line), and K68/80Q (triangles, dotted line).

Table 3.3 Second order rate constants ($/10^8$ $s^{-1}M^{-1}$) for the reduction of cyt *c*" mutants K68Q, K80Q and K68/80Q with sodium dithionite, at pH 4.5.

I (mM)	K80Q	K68Q	K68/80Q
19.5	7.10	5.72	5.21
30	6.29	5.48	4.54
50	5.58	5.82	4.38
100	4.38	3.95	3.62
150	3.92	3.54	3.20
200	3.57	3.13	2.84

As expected, the second order rate constants obtained for the mutants (Table 3.3) are smaller than those obtained at pH 4.5 for the wild type cytochrome (Table 3.2) because the removal of a positively charged residue should decrease the attractive electrostatic interaction between the negatively charged reducing agent and the protein. The mutation of K68 has a significantly larger effect on the rate constant, both on its absolute value (Table 3.3) and on its ionic strength dependence (Figure 3.7), suggesting that the access route of $SO_2^{\bullet -}$ to the haem is closer to lysine 68 than to lysine 80. The effect of the double mutation on the rate constant is roughly equal to the sum of the effects of the two single mutants and is significantly smaller than the effect of deprotonating the haem propionate at pH 7.7 (compare Tables 3.2 and 3.3 and Figures 3.5 and 3.7).

We have demonstrated that positive electrostatic interactions do play a role in the reduction of cyt *c*'' by sodium dithionite and that electron transfer is likely to occur with $SO_2^{\bullet -}$ close to the exposed haem edge. To assess the relative contribution of driving force it is necessary to compare rate constants at infinite ionic strength, so that the electrostatic interactions can be eliminated. A suitable model for this extrapolation is obtained from Marcus theory applied to the Debye-Hückel formalism (Wherland and Gray 1976):

$$\ln k = \ln k_\infty - 3.576\left(\frac{\exp(-\kappa R_1)}{1+\kappa R_2} + \frac{\exp(-\kappa R_2)}{1+\kappa R_1}\right)\left(\frac{Z_1 Z_2}{R_1 + R_2}\right) \qquad (8)$$

where k is the rate constant at ionic strength I, k_∞ is the rate constant at infinite ionic strength, $\kappa = 0.329\sqrt{I}$ Å^{-1} at 25 °C, and the Z_i and R_i are the charges and radii of the two reactants.

Eq. 8 can be used to fit the experimental data and obtain values for k_∞, the rate constant at infinite ionic strength, and Z_1, the charge on the protein surface that is relevant for the electron transfer reaction. The values of Z_2=-1, R_2=1.5 Å and R_1=5 or 8 Å were the same that were used in Eq. 7. The result of the fits is presented in

Figure 3.8. The values of the charge determined from the fit are presented in Table 3.4 and the values of the rate constants at infinite ionic strength are given in Table 3.5.

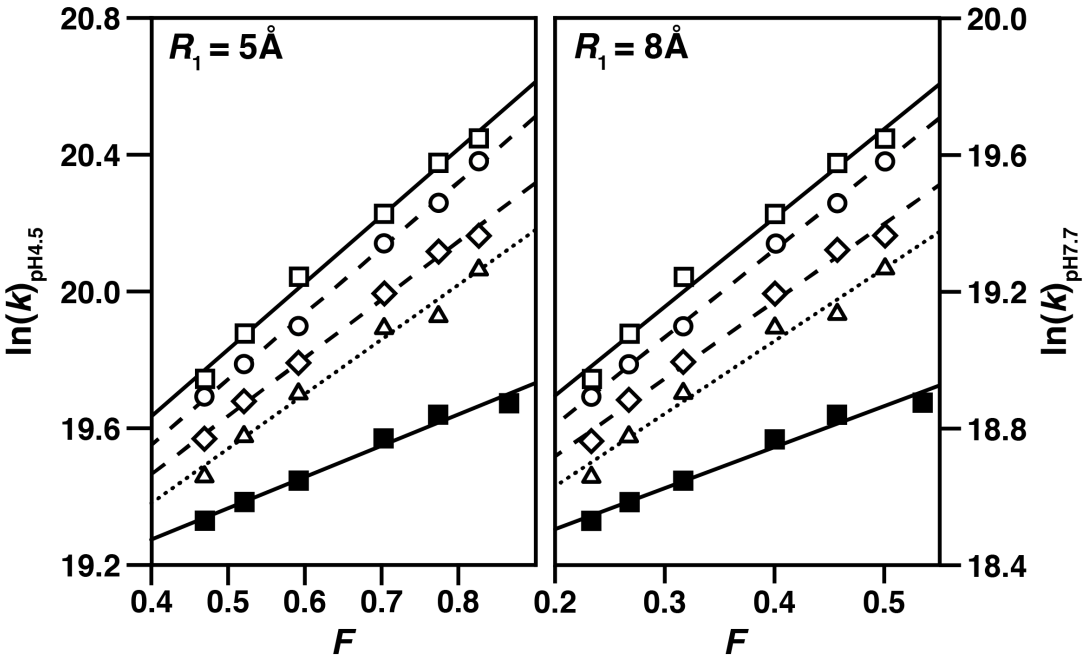

Figure 3.8 Result of the fit of Eq. 8 to the experimental rate constants. Data obtained at pH 4.5 (left scale – open symbols) and pH 7.7 (right scale – filled symbols). The lines are given by $\ln k = \ln k_\infty + Z_1 F$, where

$$F = -3.576\left(\frac{\exp(-\kappa R_1\sqrt{I})}{1+\kappa R_2\sqrt{I}} + \frac{\exp(-\kappa R_2\sqrt{I})}{1+\kappa R_1\sqrt{I}}\right)\left(\frac{Z_2}{R_1+R_2}\right).$$

The value of R_1 used in the fit is indicated in the panel. Native cyt *c*" (squares, solid line) and mutants K80Q (circles, dashed line), K68Q (diamonds dashed line), and K68/80Q (triangles, dotted line).

Table 3.4 Effective protein charge, Z_1, obtained via Eq. 8.

R_1 (Å)	wt pH 4.5	wt pH 7.7	K80Q pH 4.5	K68Q pH 4.5	K68/80Q pH 4.5
5	+1.95 ± 0.08	+0.91 ± 0.06	+1.92 ± 0.04	+1.70 ± 0.07	+1.60 ±0.10
8	+2.60 ± 0.14	+1.20 ± 0.10	+2.56 ± 0.05	+2.27 ± 0.12	+2.12 ± 0.16

Table 3.5 Rate constants for reduction of cyt *c*" at infinite ionic strength ($/10^8$ $s^{-1}M^{-1}$).

R_1 (Å)	wt pH 4.5	wt pH 7.7	K80Q pH 4.5	K68Q pH 4.5	K68/80Q pH 4.5
5	1.54 ± 0.08	0.73 ± 0.03	1.44 ± 0.04	1.44 ± 0.06	1.38 ± 0.09
8	2.13 ± 0.11	0.86 ± 0.03	1.97 ± 0.04	1.91 ± 0.09	1.80 ± 0.11

For the wild type protein, values of the protein charge, Z_1, of approximately +2 and +1 were obtained for pH 4.5 and pH 7.7, respectively. These values are plausible, taking into account the positive charges of the nearby aminoacids and the neutral haem propionate that becomes negatively charged at pH 7.7. In the single mutants there is a decrease in the calculated charge at pH 4.5, albeit a fraction of the +1 charge of the lysines. It is also noticeable that the effect of the mutation of lysine 68 on the charge is significantly larger than that of lysine 80. Moreover, the effect of the mutations seems to be roughly additive. The effect of the mutations on the rate constant at infinite ionic strength is small, which is in agreement with the small change in the reduction potentials of the mutants when compared to the wild type cytochrome.

Marcus theory for electron transfer (Marcus and Sutin 1985) can be used to calculate the change in the electron transfer rate k_{ET} expected for a given change in driving force, if it is assumed that the reorganization energy λ and the pre-exponential term do not change. Under these conditions, Eq. 9 can be used to calculate the ratio between the electron transfer rates at pH 4.5 and 7.7. Note that, when the reduction potentials, E_{cytc}, are ionic strength dependent, as it is the case at pH 7.7 (see Figure

3.4), the values used in Eq. 9 should be the values extrapolated for infinite ionic strength.

$$\frac{k_{ET}^{pH4.5}}{k_{ET}^{pH7.7}} = \exp\left(\frac{(E_{cytc}^{pH4.5} - E_{cytc}^{pH7.7})F}{2RT}\left(1 + \frac{E_{SO2}F}{\lambda} - \frac{(E_{cytc}^{pH4.5} + E_{cytc}^{pH7.7})F}{2\lambda}\right)\right) \quad (9)$$

The reduction potential of the electron donor, E_{SO2}, is equal to -0.30 V and is pH independent in this pH range (Neta *et al.* 1987). A value of 0.7 eV was used for the reorganisation energy λ (Sulpizi *et al.* 2007).

The ratio of the second order rate constants, extrapolated to infinite ionic strength to cancel out the electrostatic contributions (Table 3.5), and the ratio of the rate constants calculated with Eq. 9 using the reduction potentials of the cytochrome also extrapolated to infinite ionic strength, are presented in Table 3.6. The agreement is reasonable, showing that the driving force influences the rate of reduction of cyt *c*" by sodium dithionite according to the predictions of Marcus theory and this set of assumptions.

Table 3.6 Reduction potentials at infinite ionic strength used with Eq. 9 to calculate the ratio of ET rate constants according to Marcus theory. The ratios are compared with the ratio of experimental second order rate constants extrapolated to infinite ionic strength (values from Table 3.5). A value of λ=0.7 eV was used in the calculations (Sulpizi *et al.* 2007).

R_1 (Å)	E_{cytc} (mV)		$k_{ET}^{pH4.5} / k_{ET}^{pH7.7}$	
	pH 4.5	pH 7.7	From Eq. 9	From Table 3.5
5	68	-29	2.8	2.1 ± 0.2
8	70	-35	3.1	2.5 ± 0.2

CONCLUSIONS

This work addresses the contributions of electrostatic interactions and driving force to electron transfer rates by studying the ionic strength dependence of the reduction of cyt *c*" by sodium dithionite at different pH values. The thermodynamic modulation of electron transfer rates is adequately described by Marcus theory for electron transfer, assuming a constant value for the reorganisation energy. The studies with ionic strength showed that the region on the protein surface that is involved in the electrostatic interaction between the redox partners is positively charged and probably involves the exposed haem edge. This was tested further by single-site mutagenesis and it was concluded that the approach of the reducing agent to the haem is closer to lysine 68 than to lysine 80. The protonation state of one of the haem propionates influences the rate of reduction both by changing the reduction potential and through electrostatic repulsion. The importance of the haem propionates has also been observed in the reduction of cytochrome b_5 (Reid *et al.* 1984) and myoglobin (Tsukahara and Ishida 1991; Lim *et al.* 2006). In both cases, esterification of the propionates results in an increase in the reduction potential and the rate of reduction.

In some previous studies on the ionic strength dependence of the reduction potential and the rate of electron transfer, with a similar treatment to that used here, the full radius of the protein was used in the calculations and the values of the charges that were obtained were usually somewhat different from the expected full charge of the protein (Reid and Mauk 1982; Reid *et al.* 1982; Lim and Mauk 1985). This is particularly evident with cyt *c*" because reversing the charge of the protein by using a pH above the isoelectric point does not reverse the interaction between the protein and the reducing agent. Therefore, the effective radius appears to be more closely related to the region of accessibility of the haem to the reducing agent.

At a typical ionic strength of ca. 50 mM, the experimental rate of reduction decreases by a factor of 4.3 between pH 4.5 and pH 7.7. This may be compared with

the factor of 4.0 calculated from Marcus theory solely on the basis of the change in driving force (for I=50 mM, $E_{pH4.5}$=74 mV, $E_{pH7.7}$=-54 mV). Clearly, the effect of driving force is dominant in this case, though electrostatic interactions also play a part. This helps to explain the success of simultaneous fitting of kinetic and thermodynamic data in multihaem cytochromes over a wide pH range (Paquete *et al.* 2007b): variations in surface charge have a limited effect, and even changing the charge of a haem propionate has less effect on the electrostatic interaction with dithionite than it does on the driving force through redox-Bohr effects. Furthermore, the ionisation of the propionate of one haem in a multihaem protein is not likely to affect the rate of reduction of a different haem through electrostatic interactions, since this work also showed that the influence of charges on the protein surface is limited to a restricted area in the vicinity of the redox centre. Hence, the crucial assumption made in the method for kinetic and thermodynamic analysis of multihaem proteins, that electrostatic interactions between the protein and dithionite may be neglected, has a sound experimental basis.

CHAPTER 4

ELECTRON TRANSFER BETWEEN MULTIHAEM CYTOCHROMES C_3 FROM *DESULFOVIBRIO AFRICANUS*

Results published in:

Quintas, P. O., Oliveira, M. S., Catarino, T., and Turner, D. L. (2013) Electron transfer between multihaem cytochromes c_3 from *Desulfovibrio africanus*, Biochimica et Biophysica Acta (BBA) - Bioenergetics **1827**, 502-506.

The experimental NMR study was performed by the author of the thesis. The production and purification of the proteins was carried out by M. Oliveira.

CONTENTS

ABSTRACT

The tetrahaem type I cytochromes c_3 from *Desulfovibrionaceae* shuttle electrons from a periplasmic hydrogenase to transmembrane electron transfer complexes. In *D. africanus*, it is believed that the electrons are received by another tetrahaem cytochrome c_3, denoted type II, which is associated with the membrane complex. Thermodynamic measurements show that the type I cytochrome c_3 has the potential to transfer two electrons at a time. This study uses two-dimensional NMR to investigate the exchange of electrons between type I and type II cytochromes c_3 at equilibrium in intermediate stages of oxidation. The results indicate that the two proteins are physiological partners but that only single-electron transfers occur in solution.

INTRODUCTION

Cytochromes c_3 are a group of small tetrahaem proteins that are present in large quantities in the periplasm and are proposed to act as mediators between periplasmic hydrogenases and transmembrane electron transfer complexes (Matias *et al.* 2005). In *Desulfovibrio africanus*, the soluble cytochrome c_3, called type I (TpIc_3), is thought to receive electrons from hydrogenase and deliver them to a structurally similar tetrahaem cytochrome c_3, denoted type II (TpIIc_3), associated with the transmembrane complex (see Figure 1.6). However, despite evidence of complex formation between TpIc_3 and TpIIc_3 (Pieulle *et al.* 2005), the functional interaction between the two proteins has not been shown. Based on the thermodynamic properties of the isolated proteins (Paquete *et al.* 2007a), it has been speculated that two electrons could be transferred during the lifetime of the encounter complex. However, this two-electron transfer step has never been observed experimentally. Therefore, we attempted to determine the nature of electron transfer between *D. africanus* TpIc_3 and the soluble *D. africanus* TpIIc_3.

The study of exchange processes by NMR has a long history (Hoffman and Forsén 1966) and formed one of the earliest applications of two-dimensional NMR (Jeener *et al.* 1979). The so-called EXSY experiment is essentially identical to the normal 2D-NOESY experiment where, during the mixing time (τ_m) between the second and third 90° pulse, magnetization may be transferred between the nuclei. If the exchange rate is slow with respect to the difference of the chemical shifts of the nuclei, a cross peak appears in the 2D-spectrum with an intensity proportional to the amount of exchange that occurred during τ_m. The peculiar advantage of NMR is that nuclei are frequency labelled in individual molecules so that exchange can be studied in systems at equilibrium.

The EXSY method is not often applied to proteins because of the extensive overlap between peaks that occurs in complex spectra. However, the signals of the

methyl substituents of haems in oxidised cytochromes are pushed out of the main envelope by interaction with the paramagnetic low-spin Fe^{III}. Because the intramolecular electron exchange is fast in multihaem cytochromes but intermolecular exchange is typically slow, each haem methyl group in a protein molecule at a particular stage of oxidation gives rise to a single averaged signal. Since the tetrahaem cytochromes may release from 0 to 4 electrons, each methyl resonance has 5 possible frequencies in the macroscopic oxidation stages, which are labelled *0* to *4* (see Figure 3.1). In a solution of partially oxidised cytochrome, molecules at different stages of oxidation are in dynamic equilibrium, with intermolecular electron transfers occurring at a rate that is typically fast enough to generate cross peaks in two-dimensional exchange spectra but slow enough to cause minimal line broadening (Santos *et al.* 1984b; Salgueiro *et al.* 1992; Turner *et al.* 1996).

Individual exchange rate constants may be obtained from the initial rate of build-up of cross peak intensities with respect to the mixing time, τ_m, or, better, by non-linear fits to the full set of intensities. The matrix of intensities, $\mathbf{S}$, in a two-dimensional exchange spectrum (Jeener *et al.* 1979) of a system undergoing relatively slow exchange is given by

$$\mathbf{S}=\exp(\mathbf{L}\tau_m)\mathbf{M}_0 \tag{1}$$

where $\mathbf{M}_0$ is a diagonal matrix containing the equilibrium populations, τ_m is the mixing time, and $\mathbf{L}$ is the exchange matrix

$$\mathbf{L}=\begin{pmatrix} -R_0-\sum_j k_{j0} & k_{10} & \cdots & k_{40} \\ k_{01} & -R_1-\sum_j k_{j1} & \cdots & \cdots \\ \cdots & \cdots & \cdots & \cdots \\ k_{04} & \cdots & \cdots & -R_4-\sum_j k_{j4} \end{pmatrix} \tag{2}$$

in which k_{ij} are rate constants and R_i are longitudinal relaxation rates.

The exponential of matrix $\mathbf{X}$ is defined as the matrix resulting from the series expansion:

$$\exp(\mathbf{X}) = \sum_{n=0}^{\infty} \frac{\mathbf{X}^n}{n!}. \tag{3}$$

If $\mathbf{X}$ is transformed into $\mathbf{U}^{-1}\mathbf{X}\mathbf{U}$, where $\mathbf{U}^{-1}$ is the inverse of $\mathbf{U}$, and since

$$\left(\mathbf{U}^{-1}\mathbf{X}\mathbf{U}\right)^n = \left(\mathbf{U}^{-1}\mathbf{X}\mathbf{U}\right)\left(\mathbf{U}^{-1}\mathbf{X}\mathbf{U}\right)\cdots\left(\mathbf{U}^{-1}\mathbf{X}\mathbf{U}\right) = \mathbf{U}^{-1}\mathbf{X}^n\mathbf{U}, \tag{4}$$

then

$$\exp\left(\mathbf{U}^{-1}\mathbf{X}\mathbf{U}\right) = \sum_{n=0}^{\infty} \frac{\left(\mathbf{U}^{-1}\mathbf{X}\mathbf{U}\right)^n}{n!} = \mathbf{U}^{-1}\sum_{n=0}^{\infty}\left(\frac{\mathbf{X}^n}{n!}\right)\mathbf{U} = \mathbf{U}^{-1}\exp(\mathbf{X})\mathbf{U}, \tag{5}$$

which can be reorganized as:

$$\exp(\mathbf{X}) = \mathbf{U}\exp\left(\mathbf{U}^{-1}\mathbf{X}\mathbf{U}\right)\mathbf{U}^{-1}. \tag{6}$$

Because the forward and reverse fluxes are equal for a system at equilibrium, the matrix product $\mathbf{L}\mathbf{M}_0$ is symmetric and Eq. 1 can be reformulated as

$$\mathbf{S} = \mathbf{M}_0^{1/2}\exp\left(\mathbf{M}_0^{-1/2}\mathbf{L}\mathbf{M}_0^{1/2}\tau_m\right)\mathbf{M}_0^{1/2} \tag{7}$$

in which the exponent is a symmetric matrix.

In this work, we investigate the intermolecular electron transfer rates of TpIc_3 from *D. africanus* in intermediate stages of oxidation. Stages *0-3* are observed simultaneously, hence we must consider four populations, four relaxation rates, and six exchange rates in the analysis using Eq. 7. The exchange rates comprise three single electron transfers as well as possible two- and three-electron transfers. Adding catalytic quantities of TpIIc_3 then allows us to measure the potentially physiological electron transfer rates between the two cytochromes.

Even if only one electron could be transferred in each collision, cross peaks would appear in the NMR spectra that connect stages separated by two or more. These result from successive collisions and electron transfers occurring during the mixing period. A mechanism involving the transfer of two electrons within a single collisional event would lead to an excess of intensity in cross peaks connecting stages separated by two electrons. In this work, we compare the non-linear fits of the complete set of measured intensities to a model in which only single electron transfers are allowed, to a fit in which any number of electrons may be transferred, in order to detect the effect of possible multi-electron transfers.

MATERIALS AND METHODS

EXPRESSION AND PURIFICATION

TpIc_3 was purified from *Desulfovibrio africanus* grown as previously described (Pieulle *et al.* 1996). The soluble fraction resulting from French-press disruption was applied to a DEAE Sepharose Fast Flow anion exchange column (GE Healthcare) equilibrated with 20 mM Tris-HCl (pH 7.6) and eluted with a salt gradient from 0 to 1 M NaCl prepared in the same buffer. The non-adsorbed fractions were collected and loaded onto a SP-Sepharose cation exchange column (GE Healthcare) equilibrated and eluted as the previous step. Finally, fractions containing TpIc_3 were inserted onto a Superdex-75 gel-filtration column (GE Healthcare) equilibrated with 100 mM phosphate buffer (pH 7.6). The purification procedure was monitored by SDS-PAGE and UV-visible spectroscopy (Figure 4.1), with the pure protein presenting a purity index $\left(Abs_{552}^{red} - Abs_{570}^{red}\right) / Abs_{280}^{ox}$ of 3.6. Polyacrylamide gels were prepared with 12% acrylamide (running) and 3% acrylamide (stacking) and were stained with Coomassie blue.

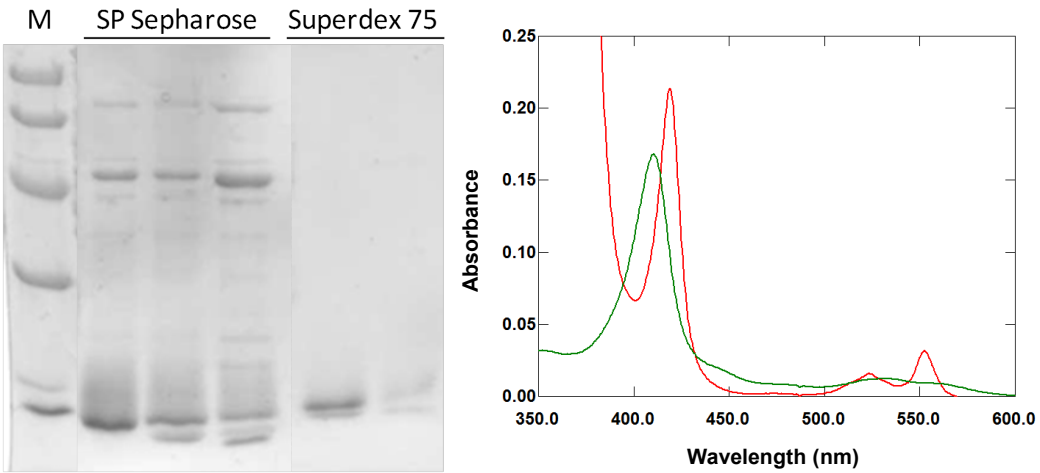

Figure 4.1 Left - SDS-PAGE gels of the purification of Type I cytochrome c_3. The lanes correspond to: the molecular weight markers (lowest to highest: 14, 20, 30, 45, 66 and 97 kDa), the fractions collected from the SP-Sepharose column, and the Superdex-75 column (pure fractions). Right - UV-visible spectrum of pure oxidised (green) and reduced TpIc_3 (red).

Attempts to purify TpIIc_3 from the native organism were not successful. We therefore sought to produce recombinant protein. The DNA sequence coding for TpIIc_3 was amplified from the genomic DNA of *D. africanus* by PCR, using primers containing restriction sites for enzymes NotI and HindIII (Fwd: 5'-GCG GCC GCC AGG AGG ACA TGA CTC ATG TG-3'; Rev: 5'-AAG CTT CTA ATT CTT CAC GTG GCA TTC-3'). This fragment was subsequently digested with NotI and HindIII and inserted into vector pVA203 (Pokkuluri *et al.* 2004) digested with the same enzymes. After the sequencing of the resulting plasmid, it was found that it was missing one nucleotide after the restriction site, which would leave the sequence out of frame and prevent the correct transcription. The missing nucleotide was inserted using the "QuikChange Site-Directed Mutagenesis Kit" from Agilent (primer: 5'-CGT TGC GGC CGC CCA GGA GGA CAT G-3'), resulting in plasmid pDAC32. The protein was produced using *E. coli* BL21 (DE3) cells co-transformed with

plasmids pDAC32 and pEC86 encoding genes for cytochrome *c* maturation (Arslan *et al.* 1998).

Cells were grown aerobically at 30 °C and 200 rpm in medium 2xYT containing 100 μg/mL of ampicillin and 25 μg/mL of chloramphenicol (antibiotic resistance conferred by pDAC32 and pEC86, respectively). After 9-10 h, expression was induced by the addition of 10 μM IPTG and the temperature was lowered to 25 °C. After 18-20 h cells were harvested by centrifugation and the periplasmic fraction was isolated as in chapter 2. The purification was performed by column chromatography in three steps: (i) anion exchange on a Q-Sepharose column (GE Healthcare) equilibrated with 20 mM Tris-HCl (pH 7.6) and eluted with a salt gradient from 0 to 1 M NaCl prepared in the same buffer, (ii) gel-filtration on Superdex- 75 column (GE Healthcare) equilibrated with 50mM Tris-HCl (pH 7.6) + 100 mM NaCl, and (iii) anion exchange on a Resource-Q column (GE Healthcare) equilibrated with 20 mM Tris-HCl (pH 7.6) and eluted as (i). The purification procedure was monitored by SDS-PAGE and UV-visible spectroscopy (Figure 4.2), with the purity index never going beyond 2.6. Despite having only one band in the SDS-PAGE gel, a homogeneous UV-visible spectrum, and the expected NMR spectrum in the reduced form, the NMR spectrum of the oxidised form shows a doubling of the most shifted peaks (Figure 4.3). We attribute this to a non-native form of TpIIc_3 in which the N-terminal glutamine is not cyclised. Expressing the protein more slowly slightly improved the yield of the native form but the two forms could not be separated and so all experiments were done with this heterogeneous material.

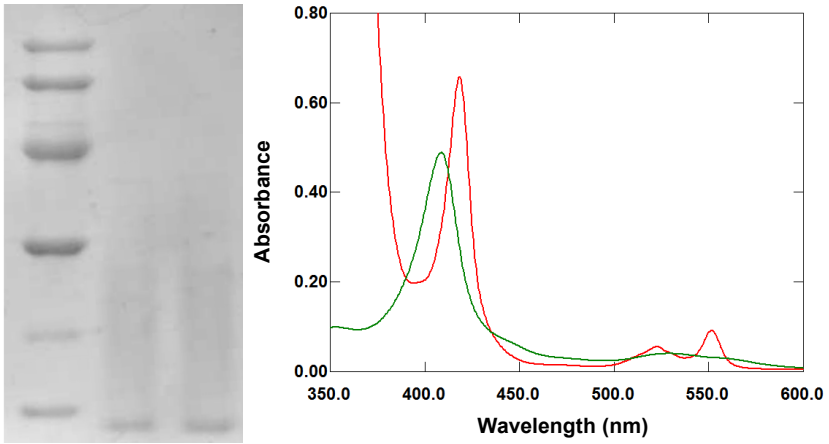

Figure 4.2 Left - SDS-PAGE gels of the pure fractions resulting from the purification of Type II cytochrome c_3. The lanes correspond to the molecular weight markers (lowest to highest: 14, 20, 30, 45, 66 and 97 kDa) and the pure fractions collected from the Resource-Q column. Right - UV-visible spectrum of pure oxidised (green) and reduced TpIIc_3 (red).

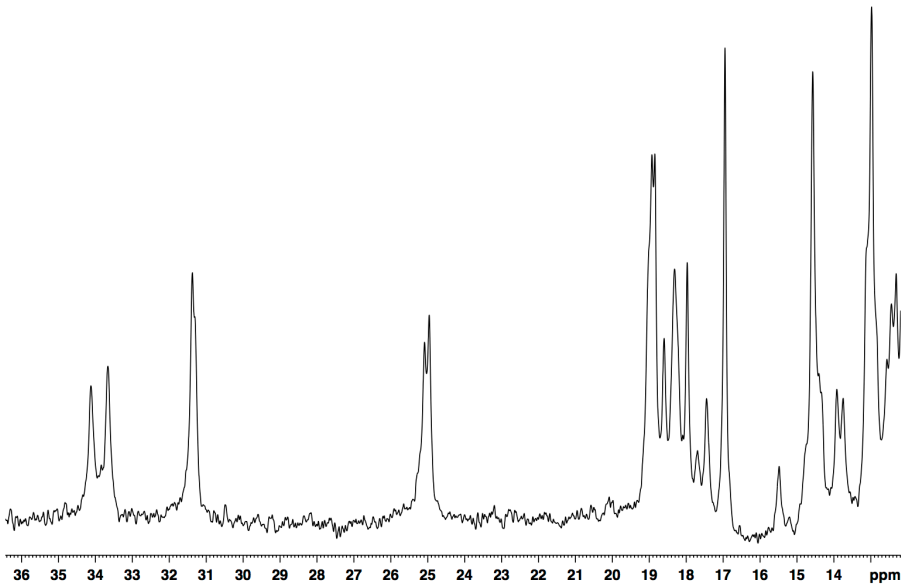

Figure 4.3 Downfield portion of the 800 MHz proton NMR spectrum of recombinant Type II cytochrome c_3 from *D. africanus* at 298 K and pH 7.6. The split peak at about 34 ppm is from the methyl group 18^1 of haem I (Pereira *et al.* 2002), which is close to the N-terminus.

NMR SAMPLE PREPARATION

Pure TpIc_3 was lyophilised and resuspended in ^2H_2O with 50 mM KCl and 0.05% NaN_3 to a final concentration of 1 mM. Partial reduction was achieved by the addition of small amounts of a sodium dithionite solution. Small amounts of a concentrated TpIIc_3 solution were added to a final concentration of 1%, 2% and 4% of that of TpIc_3. The pH of the sample was 7.6, measured after each addition. All manipulations were performed inside an anaerobic chamber (<2 ppm of O_2).

NMR EXPERIMENTS

Proton NMR spectra of partially oxidised TpIc_3 in the presence of different amounts of TpIIc_3 (0-4%) were obtained in an 800 MHz Bruker Avance III spectrometer equipped with a TXI-Z 5 mm probe. Several 2D-exchange spectroscopy (EXSY) NMR data sets were collected at 298 K with different mixing times (0.25-128 ms in pseudo-random order). Each spectrum comprised 256 increments with 32 scans and 4096 points. The spectral width was 69.4 ppm in both dimensions, centred on the water signal. Crucially, the frequency of the pulses was offset to the middle of the haem methyl signals to ensure even excitation.

DATA ANALYSIS

NMR spectra were transformed, and phase and baseline corrected using Bruker Topspin 2.1 then integrated by lineshape fitting using UCSF Sparky 3.114. Peak intensities were fitted by Eq. 7 using GNU Octave 3.6.1. Fits were performed with rate constants for the exchange of two or more electrons set to zero as well as with the complete set of variables and the results were compared by F-tests.

RESULTS AND DISCUSSION

A typical 2D exchange spectrum is shown in Figure 4.4, with assignments from (Paquete *et al.* 2007a) . Signals from methyl groups 18^1 of haems I, II and IV are visible in oxidation stages *0-3* in each spectrum. There are no signals visible for haem III, which is largely reduced in stages *0-3* and only becomes oxidised in stage *4*. This shows that the concentration of stage *4* is negligible; hence the analysis was restricted to stages *0-3*.

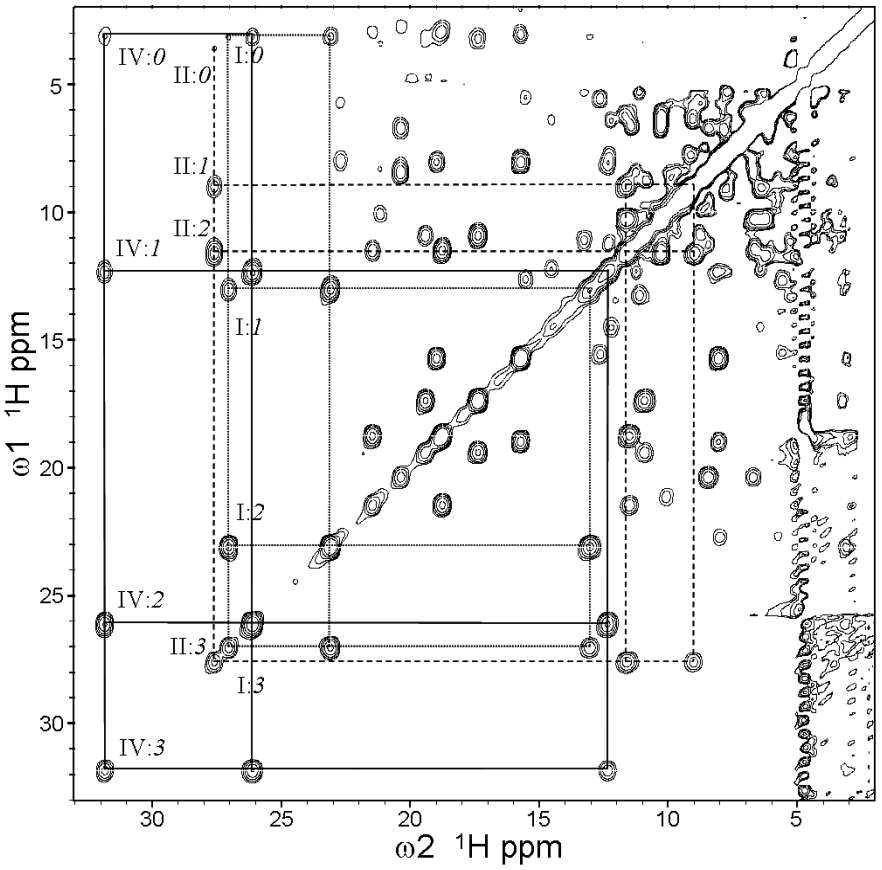

Figure 4.4 Part of the two-dimensional exchange spectrum of 1 mM type I cytochrome c_3 from *D. africanus* recorded at 800 MHz with a mixing time of 8 ms (298 K, pH 7.6). The three most shifted haem methyl resonances are labelled with the haem, indicated by a Roman numeral, and the oxidation stage in italic. In each case the cross peaks are connected by lines.

Data for the seven most shifted methyl groups were fitted separately to Eq. 7 to estimate errors. In principle, different methyl groups might have different relaxation rates, R_i, but no significant differences in relaxation rates were found within each stage and the final analysis used the average of the intensities of corresponding peaks. The fitted data for pure TpIc_3, and TpIc_3 with 4% TpIIc_3 added, are shown in Figure 4.5.

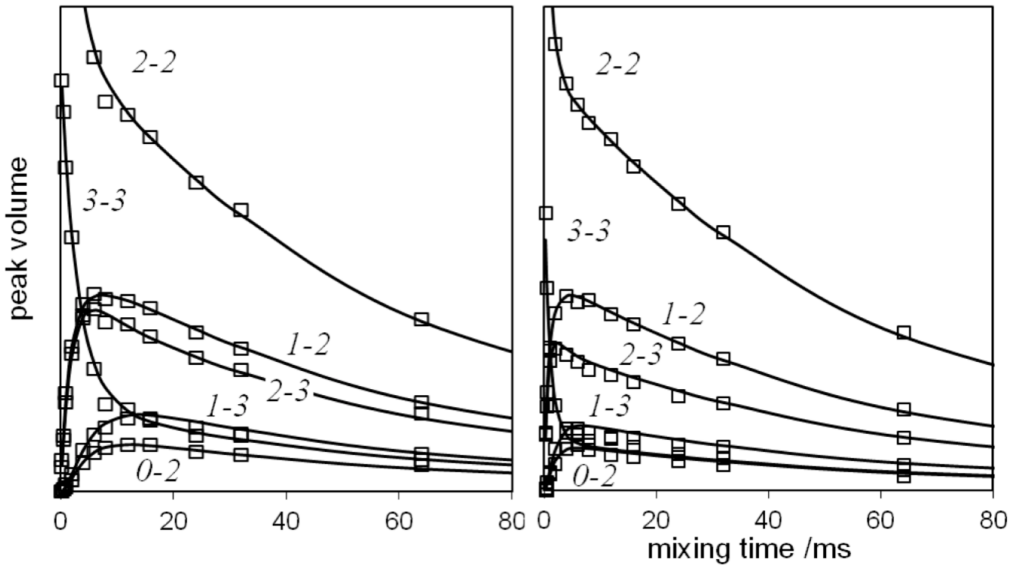

Figure 4.5 Raw NMR data and fitted curves for electron transfer in type I cytochrome c_3 from *D. africanus*. Pure TpIc_3 (left panel) and TpIc_3 with 4% TpIIc_3 (right panel). The italic numerals show the oxidation stages involved in each diagonal or cross peak. The curves were fitted using Eq. 7.

In each of the four samples, the fits to Eq. 7 showed that stage *2* was the most abundant species, forming about 50% of the total (see Table 4.1). Comparison with the proportions calculated from the thermodynamic parameters given in (Paquete *et al.* 2007a) shows that the solution potential was close to −280 mV in each case

(Figure 4.6). The fitted rates of two- or three-electron transfers were generally smaller than the uncertainties estimated by fitting the data for individual methyl groups, and an F-test showed a probability of 99.9%, 39.3%, 79.0% and 99.9% that these rates were in fact zero for exchange in the presence of 0, 1, 2, and 4% TpIIc_3, respectively. Overall, there is no evidence for the transfer of two or more electrons in a single encounter. Multi-electron exchanges were therefore neglected for the remainder of the analysis. However, cross peaks corresponding to the transfer of two or three electrons appear because of successive electron transfer events occurring during the mixing time. The fitted rate matrices are presented in Table 4.2.

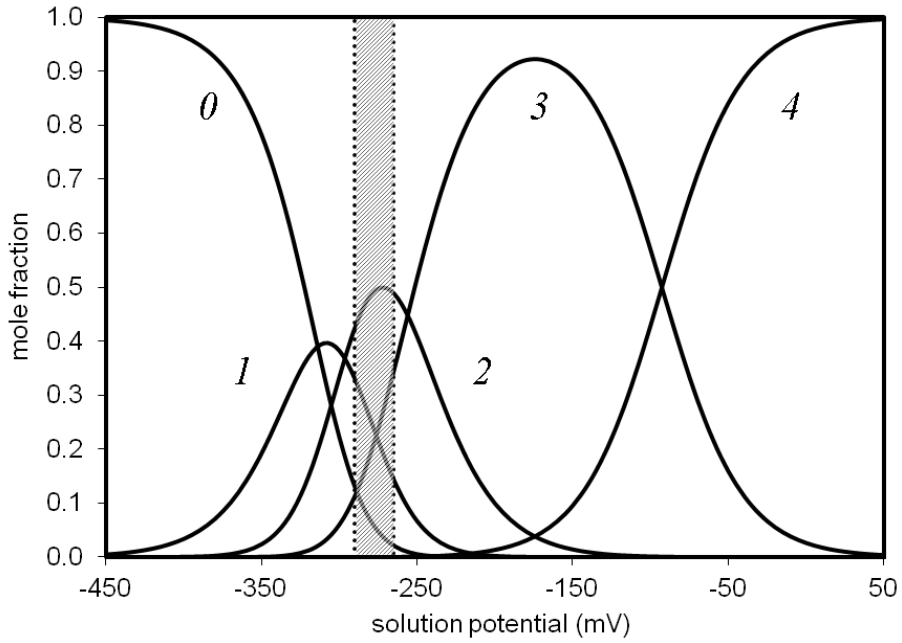

Figure 4.6 Mole fractions of the five oxidation stages of type I cytochrome c_3 from *D. africanus* as a function of solution potential. The curves were calculated for pH 7.6 using parameters from (Paquete *et al.* 2007a). The region of potentials of the NMR samples is indicated by a shaded band.

Table 4.1 Mole fractions of the oxidation stages of type I cytochrome c_3 from *D. africanus* obtained by fitting NMR data to Eq. 7. The RMSD of the fits for individual methyl groups are given in parentheses.

	Stage *0*	Stage *1*	Stage *2*	Stage *3*
1mM TpIc_3	0.06 (0.01)	0.24 (0.03)	0.48 (0.06)	0.22 (0.02)
+1% TpIIc_3	0.09 (0.02)	0.28 (0.03)	0.47 (0.04)	0.15 (0.02)
+2% TpIIc_3	0.09 (0.02)	0.28 (0.03)	0.47 (0.05)	0.16 (0.02)
+4% TpIIc_3	0.05 (0.01)	0.25 (0.02)	0.51 (0.05)	0.19 (0.02)

Table 4.2 The fitted matrices ($\mathbf{M}_0^{-1/2}\mathbf{L}\mathbf{M}_0^{1/2}$) obtained for 1 mM TpI$c_3$ in the presence of 0, 1, 2, or 4% TpIIc_3. The units are s^{-1} and the elements are ordered from oxidation stage *0* to stage *3*.

0% TpIIc_3	stage *0*	stage *1*	stage *2*	stage *3*
	-408.2	200.9	0.0	0.0
	200.9	-382.8	197.8	0.0
	0.0	197.8	-277.2	180.1
	0.0	0.0	180.1	-299.1

1% TpIIc_3	stage *0*	stage *1*	stage *2*	stage *3*
	-594.8	341.2	0.0	0.0
	341.2	-580.0	297.9	0.0
	0.0	297.9	-411.8	287.2
	0.0	0.0	287.2	-559.6

2% TpIIc_3	stage *0*	stage *1*	stage *2*	stage *3*
	-500.1	276.0	0.0	0.0
	276.0	-603.4	348.7	0.0
	0.0	348.7	-489.9	363.6
	0.0	0.0	363.6	-697.0

4% TpIIc_3	stage *0*	stage *1*	stage *2*	stage *3*
	-1195.9	560.7	0.0	0.0
	560.7	-930.6	469.2	0.0
	0.0	469.2	-623.4	479.6
	0.0	0.0	479.6	-873.1

Electron transfer may occur when two molecules in oxidation stages i and j collide:

$$C_i + C_j \rightarrow C_{i+1} + C_{j-1} \tag{8}$$

with the restrictions in the tetrahaem cytochrome that $i<4$ and $j>0$. The rate constant for this reaction can be predicted by Marcus theory (Marcus and Sutin 1985) using the energies of the individual forms (Paquete *et al.* 2007a):

$$k = Z \exp\left(\frac{-\left[\lambda - \left(e_i + e_j\right) + \left(e_{i+1} + e_{j-1}\right)\right]^2}{4\lambda RT} \right) \tag{9}$$

where λ is the reorganisation energy, which has the approximate value of 0.7 eV (0.7 F Jmol^{-1}) in this case (Sulpizi *et al.* 2007). The energies also determine the equilibrium concentrations of the forms,

$$[C_i] = [C_{tot}] \exp(-e_i / \mathrm{R}T) / \sum_j \exp(-e_j / \mathrm{R}T) \tag{10}$$

where $[C_{tot}]$ is the total concentration of cytochrome. Hence the reaction of Eq. 8 gives a flux from C_i to C_{i+1} (and equally from C_j to C_{j-1}) of $k[C_i][C_j]$. It is appropriate to use the concentrations of the oxidation stages rather than those of the haem microstates because the geometry suggests that intramolecular electron exchange should be at least as fast as the intermolecular electron exchange. There is a complication insofar as TpIc_3 has an important protonation site, and the rate of proton transfer is likely to be much slower than that of electron transfer (Turner *et al.* 1996). Therefore, protonated and deprotonated forms should be treated separately. This calculation, using the parameters at 298 K (Paquete *et al.* 2007a), pH 7.6 and a solution potential of −280 mV, assuming equal coupling in all collisions and adding terms from all possible combinations of oxidation stages, gives fluxes $C_0 \rightarrow C_1$, $C_1 \rightarrow C_2$, and $C_2 \rightarrow C_3$ in the ratio 1.0:2.7:2.4. The experimentally determined fluxes between oxidation stages are shown in Figure 4.7. The uncertainties for the flux between

stages *0* and *1* are greater because of the small population of stage *0* and the fact that cross peaks could only be measured on one side of the diagonal. However, in all cases, it is clear that the flux increases with an approximately linear dependence on the amount of TpIIc_3 added. The ratios of the fluxes determined for pure TpIc_3 are 1.0:2.9:2.5, which are in reasonable agreement with the ratios predicted by Marcus theory.

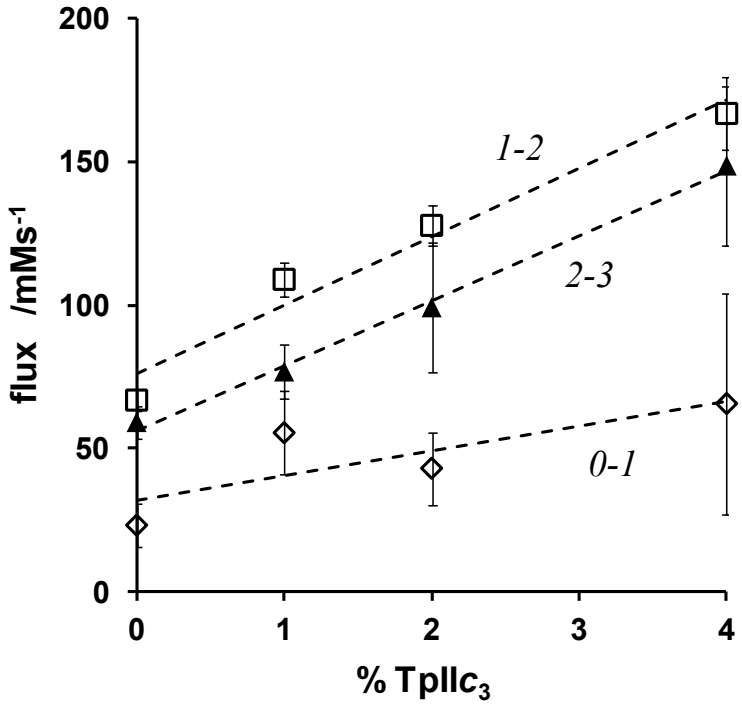

Figure 4.7 Flux between oxidation stages *1* and *2* (open squares), stages *2* and *3* (filled triangles) and stages *0* and *1* (open diamonds). The dashed lines are linear fits to the fluxes as a function of added TpIIc_3, with error bars from the RMSD of fits for individual methyl groups.

The frequency, Z in Eq. 9, may be approximated by k_{diff} the Stokes-Einstein equation for diffusion control:

$$k_{diff} = 8RT/3\eta \quad (11)$$

where the viscosity of water, η, is 0.89 cP at 298 K. This is a gross approximation, but we have no information about the equilibrium constant for the formation of the transient protein-protein complexes. The diffusion controlled fluxes in TpIc_3 are then calculated to be 770, 2080, and 1840 mMs^{-1}, about thirty times the observed values, as would be expected if not all collisions are able to lead to electron transfer.

Addition of small amounts of TpIIc_3 increases the flux between the oxidation stages of TpIc_3 molecules in an approximately linear fashion. Since the N-terminus is on the far side of a haem from the proposed binding site (Pieulle *et al.* 2005), the effect of the incomplete cyclisation of the terminal glutamine should be small. The concentrations of TpIIc_3 used here, a maximum of 40 μM, are too small for TpIIc_3 resonances to be observed directly and analysed, although its assignments are known (Pereira *et al.* 2002). However, electron transfer between TpIc_3 and TpIIc_3 adds to the fluxes between oxidation stages observed for TpIc_3. The effect on the flux between oxidation stages *0* and *1* is rather uncertain because of the low concentration of stage *0* and the proximity of signals to the residual water peak, but it agrees with the other values within experimental error: 4% TpIIc_3 increases the flux between the oxidation stages of TpIc_3 by a factor of 2.5. This implies that the rate of electron transfer between TpIc_3 and TpIIc_3 is about 37 times (*i.e.* 1.5/0.04) greater than that between TpIc_3 molecules. Allowing for the approximations in Eq. 11, this suggests that the reaction between TpIc_3 and TpIIc_3 is diffusion controlled.

CONCLUSIONS

No evidence was found for two-electron transfers occurring in the lifetime of the TpIc_3 encounter complexes. However, electron transfer between TpIc_3 and TpIIc_3 was much faster than transfer between TpIc_3 molecules and essentially diffusion controlled. This is good evidence for the two cytochromes being physiological partners; it has already been shown that TpIc_3 is the likely partner of hydrogenase and that TpIIc_3 is not (Pieulle *et al.* 1996). The failure to detect two-electron transfers between TpIc_3 and TpIIc_3 does not eliminate the possibility that TpIc_3 serves to transport two electrons and protons from the hydrogenase to the membrane. When TpIIc_3 is associated with a membrane complex, electrons should be drained by the complex such that the TpIIc_3 is mainly in the fully oxidised form (Paquete *et al.* 2007a). By contrast, there is only about 1% of TpIIc_3 oxidation stage *4* at the solution potential of about -280 mV used here. If a two-electron transfer occurs from TpIc_3 to fully oxidised TpIIc_3 then it would only be detectable in a non-equilibrium system.

Chapter 5

Concluding remarks

The importance of metal centres in proteins has been known for many years. The haem, consisting of a porphyrin structure with a central iron atom, is one of the most widespread metal centres and is involved in a variety of processes, usually involving the binding of ligands and/or electron transfer. The understanding of how haem proteins function is naturally of great importance and was the main motivation for this thesis. The work consisted of three parts: the binding of small molecules, the control of the rate of reduction, and the transfer of electrons between multihaem proteins. As models for our study, the following proteins were used: the single-haem cytochrome *c*" from *Methylophilus methylotrophus* and two cytochromes c_3 (type I and type II) from *Desulfovibrio africanus*. We have contributed incremental but significant results for the continuing study of haem proteins, and some suggestions for further work.

Many haem proteins favour the binding of some ligands while discriminating against others. They do this by adjusting the electrostatic and spatial conditions around the haem to fit the properties of the ligands. In the case of cytochrome *c*", presented in this thesis, the selectivity is towards NO, and steric hindrance seems to play a role. Another group of bacterial monohaem proteins, cytochromes *c*', has been previously found to be selective towards NO, and in *Paracoccus denitrificans* it has been implicated in the NO metabolism. They have also been used as a model for the haem domain of the human NO sensor Guanylate Cyclase. The haem is 5-coordinated in the reduced form and NO is thought to bind to the proximal side with the consequent detachment of the histidine. This is not observed in cyt *c*" where, despite the detachment of the proximal histidine, NO seems to bind to the distal side.

Understanding the mechanisms of ligand discrimination can be useful, not only in the efficient design of drugs that target these proteins, but also in the development of engineered versions that could be used as biosensors. Our results show a high selectivity of the reduced cyt *c*" towards NO. The reasons for this selectivity are not obvious but the rather restricted space around the haem may play a role. A detailed

three-dimensional structure of the protein in the NO-bound form would be a great step in clarifying this issue. It is clear however that despite the eventual detachment of the proximal histidine (see Figure 2.16), NO does not bind to that side of the haem. The reason may very well be structural, but without knowing the organization of the haem pocket in this detached form, it is not possible to draw any conclusions.

It is still not known what role cyt *c*'' plays in the cell. The high selectivity for NO could be physiologically relevant. The monohaem cytochrome *c*', which is also highly selective for NO, has been implicated in resistance to toxic levels of NO in the photosynthetic bacterium *Rhodobacter capsulatus* (Cross *et al.* 2000). A different cytochrome *c*' has been shown to bind NO reversibly in the denitrifying bacterium *Paracoccus denitrificans* (Moir 1999). NO is available in natural environments as a result disproportionation of nitrite or via nitrification and denitrification. Organisms expressing cytochrome *c*' would have a protecting mechanism against the damaging effects of NO in these environments (Moir 1999). *M. methylotrophus* is a significantly different organism but cyt *c*'' could play a similar role. This could be investigated further by studying the effect of NO in the growth profiles and the O_2 uptake of wild-type *M. methylotrophus* and mutants with the gene silenced. Cyt *c*'' is probably not required for normal growth since many attempts to produce it in the native organism yielded no protein. This was the reason why we started to produce the recombinant protein. Possibly the presence of small amounts of NO may induce the expression of cyt *c*'' as a defence mechanism.

It would also be of interest to develop an NO biosensor prepared with cyt *c*''. NO biosensors based on haem proteins have already been constructed. Haemoglobin has been used to develop an electrochemical biosensor (Fan *et al.* 2000; Fan *et al.* 2004), while an optical biosensor has been developed using the haem domain of soluble guanylate cyclase labelled with a fluorescent dye (Barker *et al.* 1999). The main features necessary for the construction of such a sensor are stability, selectivity and sensitivity. Although fairly stable and selective, the sensitivity of cyt *c*'' lags behind that

of the other proteins. However, engineering of the cyt *c*" could be attempted in order to improve the affinity for NO.

The study of multihaem cytochromes has a long history in our group. These proteins have a fundamental role in the bioenergetic metabolism of a number of bacterial organisms, some of which have proposed applications in the bioremediation of contaminated environments and in energy production. The complete characterization of these proteins is a step further in understanding their metabolism. The methodology to obtain the thermodynamic parameters has been developed in our group and relies on redox titrations followed by 2D-NMR and UV-visible spectroscopy. The kinetic characterization of each haem was also developed in our group and takes into account the thermodynamic parameters and the theory of Marcus together to analyse the results of stopped-flow experiments. A few key assumptions are made in this model, namely that, after the encounter between the protein and an external electron donor ($SO_2^{\bullet -}$ in our case), the major factor controlling the rate of electron transfer is the thermodynamic driving force, *i.e.* the difference in reduction potential between the electron donor and the acceptor. This implies that the electrostatic interactions are neglected. In order to test this assumption we studied the influence of the ionic strength on both the reduction potential and the rate of reduction of cyt *c*". By extrapolation to infinite ionic strength, we were able to eliminate the electrostatic interactions and isolate the contribution of the thermodynamic factors. The change in the rates between pH 4.5 and 7.7 was mainly due to the change in the reduction potential of cyt *c*" caused by the change in the protonation state of the haem propionate rather than a direct effect of electrostatic repulsion of $SO_2^{\bullet -}$. Additionally, three mutants were produced, in which one or two positive charges were removed close to the exposed edge of the haem, a likely point of access of the reducing agent. In none of these cases was the reduction potential or the rates of reduction at infinite ionic strength significantly changed. So, in this work, we were able to successfully separate the effects of electrostatics and reduction potential, and found that the change in

reduction potential is more important, even for a charge close to the haem, such as the propionate. The electrostatic repulsion decreases rapidly for charges further from the haem, as can be observed in the experiments with the mutants. Therefore, changes in charge can be neglected for most haems in a multihaem protein, and are relatively unimportant even for a haem whose propionate forms a redox-Bohr group.

The thermodynamic and kinetic characterization of individual proteins is unquestionably important; however, it is also desirable to obtain information about the reactions between physiological partners. In *Desulvovibrio africanus*, the type I cyt c_3 is thought to deliver the electrons it receives from the periplasmic hydrogenase to another tetrahaem cyt c_3 (type II) associated with the cytoplasmic membrane. Moreover, the cytochromes possess all the thermodynamic features necessary to allow the transfer of two electrons in a single step. We have shown that the two proteins are most likely physiological partners, but a two electron transfer step could not be observed. However, it should not be ruled out because, in contrast to the in vivo non-equilibrium situation, here we do not have a means of draining electrons from tpIIc_3.

The confirmation of the functional interaction of TpIc_3 with TpIIc_3 has elucidated a key step in the bioenergetic metabolism of *Desulfovibrionaceae*. However, this system requires further study, in particular the interaction of TpIc_3 with the periplasmic hydrogenase and TpIIc_3 with the transmembrane complex. It would be worth seeing whether a two electron transfer step could be observed in these cases. In theory this would also be viable because the oxidation of H_2 produces two electrons and, as stated before, the thermodynamic properties of TpIc_3 favour the capture of a second electron following the capture of the first one. This would be difficult in practice because TpIc_3 is rapidly and completely reduced in the presence of H_2 and hydrogenase, making it necessary to provide an electron sink. The repetition of the TpIc_3/TpIIc_3 experiments in the presence of the transmembrane complex would also be interesting but somewhat complicated since we would need a way to have the

Tmc intact and functional, and, again, a way to drain the electrons would be needed. It would be desirable to study not only the kinetics of the reactions but also the structural aspects of the interactions. This could be done by co-crystallization and determination of the x-ray structure of the two partners. However, there is no guarantee that the result would show a functional interaction, particularly in view of the fact that a fully reduced or fully oxidised sample would not have the proteins in functional states. Another method, used for the TpIc_3/TpIIc_3 system (Pieulle *et al.* 2005) could be to study how the presence of one protein affects the NMR spectrum (such as an HSQC spectrum) of the other. The more affected peaks would be in closer contact to the other protein, though, once again, the two would be in oxidation states that do not interact productively. An additional method is the computational docking of the two partners. Following the adjustment of the electrostatics of the two proteins to the correct oxidation states, the docking simulation would try to obtain the interactions that lead to the lowest energy.

The findings of chapters 3 and 4 provided significant results for the continuing study of multihaem cytochromes. This subject has gained importance since the discovery of a great number of multihaem proteins in organisms that perform the extracellular reduction of metal oxides, such as *Geobacter* and *Shewanella*. The confirmation that the driving force is the main factor controlling the rate of electron transfer encourages the further use of the model for the kinetic characterization of multihaem proteins. It also allows a more refined thermodynamic characterization by using the kinetic data together with the thermodynamic data. Several multihaem proteins have already been characterized but, given the great number of these proteins in these organisms, a considerable amount of work is yet to be done. Results from chapter 4, besides attesting the functional interaction of the two cytochromes, provides a new methodology for the study of electron transfer between multicentre redox proteins, as long as that the intramolecular electron transfer is fast and the intermolecular electron transfer is slow in the experiment time scale. Results from these experiments should

offer a clearer picture of the bioenergetic pathways in these organisms. Better knowledge of these pathways should, in turn, enable the improvement of the organisms to better perform in biotechnological applications, such as bioremediation and energy production.

References

Anderson, R.T., Vrionis, H.A., Ortiz-Bernad, I., Resch, C.T., Long, P.E., Dayvault, R., Karp, K., Marutzky, S., Metzler, D.R., Peacock, A., White, D.C., Lowe, M. and Lovley, D.R. (2003) Stimulating the in situ activity of *Geobacter* species to remove uranium from the groundwater of a uranium-contaminated aquifer. *Appl Environ Microbiol.* **69**(10):5884-91.

Andrew, C.R., Green, E.L., Lawson, D.M. and Eady, R.R. (2001) Resonance Raman studies of cytochrome c' support the binding of NO and CO to opposite sides of the heme: implications for ligand discrimination in heme-based sensors. *Biochemistry.* **40**(13):4115-22.

Andrew, C.R., George, S.J., Lawson, D.M. and Eady, R.R. (2002) Six- to five-coordinate heme-nitrosyl conversion in cytochrome c' and its relevance to guanylate cyclase. *Biochemistry*. **41**(7):2353-60.

Antonini, E. and Brunori, M. (1971). Hemoglobin and myoglobin in their reactions with ligands. North-Holland Pub. Co., Amsterdam.

Aono, S., Nakajima, H., Saito, K. and Okada, M. (1996) A novel heme protein that acts as a carbon monoxide-dependent transcriptional activator in Rhodospirillum rubrum. *Biochem Biophys Res Commun.* **228**(3):752-6.

Apel, K. and Hirt, H. (2004) Reactive oxygen species: metabolism, oxidative stress, and signal transduction. *Annu Rev Plant Biol.* **55**:373-99.

Arnoux, P., Haser, R., Izadi-Pruneyre, N., Lecroisey, A. and Czjzek, M. (2000) Functional aspects of the heme bound hemophore HasA by structural analysis of various crystal forms. *Proteins.* **41**(2):202-10.

Arslan, E., Schulz, H., Zufferey, R., Kunzler, P. and Thony-Meyer, L. (1998) Overproduction of the *Bradyrhizobium japonicum c*-type cytochrome subunits of the cbb_3 oxidase in *Escherichia coli*. *Biochem Biophys Res Commun.* **251**(3):744-7.

Atkins, P.W. and de Paula, J. (2006). Physical Chemistry, 8th ed. Oxford University Press.

Baker, N.A., Sept, D., Joseph, S., Holst, M.J. and McCammon, J.A. (2001) Electrostatics of nanosystems: application to microtubules and the ribosome. *Proc Natl Acad Sci U S A.* **98**(18):10037-41.

Balahura, R.J. and Johnson, M.D. (1987) Outer-sphere dithionite reductions of metal complexes. *Inorg Chem.* **26**(23):3860-3863.

Bamford, V.A., Bruno, S., Rasmussen, T., Appia-Ayme, C., Cheesman, M.R., Berks, B.C. and Hemmings, A.M. (2002) Structural basis for the oxidation of thiosulfate by a sulfur cycle enzyme. *EMBO J.* **21**(21):5599-610.

Barker, S.L.R., Zhao, Y.D., Marletta, M.A. and Kopelman, R. (1999) Cellular applications of a sensitive and selective fiber optic nitric oxide biosensor based on a dye-labeled heme domain of soluble guanylate cyclase. *Analytical Chemistry*. **71**(11):2071-2075.

Barton, L.L. and Fauque, G.D. (2009) Biochemistry, physiology and biotechnology of sulfate-reducing bacteria. *Adv Appl Microbiol.* **68**:41-98.

Batey, R.T., Cloutier, N., Mao, H. and Williamson, J.R. (1996) Improved large scale culture of *Methylophilus methylotrophus* for $^{13}C/^{15}N$ labeling and random fractional deuteration of ribonucleotides. *Nucleic Acids Res.* **24**(23):4836-7.

Beckman, J.S. and Koppenol, W.H. (1996) Nitric oxide, superoxide, and peroxynitrite: the good, the bad, and ugly. *Am J Physiol.* **271**(5 Pt 1):C1424-37.

Berry, M.J., George, S.J., Thomson, A.J., Santos, H. and Turner, D.L. (1990) Cytochrome *c*" isolated from *Methylophilus methylotrophus*. An example of bis-histidine-co-ordinated Fe^{3+} haem, with near-perpendicular orientation of the ligands. *Biochem J.* **270**(2):413-7.

Brennan, L., Turner, D.L., Fareleira, P. and Santos, H. (2001) Solution structure of *Methylophilus methylotrophus* cytochrome *c*": insights into the structural basis of haem-ligand detachment. *J Mol Biol.* **308**(2):353-65.

Bühler, H. and Baumann, R. (1982). Calibration of pH electrodes. Ingold booklets (E-Th5). Urdorf, Switzerland.

Carlson, H.K., Iavarone, A.T., Gorur, A., Yeo, B.S., Tran, R., Melnyk, R.A., Mathies, R.A., Auer, M. and Coates, J.D. (2012) Surface multiheme *c*-type cytochromes from *Thermincola potens* and implications for respiratory metal reduction by Gram-positive bacteria. *Proc Natl Acad Sci U S A.* **109**(5):1702-7.

Cassoly, R. and Gibson, Q. (1975) Conformation, co-operativity and ligand binding in human hemoglobin. *J Mol Biol.* **91**(3):301-13.

Catarino, T. and Turner, D.L. (2001) Thermodynamic control of electron transfer rates in multicentre redox proteins. *Chembiochem.* **2**(6):416-24.

Chen, L., Pereira, M.M., Teixeira, M., Xavier, A.V. and Le Gall, J. (1994) Isolation and characterization of a high molecular weight cytochrome from the sulfate reducing bacterium *Desulfovibrio gigas*. *FEBS Lett*. **347**(2-3):295-9.

Chien, J.C. and Dickinson, L.C. (1978) Reduction of cobalticytochrome *c* by dithionite. *J Biol Chem*. **253**(19):6965-72.

Coetser, S.E. and Cloete, T.E. (2005) Biofouling and biocorrosion in industrial water systems. *Crit Rev Microbiol*. **31**(4):213-32.

Coletta, M., Costa, H., De Sanctis, G., Neri, F., Smulevich, G., Turner, D.L. and Santos, H. (1997) pH dependence of structural and functional properties of oxidized cytochrome *c*" from *Methylophilus methylotrophus*. *J Biol Chem*. **272**(40):24800-4.

Cooper, C.E. (1999) Nitric oxide and iron proteins. *Biochim Biophys Acta*. **1411**(2-3):290-309.

Coppi, M.V., O'Neil R, A., Leang, C., Kaufmann, F., Methe, B.A., Nevin, K.P., Woodard, T.L., Liu, A. and Lovley, D.R. (2007) Involvement of *Geobacter sulfurreducens* SfrAB in acetate metabolism rather than intracellular, respiration-linked Fe(III) citrate reduction. *Microbiology*. **153**(Pt 10):3572-85.

Costa, H.S., Santos, H., Turner, D.L. and Xavier, A.V. (1992) Involvement of a labile axial histidine in coupling electron and proton transfer in *Methylophilus methylotrophus* cytochrome *c*". *Eur J Biochem*. **208**(2):427-33.

Costa, H.S., Santos, H. and Turner, D.L. (1993) Characterization of the haem environment in *Methylophilus methylotrophus* ferricytochrome *c*" by ^{1}H-NMR. *Eur J Biochem*. **215**(3):817-24.

Cox, R.P. and Hollaway, M.R. (1977) The reduction by dithionite of Fe(III) myoglobin derivatives with different ligands attached to the iron atom. A study by rapid-wavelength-scanning stopped-flow spectrophotometry. *Eur J Biochem*. **74**(3):575-87.

Cross, R., Aish, J., Paston, S.J., Poole, R.K. and Moir, J.W. (2000) Cytochrome *c*' from *Rhodobacter capsulatus* confers increased resistance to nitric oxide. *J Bacteriol*. **182**(5):1442-7.

Davis, K.L., Martin, E., Turko, I.V. and Murad, F. (2001) Novel effects of nitric oxide. *Annu Rev Pharmacol Toxicol*. **41**:203-36.

Deinum, G., Stone, J.R., Babcock, G.T. and Marletta, M.A. (1996) Binding of nitric oxide and carbon monoxide to soluble guanylate cyclase as observed with Resonance raman spectroscopy. *Biochemistry*. **35**(5):1540-7.

Di Paolo, R.E., Pereira, P.M., Gomes, I., Valente, F.M., Pereira, I.A. and Franco, R. (2006) Resonance Raman fingerprinting of multiheme cytochromes from the cytochrome c_3 family. *J Biol Inorg Chem*. **11**(2):217-24.

Dixon, M. (1971) The acceptor specificity of flavins and flavoproteins. I. Techniques for anaerobic spectrophotometry. *Biochim Biophys Acta*. **226**(2):241-58.

Dolinsky, T.J., Nielsen, J.E., McCammon, J.A. and Baker, N.A. (2004) PDB2PQR: an automated pipeline for the setup of Poisson-Boltzmann electrostatics calculations. *Nucleic Acids Res*. **32**(Web Server issue):W665-7.

Dröge, W. (2002) Free radicals in the physiological control of cell function. *Physiol Rev*. **82**(1):47-95.

Enguita, F.J., Pohl, E., Turner, D.L., Santos, H. and Carrondo, M.A. (2006) Structural evidence for a proton transfer pathway coupled with haem reduction of cytochrome *c*'' from *Methylophilus methylotrophus*. *J Biol Inorg Chem*. **11**(2):189-96.

Fan, C.H., Li, G.X., Zhu, J.Q. and Zhu, D.X. (2000) A reagentless nitric oxide biosensor based on hemoglobin-DNA films. *Analytica Chimica Acta*. **423**(1):95-100.

Fan, C.H., Liu, X.J., Pang, J.T., Li, G.X. and Scheer, H. (2004) Highly sensitive voltammetric biosensor for nitric oxide based on its high affinity with hemoglobin. *Analytica Chimica Acta*. **523**(2):225-228.

Fernhoff, N.B., Derbyshire, E.R. and Marletta, M.A. (2009) A nitric oxide/cysteine interaction mediates the activation of soluble guanylate cyclase. *Proc Natl Acad Sci U S A*. **106**(51):21602-7.

Fredrickson, J.K., Romine, M.F., Beliaev, A.S., Auchtung, J.M., Driscoll, M.E., Gardner, T.S., Nealson, K.H., Osterman, A.L., Pinchuk, G., Reed, J.L., Rodionov, D.A., Rodrigues, J.L., Saffarini, D.A., Serres, M.H., Spormann, A.M., Zhulin, I.B. and Tiedje, J.M. (2008) Towards environmental systems biology of *Shewanella*. *Nat Rev Microbiol*. **6**(8):592-603.

Fulop, V., Moir, J.W., Ferguson, S.J. and Hajdu, J. (1995) The anatomy of a bifunctional enzyme: structural basis for reduction of oxygen to water and synthesis of nitric oxide by cytochrome cd_1. *Cell*. **81**(3):369-77.

Goldkorn, T. and Schejter, A. (1979) Electrostatic effects on the kinetics of oxidation-reduction reactions of *c*-type cytochromes. *J Biol Chem*. **254**(24):12562-6.

Gong, W., Hao, B., Mansy, S.S., Gonzalez, G., Gilles-Gonzalez, M.A. and Chan, M.K. (1998) Structure of a biological oxygen sensor: a new mechanism for heme-driven signal transduction. *Proc Natl Acad Sci U S A*. **95**(26):15177-82.

Gong, W., Hao, B. and Chan, M.K. (2000) New mechanistic insights from structural studies of the oxygen-sensing domain of Bradyrhizobium japonicum FixL. *Biochemistry*. **39**(14):3955-62.

Gullotta, F., di Masi, A., Coletta, M. and Ascenzi, P. (2012) CO metabolism, sensing, and signaling. *Biofactors*. **38**(1):1-13.

Hamilton, W.A. (2003) Microbially influenced corrosion as a model system for the study of metal microbe interactions: a unifying electron transfer hypothesis. *Biofouling*. **19**(1):65-76.

Hansen, T.A. (1994) Metabolism of sulfate-reducing prokaryotes. *Antonie Van Leeuwenhoek*. **66**(1-3):165-85.

Hodges, H.L., Holwerda, R.A. and Gray, H.B. (1974) Kinetic studies of the reduction of ferricytochrome *c* by $Fe(EDTA)^{2-}$. *J Am Chem Soc*. **96**(10):3132-7.

Hoffman, R.A. and Forsén, S. (1966) High resolution nuclear magnetic double and multiple resonance. *Prog Nucl Magn Reson Spectrosc*. **1**(0):15-204.

Ishimoto, M., Koyama, J. and Nagai, Y. (1954) A Cytochrome and a Green Pigment of Sulfate-reducing Bacteria. *Bull Chem Soc Jpn*. **27**(8):564b-565.

Jain, R. and Chan, M.K. (2003) Mechanisms of ligand discrimination by heme proteins. *J Biol Inorg Chem*. **8**(1-2):1-11.

Jeener, J., Meier, B.H., Bachmann, P. and Ernst, R.R. (1979) Investigation of Exchange Processes by 2-Dimensional Nmr-Spectroscopy. *J Chem Phys*. **71**(11):4546-4553.

Jenkins, O., Byrom, D. and Jones, D. (1987) *Methylophilus*: a New Genus of Methanol-Utilizing Bacteria. *Int J Syst Bacteriol.* **37**(4):446-448.

Jones, M.G., Bickar, D., Wilson, M.T., Brunori, M., Colosimo, A. and Sarti, P. (1984) A re-examination of the reactions of cyanide with cytochrome c oxidase. *Biochem J.* **220**(1):57-66.

Kassner, R.J. (1991) Ligand binding properties of cytochromes c'. *Biochim Biophys Acta.* **1058**(1):8-12.

Keefer, L.K., Nims, R.W., Davies, K.M. and Wink, D.A. (1996) "NONOates" (1-substituted diazen-1-ium-1,2-diolates) as nitric oxide donors: convenient nitric oxide dosage forms. *Methods Enzymol.* **268**:281-93.

Kuchinskas, M., Li, H., Conrad, M., Roberts, G. and Poulos, T.L. (2006) The role of the DNA-binding domains in CooA activation. *Biochemistry.* **45**(23):7148-53.

Lawson, D.M., Stevenson, C.E., Andrew, C.R. and Eady, R.R. (2000) Unprecedented proximal binding of nitric oxide to heme: implications for guanylate cyclase. *EMBO J.* **19**(21):5661-71.

Lee, B., Usov, O.M., Grigoryants, V.M., Myers, W.K., Shapleigh, J.P. and Scholes, C.P. (2009) The role of arginine-127 at the proximal NO-binding site in determining the electronic structure and function of 5-coordinate NO-heme in cytochrome c' of Rhodobacter sphaeroides. *Biochemistry.* **48**(38):8985-93.

Leys, D., Backers, K., Meyer, T.E., Hagen, W.R., Cusanovich, M.A. and Van Beeumen, J.J. (2000) Crystal structures of an oxygen-binding cytochrome *c* from *Rhodobacter sphaeroides*. *J Biol Chem.* **275**(21):16050-6.

Li, H., Robertson, A.D. and Jensen, J.H. (2005) Very fast empirical prediction and rationalization of protein pK_a values. *Proteins.* **61**(4):704-21.

Lim, A.R. and Mauk, A.G. (1985) Kinetic analysis of metsulphmyoglobin and metmyoglobin reduction by $Fe(EDTA)^{2-}$. *Biochem J.* **229**(3):765-9.

Lim, A.R., Sishta, B.P. and Grant Mauk, A. (2006) Contribution of the heme propionate groups to the electron transfer and electrostatic properties of myoglobin. *J Inorg Biochem.* **100**(12):2017-23.

Liu, M.C., Costa, C., Coutinho, I.B., Moura, J.J., Moura, I., Xavier, A.V. and LeGall, J. (1988) Cytochrome components of nitrate- and sulfate-respiring *Desulfovibrio desulfuricans* ATCC 27774. *J Bacteriol.* **170**(12):5545-51.

Logan, B.E. (2009) Exoelectrogenic bacteria that power microbial fuel cells. *Nat Rev Microbiol*. **7**(5):375-81.

Louro, R.O. (2007) Proton thrusters: overview of the structural and functional features of soluble tetrahaem cytochromes c_3. *J Biol Inorg Chem*. **12**(1):1-10.

Lovley, D.R., Baedecker, M.J., Lonergan, D.J., Cozzarelli, I.M., Phillips, E.J.P. and Siegel, D.I. (1989) Oxidation of Aromatic Contaminants Coupled to Microbial Iron Reduction. *Nature*. **339**(6222):297-300.

Lovley, D.R., Coates, J.D., BluntHarris, E.L., Phillips, E.J.P. and Woodward, J.C. (1996) Humic substances as electron acceptors for microbial respiration. *Nature*. **382**(6590):445-448.

Lovley, D.R. (1997) Potential for anaerobic bioremediation of BTEX in petroleum-contaminated aquifers. *Journal of Industrial Microbiology & Biotechnology*. **18**(2-3):75-81.

Lovley, D.R. (2001) Bioremediation. Anaerobes to the rescue. *Science*. **293**(5534):1444-6.

Lovley, D.R., Holmes, D.E. and Nevin, K.P. (2004) Dissimilatory Fe(III) and Mn(IV) reduction. *Adv Microb Physiol*. **49**:219-86.

Lovley, D.R. (2006a) Bug juice: harvesting electricity with microorganisms. *Nat Rev Microbiol*. **4**(7):497-508.

Lovley, D.R. (2006b) Microbial fuel cells: novel microbial physiologies and engineering approaches. *Curr Opin Biotechnol*. **17**(3):327-32.

Lukat-Rodgers, G.S. and Rodgers, K.R. (1997) Characterization of ferrous FixL-nitric oxide adducts by resonance Raman spectroscopy. *Biochemistry*. **36**(14):4178-87.

Magro, V., Pieulle, L., Forget, N., Guigliarelli, B., Petillot, Y. and Hatchikian, E.C. (1997) Further characterization of the two tetraheme cytochromes c_3 from *Desulfovibiro africanus*: nucleotide sequences, EPR spectroscopy and biological activity. *Biochim Biophys Acta*. **1342**(2):149-63.

Makhatadze, G.I. (1999) Thermodynamics of protein interactions with urea and guanidinium hydrochloride. *J Phys Chem B*. **103**(23):4781-4785.

Makino, R., Matsuda, H., Obayashi, E., Shiro, Y., Iizuka, T. and Hori, H. (1999) EPR characterization of axial bond in metal center of native and cobalt-substituted guanylate cyclase. *J Biol Chem.* **274**(12):7714-23.

Marcus, R.A. and Sutin, N. (1985) Electron transfers in chemistry and biology. *Biochim Biophys Acta.* **811**(3):265-322.

Matias, P.M., Coelho, R., Pereira, I.A., Coelho, A.V., Thompson, A.W., Sieker, L.C., Gall, J.L. and Carrondo, M.A. (1999) The primary and three-dimensional structures of a nine-haem cytochrome *c* from *Desulfovibrio desulfuricans* ATCC 27774 reveal a new member of the Hmc family. *Structure.* **7**(2):119-30.

Matias, P.M., Soares, C.M., Saraiva, L.M., Coelho, R., Morais, J., Le Gall, J. and Carrondo, M.A. (2001) [NiFe] hydrogenase from *Desulfovibrio desulfuricans* ATCC 27774: gene sequencing, three-dimensional structure determination and refinement at 1.8 A and modelling studies of its interaction with the tetrahaem cytochrome c_3. *J Biol Inorg Chem.* **6**(1):63-81.

Matias, P.M., Pereira, I.A., Soares, C.M. and Carrondo, M.A. (2005) Sulphate respiration from hydrogen in *Desulfovibrio* bacteria: a structural biology overview. *Prog Biophys Mol Biol.* **89**(3):292-329.

Mauk, A.G., Scott, R.A. and Gray, H.B. (1980) Distances of electron-transfer to and from metalloprotein redox sites in reactions with inorganic complexes. *J Am Chem Soc.* **102**(13):4360-4363.

Mayburd, A.L. and Kassner, R.J. (2002) Mechanism and biological role of nitric oxide binding to cytochrome c'. *Biochemistry.* **41**(39):11582-91.

McArdle, J.V., Gray, H.B., Creutz, C. and Sutin, N. (1974) Kinetic studies of the oxidation of ferrocytochrome *c* from horse heart and *Candida krusei* by tris(1,10-phenanthroline)cobalt(III). *J Am Chem Soc.* **96**(18):5737-41.

Meier, M., Janosik, M., Kery, V., Kraus, J.P. and Burkhard, P. (2001) Structure of human cystathionine beta-synthase: a unique pyridoxal 5'-phosphate-dependent heme protein. *EMBO J.* **20**(15):3910-6.

Messias, A.C., Kastrau, D.H., Costa, H.S., LeGall, J., Turner, D.L., Santos, H. and Xavier, A.V. (1998) Solution structure of *Desulfovibrio vulgaris* (Hildenborough) ferrocytochrome c_3: structural basis for functional cooperativity. *J Mol Biol.* **281**(4):719-39.

Moir, J.W. (1999) Cytochrome *c'* from *Paracoccus denitrificans*: spectroscopic studies consistent with a role for the protein in nitric oxide metabolism. *Biochim Biophys Acta*. **1430**(1):65-72.

Moncada, S., Palmer, R.M. and Higgs, E.A. (1991) Nitric oxide: physiology, pathophysiology, and pharmacology. *Pharmacol Rev*. **43**(2):109-42.

Moore, E.G. and Gibson, Q.H. (1976) Cooperativity in the dissociation of nitric oxide from hemoglobin. *J Biol Chem*. **251**(9):2788-94.

Moss, G.P. (1988) Nomenclature of tetrapyrroles. Recommendations 1986 IUPAC-IUB Joint Commission on Biochemical Nomenclature (JCBN). *Eur J Biochem*. **178**(2):277-328.

Moura, J.J., Santos, H., Moura, I., LeGall, J., Moore, G.R., Williams, R.J. and Xavier, A.V. (1982) NMR redox studies of *Desulfovibrio vulgaris* Cytochrome c_3. Electron transfer mechanisms. *Eur J Biochem*. **127**(1):151-5.

Muyzer, G. and Stams, A.J. (2008) The ecology and biotechnology of sulphate-reducing bacteria. *Nat Rev Microbiol*. **6**(6):441-54.

Nealson, K.H. and Saffarini, D. (1994) Iron and manganese in anaerobic respiration: environmental significance, physiology, and regulation. *Annu Rev Microbiol*. **48**:311-43.

Neta, P., Huie, R.E. and Harriman, A. (1987) One-electron-transfer reactions of the couple SO_2/SO_2^- in aqueous solutions. Pulse radiolytic and cyclic voltammetric studies. *J Phys Chem*. **91**(6):1606-1611.

Nørager, S., Legrand, P., Pieulle, L., Hatchikian, C. and Roth, M. (1999) Crystal structure of the oxidised and reduced acidic cytochrome c_3 from *Desulfovibrio africanus*. *J Mol Biol*. **290**(4):881-902.

Ogata, M., Kiuchi, N. and Yagi, T. (1993) Characterization and redox properties of high molecular mass cytochrome c_3 (Hmc) isolated from *Desulfovibrio vulgaris* Miyazaki. *Biochimie*. **75**(11):977-83.

Olson, J.S. and Phillips, G.N. (1997) Myoglobin discriminates between O-2, NO, and CO by electrostatic interactions with the bound ligand. *J Biol Inorg Chem*. **2**(4):544-552.

Othman, S., Richaud, P., Vermeglio, A. and Desbois, A. (1996) Evidence for a proximal histidine interaction in the structure of cytochromes c in solution: a resonance Raman study. *Biochemistry*. **35**(28):9224-34.

Paquete, C.M., Pereira, P.M., Catarino, T., Turner, D.L., Louro, R.O. and Xavier, A.V. (2007a) Functional properties of type I and type II cytochromes c_3 from *Desulfovibrio africanus*. *Biochim Biophys Acta*. **1767**(2):178-88.

Paquete, C.M., Turner, D.L., Louro, R.O., Xavier, A.V. and Catarino, T. (2007b) Thermodynamic and kinetic characterisation of individual haems in multicentre cytochromes c_3. *Biochim Biophys Acta*. **1767**(9):1169-79.

Paquete, C.M., Saraiva, I.H., Calcada, E. and Louro, R.O. (2010) Molecular basis for directional electron transfer. *J Biol Chem*. **285**(14):10370-5.

Park, J.S., Ohmura, T., Kano, K., Sagara, T., Niki, K., Kyogoku, Y. and Akutsu, H. (1996) Regulation of the redox order of four hemes by pH in cytochrome c_3 from *D. vulgaris* Miyazaki F. *Biochim Biophys Acta*. **1293**(1):45-54.

Pereira, P.M., Pacheco, I., Turner, D.L. and Louro, R.O. (2002) Structure-function relationship in type II cytochrome c_3 from *Desulfovibrio africanus*: a novel function in a familiar heme core. *J Biol Inorg Chem*. **7**(7-8):815-22.

Pessanha, M., Morgado, L., Louro, R.O., Londer, Y.Y., Pokkuluri, P.R., Schiffer, M. and Salgueiro, C.A. (2006) Thermodynamic characterization of triheme cytochrome PpcA from *Geobacter sulfurreducens*: evidence for a role played in e^-/H^+ energy transduction. *Biochemistry*. **45**(46):13910-7.

Pettigrew, G.W. and Moore, G.R. (1987). Cytochromes *c*: Biological Aspects. Springer-Verlag.

Pieulle, L., Haladjian, J., Bonicel, J. and Hatchikian, E.C. (1996) Biochemical studies of the *c*-type cytochromes of the sulfate reducer *Desulfovibrio africanus*. Characterization of two tetraheme cytochromes c_3 with different specificity. *Biochim Biophys Acta*. **1273**(1):51-61.

Pieulle, L., Morelli, X., Gallice, P., Lojou, E., Barbier, P., Czjzek, M., Bianco, P., Guerlesquin, F. and Hatchikian, E.C. (2005) The type I/type II cytochrome c_3 complex: an electron transfer link in the hydrogen-sulfate reduction pathway. *J Mol Biol*. **354**(1):73-90.

Pokkuluri, P.R., Londer, Y.Y., Duke, N.E., Erickson, J., Pessanha, M., Salgueiro, C.A. and Schiffer, M. (2004) Structure of a novel c_7-type three-heme cytochrome domain from a multidomain cytochrome *c* polymer. *Protein Sci*. **13**(6):1684-92.

Pollock, W.B., Loutfi, M., Bruschi, M., Rapp-Giles, B.J., Wall, J.D. and Voordouw, G. (1991) Cloning, sequencing, and expression of the gene encoding the high-molecular-weight cytochrome *c* from *Desulfovibrio vulgaris* Hildenborough. *J Bacteriol.* **173**(1):220-8.

Postgate, J.R. (1954) Dependence of sulphate reduction and oxygen utilization on a cytochrome in *Desulphovibrio*. *Biochem J.* **58**(330th Meeting):ix.

Price, N.J., Brennan, L., Faria, T.Q., Vijgenboom, E., Canters, G.W., Turner, D.L. and Santos, H. (2000) High yield of *Methylophilus methylotrophus* cytochrome *c*" by coexpression with cytochrome *c* maturation gene cluster from *Escherichia coli*. *Protein Expr Purif.* **20**(3):444-50.

Reid, L.S. and Mauk, A.G. (1982) Kinetic analysis of cytochrome b_5 reduction by $Fe(EDTA)^{2-}$. *J Am Chem Soc.* **104**(3):841-845.

Reid, L.S., Taniguchi, V.T., Gray, H.B. and Mauk, A.G. (1982) Oxidation-reduction equilibrium of cytochrome b_5. *J Am Chem Soc.* **104**(26):7516-7519.

Reid, L.S., Mauk, M.R. and Mauk, A.G. (1984) Role of heme propionate groups in cytochrome b_5 electron transfer. *J Am Chem Soc.* **106**(7):2182-2185.

Reynolds, M.F., Parks, R.B., Burstyn, J.N., Shelver, D., Thorsteinsson, M.V., Kerby, R.L., Roberts, G.P., Vogel, K.M. and Spiro, T.G. (2000) Electronic absorption, EPR, and resonance raman spectroscopy of CooA, a CO-sensing transcription activator from R. rubrum, reveals a five-coordinate NO-heme. *Biochemistry*. **39**(2):388-96.

Rivas, L., Murgida, D.H. and Hildebrandt, P. (2001) Surface-enhanced resonance Raman study of cytochrome *c*" from Methylophilus methylotrophus. *J Mol Struct*. **565**:193-196.

Russwurm, M. and Koesling, D. (2004) NO activation of guanylyl cyclase. *EMBO J.* **23**(22):4443-50.

Salgueiro, C.A., Turner, D.L., Santos, H., LeGall, J. and Xavier, A.V. (1992) Assignment of the redox potentials to the four haems in *Desulfovibrio vulgaris* cytochrome c_3 by 2D-NMR. *FEBS Lett*. **314**(2):155-8.

Santos, H., Moura, J.J., Moura, I., LeGall, J. and Xavier, A.V. (1984a) NMR studies of electron transfer mechanisms in a protein with interacting redox centres: *Desulfovibrio gigas* cytochrome c_3. *Eur J Biochem*. **141**(2):283-96.

Santos, H., Turner, D.L. and Xavier, A.V. (1984b) Two-Dimensional Nmr-Studies of Electron-Transfer in Cytochrome c_3. *J Magn Reson.* **59**(1):177-180.

Santos, H. and Turner, D.L. (1988) Characterization and NMR studies of a novel cytochrome *c* isolated from *Methylophilus methylotrophus* which shows a redox-linked change of spin state. *Biochim Biophys Acta.* **954**:277-286.

Schejter, A., Ryan, M.D., Blizzard, E.R., Zhang, C., Margoliash, E. and Feinberg, B.A. (2006) The redox couple of the cytochrome c cyanide complex: the contribution of heme iron ligation to the structural stability, chemical reactivity, and physiological behavior of horse cytochrome c. *Protein Sci.* **15**(2):234-41.

Shelobolina, E.S., Coppi, M.V., Korenevsky, A.A., DiDonato, L.N., Sullivan, S.A., Konishi, H., Xu, H., Leang, C., Butler, J.E., Kim, B.C. and Lovley, D.R. (2007) Importance of *c*-Type cytochromes for U(VI) reduction by *Geobacter sulfurreducens*. *BMC Microbiol.* **7**:16.

Shi, L., Squier, T.C., Zachara, J.M. and Fredrickson, J.K. (2007) Respiration of metal (hydr)oxides by *Shewanella* and *Geobacter*: a key role for multihaem *c*-type cytochromes. *Mol Microbiol.* **65**(1):12-20.

Soldatova, A.V., Ibrahim, M., Olson, J.S., Czernuszewicz, R.S. and Spiro, T.G. (2010) New light on NO bonding in Fe(III) heme proteins from resonance Raman spectroscopy and DFT modeling. *J Am Chem Soc.* **132**(13):4614-25.

Springer, B.A., Sligar, S.G., Olson, J.S. and Phillips, G.N. (1994) Mechanisms of Ligand Recognition in Myoglobin. *Chem Rev.* **94**(3):699-714.

Stephen, H., Stephen, T. and Kafarov, V.V. (1963). Solubilities of inorganic and organic compounds. Pergamon Press, Oxford, UK.

Stone, J.R. and Marletta, M.A. (1994) Soluble guanylate cyclase from bovine lung: activation with nitric oxide and carbon monoxide and spectral characterization of the ferrous and ferric states. *Biochemistry.* **33**(18):5636-40.

Stone, J.R. and Marletta, M.A. (1995) The ferrous heme of soluble guanylate cyclase: formation of hexacoordinate complexes with carbon monoxide and nitrosomethane. *Biochemistry.* **34**(50):16397-403.

Stone, J.R., Sands, R.H., Dunham, W.R. and Marletta, M.A. (1996) Spectral and ligand-binding properties of an unusual hemoprotein, the ferric form of soluble guanylate cyclase. *Biochemistry.* **35**(10):3258-62.

Sulpizi, M., Raugei, S., VandeVondele, J., Carloni, P. and Sprik, M. (2007) Calculation of redox properties: understanding short- and long-range effects in rubredoxin. *J Phys Chem B*. **111**(15):3969-76.

Thannickal, V.J. and Fanburg, B.L. (2000) Reactive oxygen species in cell signaling. *Am J Physiol Lung Cell Mol Physiol*. **279**(6):L1005-28.

The PyMOL Molecular Graphics System, Version 0.99rc6, Schrodinger, LLC, 2006.

Thorneley, R.N. and Lowe, D.J. (1983) Nitrogenase of *Klebsiella pneumoniae*. Kinetics of the dissociation of oxidized iron protein from molybdenum-iron protein: identification of the rate-limiting step for substrate reduction. *Biochem J*. **215**(2):393-403.

Tsukahara, K. and Ishida, K. (1991) Kinetics and Mechanism of Reduction of Metmyoglobins by Dithionite. Role of the Heme Propionates. *Bull Chem Soc Jpn*. **64**(8):2378-2382.

Turner, D.L., Salgueiro, C.A., Catarino, T., Legall, J. and Xavier, A.V. (1996) NMR studies of cooperativity in the tetrahaem cytochrome c_3 from *Desulfovibrio vulgaris*. *Eur J Biochem*. **241**(3):723-31.

Turner, D.L. and Catarino, T. (2012) Homotropic and heterotropic interactions in cytochromes c_3 from sulphate reducing bacteria. *FEBS Lett*. **586**(5):494-503.

Valente, F.M., Saraiva, L.M., LeGall, J., Xavier, A.V., Teixeira, M. and Pereira, I.A. (2001) A membrane-bound cytochrome c_3: a type II cytochrome c_3 from *Desulfovibrio vulgaris* Hildenborough. *Chembiochem*. **2**(12):895-905.

Watanabe, T. and Honda, K. (1982) Measurement of the Extinction Coefficient of the Methyl Viologen Cation Radical and the Efficiency of Its Formation by Semiconductor Photocatalysis. *J Phys Chem*. **86**(14):2617-2619.

Wherland, S. and Gray, H.B. (1976) Metalloprotein electron transfer reactions: analysis of reactivity of horse heart cytochrome *c* with inorganic complexes. *Proc Natl Acad Sci U S A*. **73**(9):2950-4.

Windass, J.D., Worsey, M.J., Pioli, E.M., Pioli, D., Barth, P.T., Atherton, K.T., Dart, E.C., Byrom, D., Powell, K. and Senior, P.J. (1980) Improved conversion of methanol to single-cell protein by *Methylophilus methylotrophus*. *Nature*. **287**(5781):396-401.

Wyman, J., Jr. (1964) Linked Functions and Reciprocal Effects in Hemoglobin: A Second Look. *Adv Protein Chem*. **19**:223-86.

Xavier, A.V. (2002) A mechano-chemical model for energy transduction in cytochrome *c* oxidase: the work of a Maxwell's god. *FEBS Lett.* **532**(3):261-6.

Zhao, Y., Brandish, P.E., Ballou, D.P. and Marletta, M.A. (1999) A molecular basis for nitric oxide sensing by soluble guanylate cyclase. *Proc Natl Acad Sci U S A.* **96**(26):14753-8.

Zumft, W.G. (1993) The biological role of nitric oxide in bacteria. *Arch Microbiol.* **160**(4):253-64.

Appendix

Pulse program for the acquisition of EXSY spectra

```
;noesyphprd04ofrex.dlt
;avance-version (07/04/04)
;2D homonuclear correlation via dipolar coupling
;dipolar coupling may be due to noe or chemical exchange.
;phase sensitive
;with presaturation during relaxation delay and mixing time
;with initial d0 of 4u and excitation offset given by frequency list
;
;$CLASS=HighRes
;$DIM=2D
;$TYPE=
;$SUBTYPE=
;$COMMENT=

#include <Avance.incl>

"d11=30m"
"d12=20u"
"d13=4u"

"in0=inf1"

"d0=4u"

"acqt0=-p1*2/3.1416"

1 ze
2 d11
3 d12 fq1:f1
  d12 pl9:f1
  d1 cw:f1 ph29
  d13 do:f1
  d12 fq1:f1
  d12 pl1:f1
  p1 ph1
  d0
  p1 ph2
  ;d12 fq1:f1
  ;d12 pl9:f1
  d8 ;cw:f1
  ;d13 do:f1
  ;d12 fq1:f1
  ;d12 pl1:f1
  p1 ph3
  go=2 ph31
  d11 mc #0 to 2 F1PH(ip1 & ip29, id0)
exit
```

```
ph1=0 2
ph2=0 0 0 0 0 0 0 0 2 2 2 2 2 2 2 2
ph3=0 0 2 2 1 1 3 3
ph29=0
ph31=0 2 2 0 1 3 3 1 2 0 0 2 3 1 1 3

;pl1 : f1 channel - power level for pulse (default)
;pl9 : f1 channel - power level for presaturation
;p1 : f1 channel -  90 degree high power pulse
;d0 : incremented delay (2D)
;d1 : relaxation delay; 1-5 * T1
;d8 : mixing time
;d11: delay for disk I/O                              [30 msec]
;d12: delay for power switching                       [20 usec]
;d13: short delay                                     [4 usec]
;inf1: 1/SW = 2 * DW
;in0: 1/(1 * SW) = 2 * DW
;nd0: 1
;NS: 8 * n
;DS: 16
;td1: number of experiments
;FnMODE: States-TPPI, TPPI, States or QSEQ

;Processing

;PHC0(F1): 90
;PHC1(F1): -180
;FCOR(F1): 1

;$Id: noesyphpr,v 1.7 2007/04/11 13:34:31 ber Exp $
```

ITQB-UNL | Av. da República, 2780-157 Oeiras, Portugal
Tel (+351) 214 469 100 | Fax (+351) 214 411 277

www.itqb.unl.pt